Interaction Notes

Note 335

December 1976

Induced Currents and Charges on Cylinders and Crossed Cylinders by an Electromagnetic Field

Ronold W. P. King
R. W. Burton
L. C. Shen

Harvard University
Cambridge, Massachusetts

ABSTRACT

An introduction is given to the problem of determining the distributions of surface current and charge on crossed metal structures, particularly tubular cylinders. Pertinent knowledge about distributions of current and charge induced in thin wires, crossed thin wires, and cross-sectionally large tubes is presented as a foundation for acquiring an understanding for currents and charges induced in crossed electrically thick cylinders. It is shown that a representation of the distribution of current along a conductor excited by an E-polarized plane wave in terms of the transverse Fourier components and suitable combinations of forced and resonant components offers an attractive, relatively simple approximation. Preliminary experimental investigation of crossed cylinders with ka = 1 indicates that the original standing-wave distributions of charge and current density are not greatly altered by the addition of the horizontal cylinder except in the vicinity of that member. Outside this vicinity the general nature of the standing waves is not changed significantly with respect to their location but large changes in the relative distributions of amplitude can occur.

ACKNOWLEDGEMENT

In addition to support from the Air Force Contract Management Division, Kirtland Air Force Base, under Contract F29601-75-C-0119, the research described in this report was also supported in part by the Joint Services Electronics Program under Contract N00014-75-C-0648 with Harvard University.

TABLE OF CONTENTS

		Page
	LIST OF ILLUSTRATIONS	4
SECTION		
I	INTRODUCTION	11
II	THE INFINITELY LONG CYLINDER IN A PLANE-WAVE FIELD	15
III	DISTRIBUTIONS OF CURRENT AND CHARGE PER UNIT LENGTH INDUCED IN THIN WIRES BY A PLANE-WAVE FIELD	24
IV	CURRENTS AND CHARGES ON CROSSED THIN WIRES IN A PLANE-WAVE FIELD	38
V	THEORY OF THE TUBULAR CYLINDER OF FINITE LENGTH	55
VI	THEORETICAL CURRENTS AND CHARGES ON A TUBULAR CYLINDER	65
VII	EXPERIMENTAL VERIFICATION; CYLINDER WITH ka = 1, kh = 3.5π	87
VIII	FOURIER COMPONENTS OF THE TOTAL CURRENT	100
IX	CROSSED ELECTRICALLY THICK TUBES; ka = 1	110
X	CONCLUSIONS	127
	REFERENCES	128

LIST OF ILLUSTRATIONS

Figure		Page
1	Plane wave (top) and cylindrical wave (bottom) normally incident on infinitely long cylinder with radius a.	16
2	Surface densities of current on infinitely long cylinder in normally incident, plane-wave field	20
3	Surface density of charge on infinitely long cylinder in normally incident, plane-wave field. H-polarization; $E_x^{inc} = cB_z^{inc} = 1$ volt/m; $c = 3 \times 10^8$ m/sec.	22
4	Theoretical distributions of current and charge per unit length in parasitic antenna in normally incident, plane-wave field; $h = 7\lambda/4$.	26
5	Theoretical distributions of current and charge per unit length in parasitic antenna in normally incident, plane-wave field; $h = 1.5\lambda$.	27
6	Theoretical distributions of current and charge per unit length in parasitic antenna in normally incident, plane-wave field; $h = 5\lambda/4$.	28
7	Measured distributions of current and charge per unit length in parasitic antenna in normally incident, plane-wave field; $h = 5\lambda/4$.	29
8	Real and imaginary currents on parasitic antenna in normally incident, plane-wave field.	31
9	The function $e(kz)$.	32
10	Real and imaginary currents on parasitic antenna in normally incident, plane-wave field; $kh = 3\pi/4$.	35
11	Real and imaginary currents on parasitic antenna in normally incident, plane-wave field; $kh = 0.95\pi$.	36

Figure		Page
12	Induced current in parasitic antenna. $\theta = 90°$ is normal incidence with E parallel to axis.	37
13	Crossed wires in normally incident, plane-wave field.	39
14	Current on parasitic antenna (King-Wu theory).	43
15	Theoretical distributions of current and charge per unit length on crossed antenna in normally incident, plane-wave field; $kh_1 = 5\pi/2$, $kh_2 = k\ell_1 = k\ell_2 = \pi/2$.	45
16	Theoretical distributions of current and charge per unit length on crossed antenna in normally incident, plane-wave field; $kh_1 = 3\pi$, $kh_2 = k\ell_1 = k\ell_2 = \pi$.	47
17	Theoretical distributions of current and charge per unit length on crossed antenna in normally incident, plane-wave field; $kh_1 = 4\pi$, $kh_2 = 2\pi$, $k\ell_1 = k\ell_2 = \pi$.	48
18	Theoretical distributions of current and charge per unit length on crossed antenna in normally incident, plane-wave field; $kh_1 = 4\pi$, $kh_2 = k\ell_1 = k\ell_2 = \pi$.	50
19	Measured distributions of current and charge per unit length on antenna with and without cross in normally incident, plane-wave field. Junction at maximum current, minimum charge.	52
20	Measured distributions of current and charge per unit length on antenna with and without cross in normally incident, plane-wave field. Junction at maximum of charge.	54
21a	Theoretical amplitude of surface density of total axial current on tubular cylinder; E-polarization, normal incidence.	66

Figure		Page
21b	Theoretical phase of surface density of total axial current on tubular cylinder; E-polarization, normal incidence.	67
21c	Real and imaginary parts of $K_z(\theta,z)$ on tubular cylinder; E-polarization, normal incidence.	68
22a	Theoretical amplitude of surface density of total axial current on tubular cylinder; E-polarization, normal incidence.	69
22b	Theoretical phase of surface density of total axial current on tubular cylinder; E-polarization, normal incidence.	70
22c	Real and imaginary parts of $K_z(\theta,z)$ on tubular cylinder; E-polarization, normal incidence. $K_z(\theta)$ with $kh = \infty$.	71
23a	Theoretical amplitude of surface density of transverse current on tubular cylinder; E-polarization, normal incidence.	73
23b	Theoretical phase of surface density of transverse current on tubular cylinder; E-polarization, normal incidence.	74
23c	Real and imaginary parts of $K_\theta(\theta,z)$ on tubular cylinder; E-polarization, normal incidence.	75
24	$\vec{K}_R(\theta,z)$ and $\vec{K}_I(\theta,z)$ on tubular cylinder; E-polarization, normal incidence; $kh = 1.5\pi$, $ka = 1$.	76
25	Theoretical polarization ellipses of $\vec{K}(\theta,z)$ on tubular cylinder; E-polarization, normal incidence; $kh = 1.5\pi$, $ka = 1$.	77

Figure		Page
26a	Theoretical magnitude of surface density of charge on tubular cylinder, $\eta = \|\eta\|\exp(i\theta_\eta)$; E-polarization, normal incidence.	78
26b	Theoretical phase of surface density of charge on tubular cylinder, $\eta = \|\eta\|\exp(i\theta_\eta)$; E-polarization, normal incidence.	79
27a	Theoretical contours of magnitude of surface density of charge on tubular cylinder; E-polarization, normal incidence.	81
27b	Theoretical contours of constant phase of surface density of charge on tubular cylinder; E-polarization, normal incidence.	82
28	Surface density of axial current on tubular cylinder, $K_z(\theta,z) = K_{zR} + iK_{zI}$; E-polarization, normal incidence; $ka = 1$.	83
29	Theoretical magnitude of surface density of outside charge on tubular cylinder; E-polarization, normal incidence.	84
30	Contour diagram of theoretical surface density of outside charge on tubular cylinder; E-polarization, normal incidence; $kh = 3\pi$, $ka = 1$.	85
31	Schematic diagrams of (a) scattering cylinder on ground plane, (b) cross section of groove in cylinder, and (c) probes on slider.	88
32	Theoretical magnitude and phase of surface density of outside axial current on tubular cylinder; E-polarization, normal incidence; $kh = 3.5\pi$, $ka = 1$.	89

Figure		Page
33	Measured magnitude and phase of surface density of outside axial current on tubular cylinder; E-polarization, normal incidence; kh = 3.5π, ka = 1, λ = 48.0 cm.	90
34	Theoretical amplitude and phase of surface density of outside transverse current on tubular cylinder; E-polarization, normal incidence; kh = 3.5π, ka = 1.	92
35	$\vec{K}_R(\theta,z)$ and $\vec{K}_I(\theta,z)$ on tubular cylinder; E-polarization, normal incidence; kh = 3.5π, ka = 1.	93
36	Theoretical polarization ellipses of $\vec{K}(\theta,z)$ on tubular cylinder; E-polarization, normal incidence; kh = 3.5π, ka = 1.	94
37	Measured polarization ellipses of $\vec{K}(\theta,z)$ on tubular cylinder; E-polarization, normal incidence; kh = 3.5π, ka = 1.	95
38	Theoretical magnitude of surface density of outside charge on tubular cylinder; E-polarization, normal incidence.	96
39	Measured magnitude of surface density of outside charge on tubular cylinder; E-polarization, normal incidence.	97
40	Contour diagram of theoretical surface density of outside charge on tubular cylinder; E-polarization, normal incidence; kh = 3.5π, ka = 1.	98
41	Contour diagram of measured surface density of outside charge on tubular cylinder; E-polarization, normal incidence; kh = 3.5π, ka = 1, λ = 48.0 cm.	99
42	Fourier coefficients of surface density of axial current on tubular cylinder, $K_z(\theta,z) = A(kz) + B(kz)\cos\theta + C(kz) \times \cos 2\theta + D(kz)\cos 3\theta$; E-polarization, normal incidence; ka = 1.	101

Figure		Page
43	Fourier coefficients of surface density of axial current on tubular cylinder, $K_z(\theta,z) = A(kz) + B(kz)\cos\theta + C(kz) \times \cos 2\theta + D(kz)\cos 3\theta$; E-polarization, normal incidence; $ka = 1$.	102
44	Fourier coefficients A(kz) and B(kz) of $K_z(\theta,z)$ resolved into resonant and forced components.	104
45	Theoretical (left) and approximate (right) Fourier coefficients of surface density of axial current $K_z(\theta,z)$ on tubular cylinder; E-polarization, normal incidence.	106
46	Components in the approximate representation shown on right in Fig. 45: $A(kz) = (A - A_r)e(kz) + A_r(\cos kz + 1)$, $B(kz) = (B - B_r)e(kz) + B_r(\cos kz + 1)$.	107
47	Diagram of crossed electrically thick cylinders illuminated by normally incident, plane-wave field.	111
48	Measured surface density of charge on crossed cylinder; E-polarization, normal incidence; $kh_1 = 2.5\pi$, $kh_2 = \pi$, $k\ell_1 = k\ell_2 = \pi$.	115
49	Measured surface densities of current on crossed cylinders; E-polarization, normal incidence; $kh_1 = 2.5\pi$, $kh_2 = k\ell_1 = k\ell_2 = \pi$.	117
50	Measured surface density of charge on crossed cylinders; E-polarization, normal incidence; $kh_1 = 2\pi$, $kh_2 = k\ell_1 = k\ell_2 = 1.5\pi$.	118
51	Measured surface densities of current on crossed cylinders; E-polarization, normal incidence; $kh_1 = 2\pi$, $kh_2 = k\ell_1 = k\ell_2 = 1.5\pi$.	119

Figure		Page
52	Measured magnitude of surface density of charge on vertical member of crossed cylinders; E-polarization, normal incidence.	120
53	Measured contours of constant density of charge on vertical member of crossed cylinders; E-polarization, normal incidence.	121
54	Measured magnitude of surface density of axial current on vertical member of crossed cylinders; E-polarization, normal incidence.	123
55	Measured magnitude of surface density of charge on horizontal member of crossed cylinders; E-polarization for vertical cylinder, normal incidence.	124
56	Measured magnitudes of surface densities of charge and current on horizontal member of crossed cylinders; E-polarization for vertical cylinder, normal incidence.	125
57	Measured magnitudes of surface densities of current on horizontal member of crossed cylinders; E-polarization for vertical cylinder, normal incidence.	126

SECTION I
INTRODUCTION

The currents and charges that are induced on the surfaces of rockets, aircraft, shielded transmission lines and other metal-clad, three-dimensional structures by an electromagnetic field in the form of a standing or traveling wave or a pulse are of interest for several reasons. One is the determination of the scattered far field from which is derived the radar cross section. Another is to understand the near field, specifically in its relationship to the imperfect shielding properties of the metal walls either when interrupted by small apertures [1], [2] or because of their finite conductivity [3]. Closely related and also involving the near field is the coupling between the exterior and interior regions by exposed conductors that pass through the walls [4]. In all of these examples the field and the associated currents and charges on conductors in the interior of the metal structure are directly related to the currents and charges induced on its outside surfaces. The currents induced in circuits within a cylindrical sheath that simulates a rocket or missile due either to fields that penetrate the imperfectly conducting walls or that enter through slots, holes or other apertures have been studied [1]-[4]. However, the scope of the investigations has been limited to cylinders (with radius a and half-length h) that are electrically very thin ($ka \ll 1$) and relatively short ($kh < 2\pi$). This range of study is

inadequate at frequencies for which the cylinder is electrically thick or long or when the exciting field is a pulse.

To determine surface currents and charges on metal structures like aircraft is more difficult owing to the awkward geometry of the boundaries and the presence of a junction region with intersecting surfaces. Numerical methods have been used [5]-[9] to determine the currents on electrically very thin crossed wires when the arms were quite short, ranging between 0.1 and 0.3 wavelength. Unfortunately, the critical problem of the junction was not treated completely since only the continuity of the confluent currents but not of their slopes was enforced at the junction. The results obtained are adequate for calculating far fields but not near electric fields since spurious concentrations of charge occur where the slopes of the currents are discontinuous. This difficulty was overcome in an analysis of the distributions of both current and charge per unit length on mutually perpendicular, electrically thin, crossed wires that are not restricted in length but are assumed to have equal radii [10]. Conditions were imposed that assured the continuity of both current and charge per unit length at the junction. The generalization of these to intersecting electrically thin wires with different radii has been formulated [11]. Unfortunately, the quasi-one-dimensional theory of electrically thin crossed conductors is not adequate to describe the distributions of current and charge on structures with members that have electrically large cross sections. This is a consequence of one of the basic assumptions characteristic of electrical thinness, namely, that transverse currents be negligible. As soon as the cross section is large enough to support significant transverse currents on any of the conductors, thin-wire theory is inadequate. Nevertheless, computations have been made to determine currents on electrically thick structures by applying electrically thin

theory and junction conditions [12] to crossed electrically thick cylinders!

The distribution of current on an electrically thick cylinder in an incident plane-wave field is well known for any polarization when the cylinder is infinitely long [13]. But this is quite different from the current on a similar cylinder that is finite in length, as is evident from the analysis of the electrically thick tubular cylinder of finite length by C. C. Kao [14]-[17] and the associated extensive computations of the distributions of the surface densities of current and charge by King et al. [18]. Since no theory is available for the distributions of current and charge on the surfaces of two crossed electrically thick cylinders, recourse must be taken to the direct measurement of these quantities. Since this involves the use of movable calibrated electric and magnetic field probes traveling in slots and the generation of a plane electromagnetic wave, a thorough study of the accuracy of such measurements is essential. These have been carried out for electrically thin wires and crossed wires by Burton and King [19], [20] and for thick tubular cylinders by Kao [21] and Burton et al. [22]. They reveal both the possibilities and the difficulties associated with the experimental simulation of a plane electromagnetic wave and the measurement of the currents and charges induced by it on extended conducting surfaces. Only after a complete validation of the apparatus and techniques of measurement on structures for which theoretical results are available has been achieved, can the experimental methods be applied with confidence to the measurement of the currents and charges on crossed metal structures including especially those with cross sections that are electrically large. From a study of the measured currents and charges on the crossed thick cylinders - especially in and near the junction region - and the knowledge of forced and resonant distributions on isolated thin and thick cylinders and on crossed thin cylinders, an understanding

can be sought of the basic phenomena that determine the distributions of currents and charges on crossed thick cylinders.

It is the purpose of the following sections to lay the foundations for such an understanding by reviewing the induced currents and charges on circular highly conducting cylinders in an incident plane-wave field in the following sequence: 1) Infinitely long cylinders with unrestricted radii; 2) Electrically thin cylinders of finite length; 3) Electrically thin crossed cylinders; 4) Tubular cylinders with unrestricted radii and finite length; 5) Crossed electrically thick cylinders.

SECTION II

THE INFINITELY LONG CYLINDER IN A PLANE-WAVE FIELD

A section of an infinitely long, perfectly conducting cylinder with radius a is shown at the top and center of Fig. 1. It is illuminated by a normally incident plane electromagnetic wave traveling in the direction of the positive y axis. The electric and magnetic vectors are mutually perpendicular and lie in the xz-plane. It is well known that Maxwell's equations (with the time dependence $e^{-i\omega t}$), $\nabla \times \vec{E} = i\omega\vec{B}$, $\nabla \times \vec{B} = -i(k^2/\omega)\vec{E}$, are separable into two independent groups when $\partial\vec{E}/\partial z = 0$, $\partial\vec{B}/\partial z = 0$ as is true when the scattering cylinder is infinitely long. In the one group, the induced currents are entirely axial and are derivable from E_z^{inc} (E-polarization). In the second group, the induced currents are exclusively transverse and depend only on B_z^{inc} (H-polarization). With the cylindrical coordinates (ρ,θ,z), the induced surface density of axial current, $K_z(\theta)$, with E-polarization satisfies the integral equation

$$E_z^i e^{ika\cos\theta} + i\omega\mu_0 a \int_0^{2\pi} K_z(\theta')G(a,\theta;a',\theta')\,d\theta' = 0 \qquad (2.1)$$

The induced surface density of transverse current with H-polarization satisfies the equation

$$\frac{\partial}{\partial\rho}\left[B_z^i e^{ika\cos\theta}\right] - \mu_0 a \int_0^{2\pi} K_\theta(\theta')\left[\frac{\partial^2}{\partial\rho\,\partial\rho'}G(\rho,\theta;\rho',\theta')\right]_{\rho=\rho'=a} d\theta' = 0 \qquad (2.2)$$

In (2.1) and (2.2), $G(\rho,\theta;\rho',\theta') = (i/4)H_0^{(1)}(kR)$ with $R = [\rho^2 + \rho'^2 - 2\rho\rho'\cos(\theta - \theta')]^{1/2}$. When ka is not too large, the eigenfunction expansions [13], [22] are convenient solutions. They are

$$\frac{K_z(\theta)}{E_z^{inc}} = \frac{2}{\pi\zeta_0 ka}\sum_{m=0}^{\infty}\varepsilon_m i^m \frac{\cos m\theta}{H_m^{(1)}(ka)} \qquad (2.3)$$

and

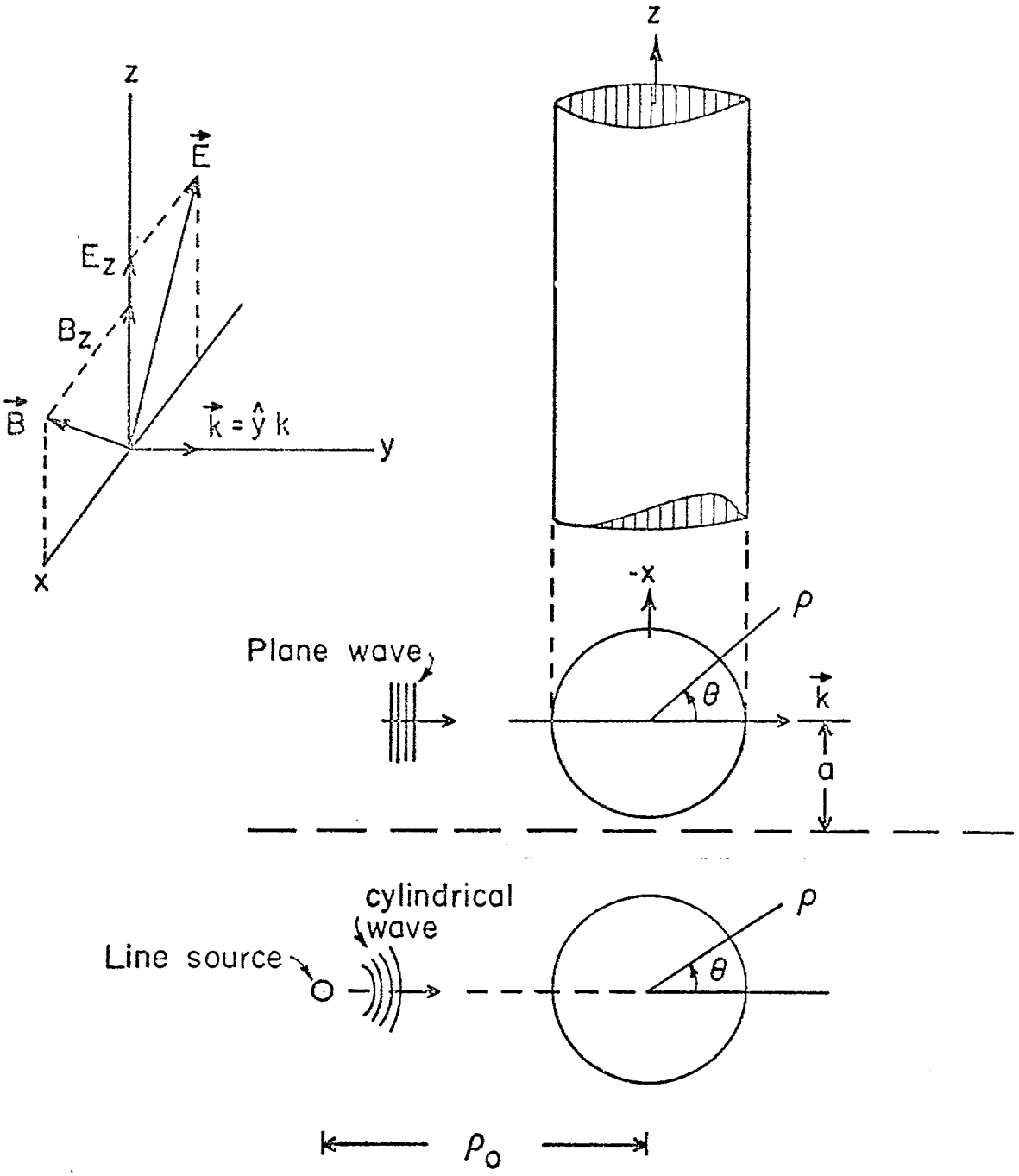

Fig. 1. Plane wave (top) and cylindrical wave (bottom) normally incident on infinitely long cylinder with radius a.

$$\frac{K_\theta(\theta)}{E_y^{inc}} = \frac{2}{\pi\zeta_0 ka} \sum_{m=0}^{\infty} \varepsilon_m i^{m-1} \frac{\cos m\theta}{H_m^{(1)'}(ka)} \tag{2.4}$$

where $\varepsilon_m = 1$ for $m = 0$, 2 for $m \neq 0$; $\zeta_0 = (\mu_0/\varepsilon_0)^{1/2} \doteq 120\pi$ ohms. $H_m^{(1)}(ka)$ is the Hankel function, $H_m^{(1)'}(ka)$ its derivative with respect to the argument. Note that in (2.4), $E_x^{inc}/\zeta_0 = B_z^{inc}/\mu_0 = H_z^{inc}$.

In subsequent discussions interest centers on conductors that are electrically thin with ka = 0.04 and electrically thick with ka = 1. In the former, the first rotationally symmetric term with m = 0 dominates for both E- and H-polarizations. With $H_0^{(1)}(ka) \doteq 1 - (2i/\pi)[\ell n(2/ka) + C]$ and $H_0^{(1)'}(ka) \doteq (2i/\pi ka)$, $H_1^{(1)}(ka) = -(2i/\pi ka)$ and $H_1^{(1)'}(ka) = (2i/\pi k^2 a^2)$. It follows that

$$\frac{K_z(\theta)}{E_z^{inc}} = \frac{2}{\pi\zeta_0 ka} \left\{ \frac{1}{1 - (2i/\pi)[\ell n(2/ka) + C]} + 2ka \cos\theta \right\} \tag{2.5}$$

The leading rotationally symmetric part can be expressed in terms of the total axial current, $I_z = 2\pi a K_z$, in the normalized form:

$$\frac{kaK_z}{E_z^{inc}} = \frac{I_z}{\lambda E_z^{inc}} = \frac{2}{\pi\zeta_0} \left\{ \frac{1 + (2i/\pi)[\ell n(2/ka) + C]}{1 + (4/\pi)^2[\ell n(2/ka) + C]^2} \right\} \tag{2.6}$$

For the H-polarization

$$\frac{K_\theta(\theta)}{E_x^{inc}} = -\frac{1}{\zeta_0}(1 + 2ika \cos\theta) \tag{2.7}$$

where the leading rotationally symmetric term is simply $K_\theta(\theta) = -E_x^{inc}/\zeta_0 = -H_z^{inc} = -B_z^{inc}/\mu_0$, which is independent of ka so long as this is sufficiently small.

With ka = 0.04,

$$kaK_z/E_z^{inc} = I_z/\lambda E_z^{inc} = 0.184 + i0.526 \text{ mA/V} \tag{2.8}$$

When ka = 1, the densities of surface current in (2.3) and (2.4) can be expressed as follows:

E-polarization:

$$\frac{K_z(\theta)}{E_z^{inc}} = A + B\cos\theta + C\cos 2\theta + D\cos 3\theta + E\cos 4\theta + F\cos 5\theta + \ldots \qquad (2.9)$$

H-polarization:

$$\frac{K_\theta(\theta)}{E_x^{inc}} = A_H + B_H\cos\theta + C_H\cos 2\theta + D_H\cos 3\theta + E_H\cos 4\theta + F_H\cos 5\theta + \ldots \qquad (2.10)$$

where the complex Fourier coefficients $A = A_R + iA_I$ through $F = F_R + iF_I$ (with and without the subscript H) are given in Table 1. It is seen that in each case only the first four coefficients are significant. The transverse distributions of $K_z(\theta)$ and $K_\theta(\theta)$ are shown graphically in Fig. 2. Note that $K_\theta(\theta)$ decays much less rapidly than $K_z(\theta)$ from the center of the illuminated side at $\theta = 180°$ to the center of the shadow side at $\theta = 0°$. The real and imaginary parts are of interest since they are contained individually in (2.3) or (2.4) and $|K|$ and θ are determined from them.

The surface density of charge $\eta(\theta)$ on the infinite cylinder is, for E-polarization,

$$\eta(\theta) = \frac{i}{\omega}\frac{\partial K_z(\theta)}{\partial z} = 0 \qquad (2.11)$$

For H-polarization with (2.4),

$$\frac{\eta(\theta)}{E_x^{inc}} = \frac{i}{\omega E_x^{inc}}\frac{\partial K_\theta(\theta)}{a\,\partial\theta} = -\frac{2i\varepsilon_0}{\pi k^2 a^2}\sum_{m=0}^{\infty}\varepsilon_m i^{m-1}\frac{m\sin m\theta}{H_m^{(1)\prime}(ka)} \qquad (2.12)$$

With ka = 1, $c\eta(\theta)/E_x^{inc} = -i[B_H\sin\theta + 2C_H\sin 2\theta + 3D_H\sin 3\theta + 4E_H\sin 4\theta + \ldots]$.

TABLE 1

FOURIER COEFFICIENTS IN mA/V FOR INFINITELY LONG CYLINDER; ka = 1

	A	B	C	D	E	F
$K_z(\theta)$	2.18 - i0.25	-3.28 + i1.85	-0.14 - i2.04	0.58 + i0.00	0.00 + i0.10	0.01 + i0.00
	A_H	B_H	C_H	D_H	E_H	F_H
$K_\theta(\theta)$	-1.64 + i0.93	1.27 - i3.41	1.33 + i0.11	0.00 + i0.21	0.03 + i0.00	0.00 + i0.00

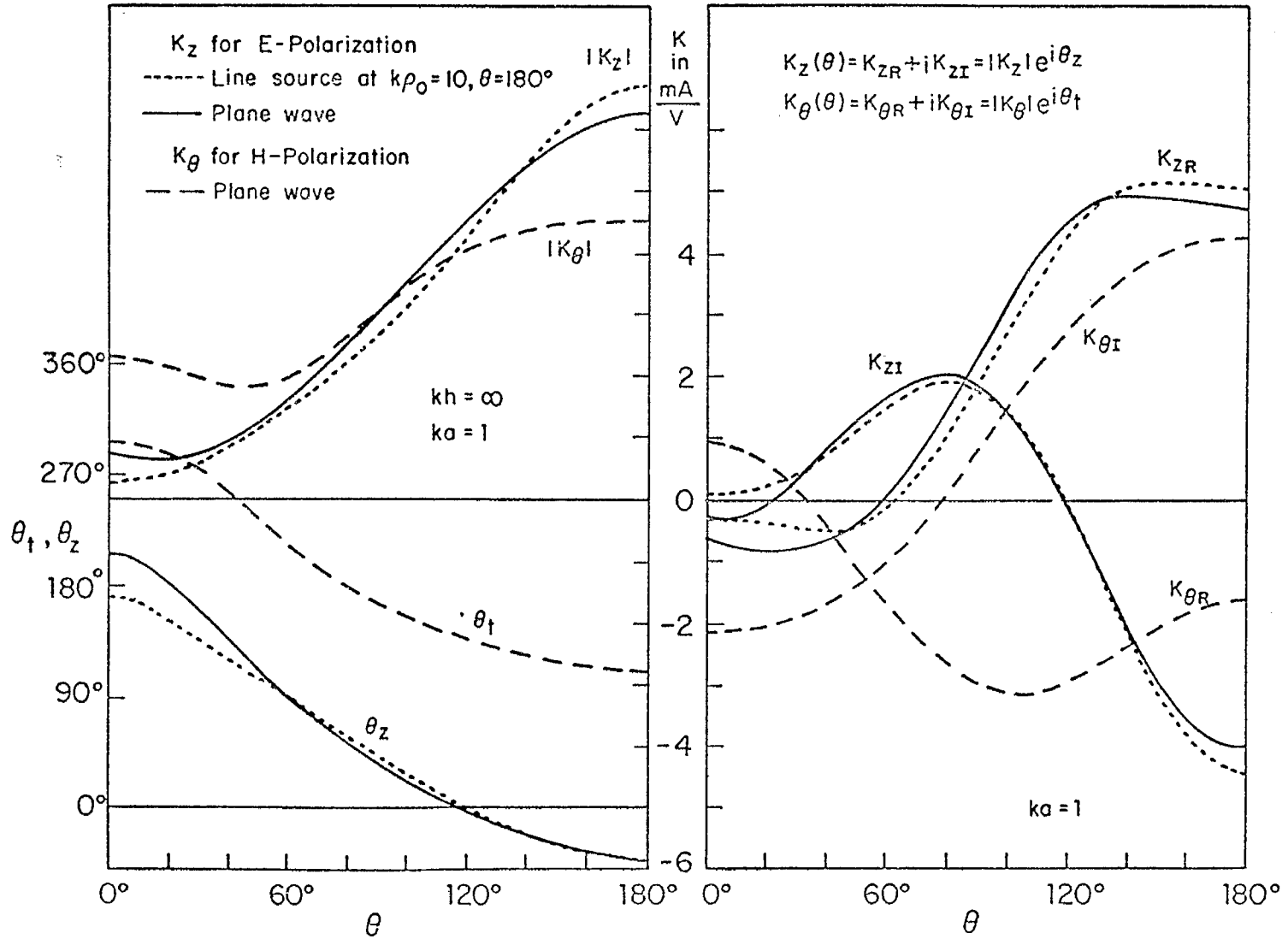

Fig. 2. Surface densities of current on infinitely long cylinder in normally incident, plane-wave field.

This quantity is shown in Fig. 3 in its magnitude and phase on the left, its real and imaginary parts on the right.

Since the problem of generating a plane wave in the laboratory for purposes of testing is formidable, a knowledge of the distributions of current and charge density induced by an incident cylindrical wave is of interest. With a line source at $\rho = \rho_0$, $\theta = 180°$ (Fig. 1, bottom), the appropriate eigenfunction expansion for E-polarization is [23]:

$$\frac{K_z(\theta)}{E_z^{inc}} = \frac{2}{\pi ka\zeta_0 H_0^{(1)}(k\rho_0)} \sum_{m=0}^{\infty} \epsilon_m \frac{(-1)^m H_m^{(1)}(k\rho_0)}{H_m^{(1)'}(ka)} \cos m\theta \qquad (2.13)$$

When $k\rho_0$ is sufficiently large so that the asymptotic formula

$$H_m^{(1)}(k\rho_0) \doteq \sqrt{2/\pi k\rho_0}\, e^{i(k\rho_0 - \pi/4 - m\pi/2)} = (-1)^m \sqrt{2/\pi k\rho_0}\, e^{i(k\rho_0 - \pi/4)} \qquad (2.14)$$

is a satisfactory approximation, (2.13) reduces to (2.3). For $ka = 1$, only four or five terms in (2.13) are needed and (2.14) is an adequate approximation when $k\rho_0 > 10$. The current density in (2.13) has been evaluated accurately for $ka = 1$ and $k\rho_0 = 10$ and shown graphically in dotted lines in Fig. 2 along with the corresponding components of the current excited by an incident plane wave. The calculations assume that the line source at $\rho_0 = (10/2\pi)\lambda = 1.59\lambda$ maintain the same electric field, viz., 1 volt/m, along the axis of the cylinder with $ka = 1$ as the plane wave. It is seen that the currents with the plane- and cylindrical-wave excitations are quite similar even when the line source is only 1.59λ from the axis of the cylinder. The largest relative differences are in the shadow region. Evidently with a thin-wire source at distances of $\rho_0 = 4\lambda$, 7.5λ and 10λ (used in actual measurements) or $k\rho_0 = 25.1$, 47.1 and 62.8, the slight curvature of the wave front in each transverse

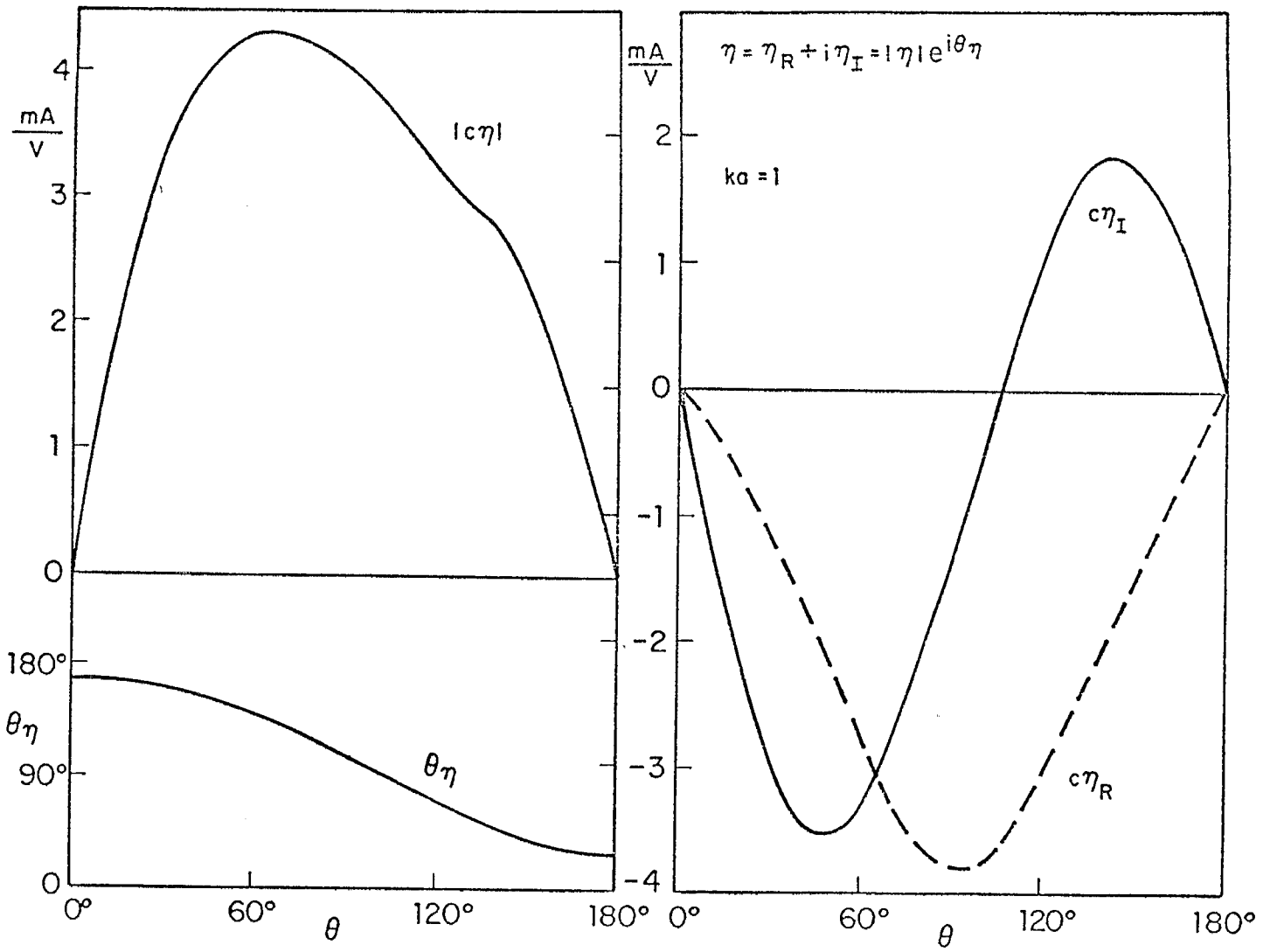

Fig. 3. Surface density of charge on infinitely long cylinder in normally incident, plane-wave field. H-polarization; $E_x^{inc} = cB_z^{inc} = 1$ volt/m; $c = 3 \times 10^8$ m/sec.

plane cannot significantly alter the induced currents and charges. The spherical curvature in the vertical plane is a different matter.

SECTION III

DISTRIBUTIONS OF CURRENT AND CHARGE PER UNIT LENGTH INDUCED IN THIN WIRES BY A PLANE-WAVE FIELD

The original interest in the current distribution along electrically thin conductors excited by an electromagnetic wave was in connection with their reradiating or scattering properties. In early work [24]-[26] approximate expressions for the current were derived or postulated as trial functions in variational methods for calculating the backscattering cross section. This is an average quantity not very sensitive to the detailed distribution of current. For the determination of the near fields, especially in small apertures on the cylindrical surface, more accurate formulas are needed. These have been obtained for the currents in both shorter and longer thin wires in the ranges of half-lengths h given by $0 \leq h/\lambda \leq 0.625$ [27], [28] and $0.25 \leq h/\lambda < \infty$ [29], [30]. For present purposes the formulation for the longer lengths is required.

When the electric field is normally incident and parallel to the axis of the wire, the induced current I(z) and charge per unit length q(z) are given in normalized form by [29]:

$$\frac{I(z)}{\lambda E_z^{inc}} = \frac{i}{4\pi^2 \zeta_0} \left\{ \frac{4\pi^2}{\Omega_1} - \frac{2\pi i}{k} [M(h+z) + M(h-z)] + \frac{C_s}{2} [U(h+z) + U(h-z)] \times \cos kz + C_s [S(h+z) - S(h-z)] \sin kz \right\} \tag{3.1}$$

$$\frac{q(z)}{\lambda E_z^{inc}} = -\frac{\varepsilon_0}{8\pi^3} \left\{ \frac{2\pi}{k} [1 + C_s \cos kh][M(h+z) + M(h-z)] + \frac{C_s}{2} [S(h+z) - S(h-z)] \cos kz + \frac{C_s}{2} [U(h+z) + U(h-z)] \sin kz \right\} \tag{3.2}$$

where $\zeta_0 = (\mu_0/\varepsilon_0)^{1/2} \doteq 120\pi$ ohms, $k = \omega(\mu_0 \varepsilon_0)^{1/2} = \omega/c = 2\pi/\lambda$ and

$$C_s = -\frac{4\pi^2/\Omega_1 - (2\pi i/k) M(2h)}{T(2h) \cos kh + S(2h) \sin kh} \tag{3.3}$$

Also, $\Omega_1 = \Omega_0 + i\pi/2$; $\Omega_0 = \ell n(2/ka) - 0.5772$; $M(X) = \frac{2i}{X} \exp(ikX) [\frac{1}{\Omega_2(X)} - \frac{1}{\Omega_3(X)}]$; $\Omega_2(X) = 2[\ell n(1/ka) - 0.5772] + \ell n(2kX) + 0.5772 - i\pi/2$; and $\Omega_3(X) = \Omega_2(X) + 2\pi$.

$$\left.\begin{matrix} S(X)/2 \\ T(X)/2\pi i \end{matrix}\right\} = -\ell n[1 + i\pi(\Omega_0 - \ell n\ 2)^{-1}] - (\pi^2/12)[(\Omega_0 - 2\ \ell n\ 2)^{-2} - (\Omega_0 - 2\ \ell n\ 2 + i\pi)^{-2}] \pm \ell n[\Omega_3(X)/\Omega_2(X)] + 0.825[\Omega_2^{-2}(X) - \Omega_3^{-2}(X)] - M(X)/4k \tag{3.4}$$

$$-U(X)/4\pi i = \ell n[\Omega_3(X)/\Omega_2(X)] + 0.825[\Omega_2^{-2}(X) - \Omega_3^{-2}(X)] + M(X)/4k \tag{3.5}$$

These formulas were derived with the time dependence $e^{-i\omega t}$. They are not good approximations within a quarter wavelength of the ends where the current is known to vanish so that a simple extrapolation is possible. Their derivation assumes the conditions: $ka << 1$ and $kh > \pi/2$. The approximation improves with increasing length of the wire.

The distributions of current and charge in the forms

$$I(z) = I_R + iI_I = |I|e^{i\theta_I} \quad ; \quad q(z) = q_R + iq_I = |q|e^{i\theta_q} \tag{3.6}$$

as calculated from (3.1) and (3.2) are shown graphically in Figs. 4 through 6 for three thin and moderately long wires with electrical half-lengths $kh = 3.5\pi$, 3π and 2.5π. The first and third are near resonance, the second near antiresonance. For all three, the electrical radius is $ka = 0.04$. Extensive comparisons with measurements have been reported [19] with generally good agreement with theory. An example is in Fig. 7 for comparison with Fig. 6.

A glance at Figs. 3 through 7 reveals that the distributions of charge per unit length are very simple in form with $q(z) \sim \sin kz$ an excellent approximation. The more complicated form of the currents can be understood from the components in phase and in phase quadrature with the incident field

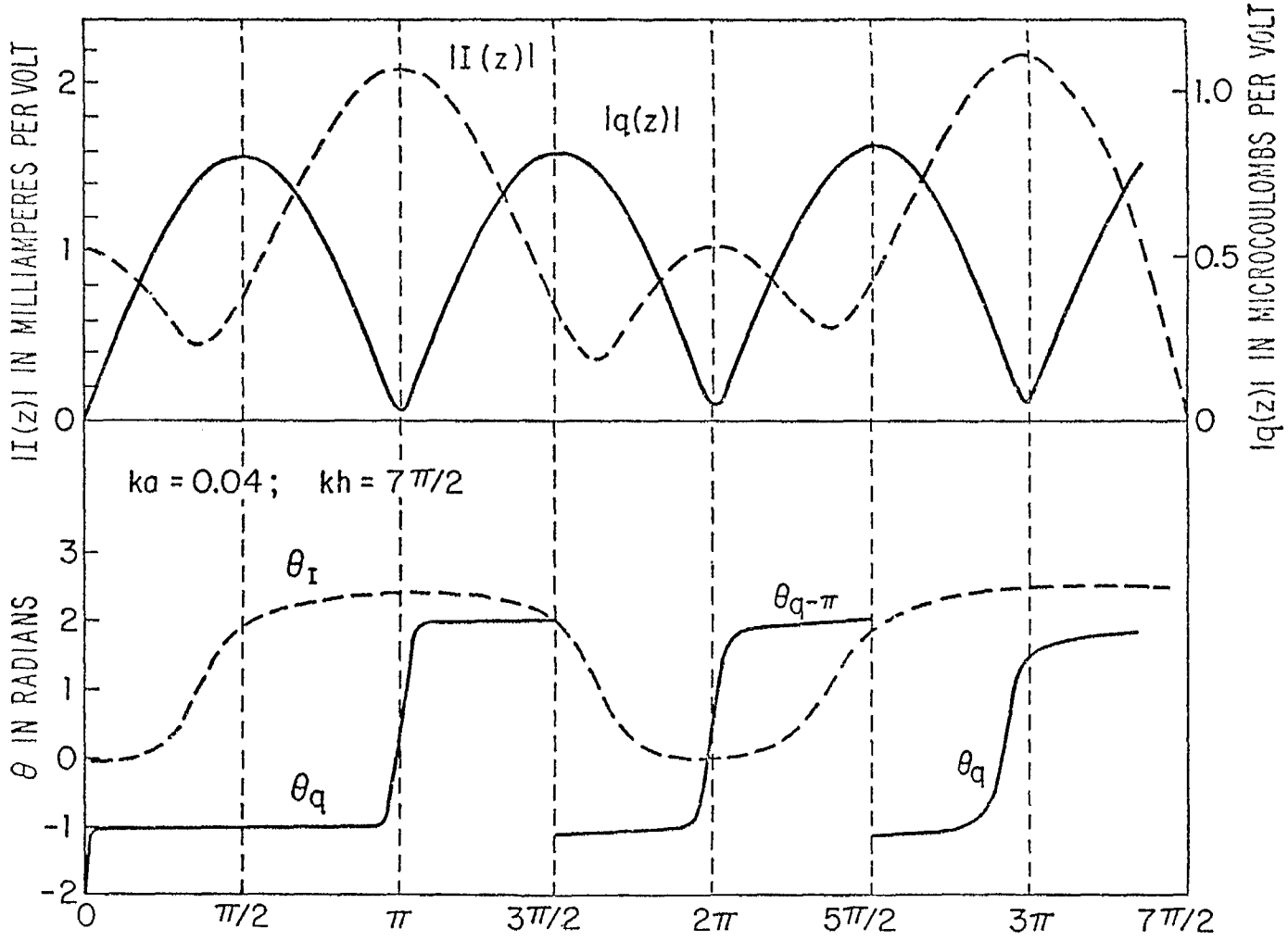

Fig. 4. Theoretical distributions of current and charge per unit length in parasitic antenna in normally incident, plane-wave field; h = 7λ/4.

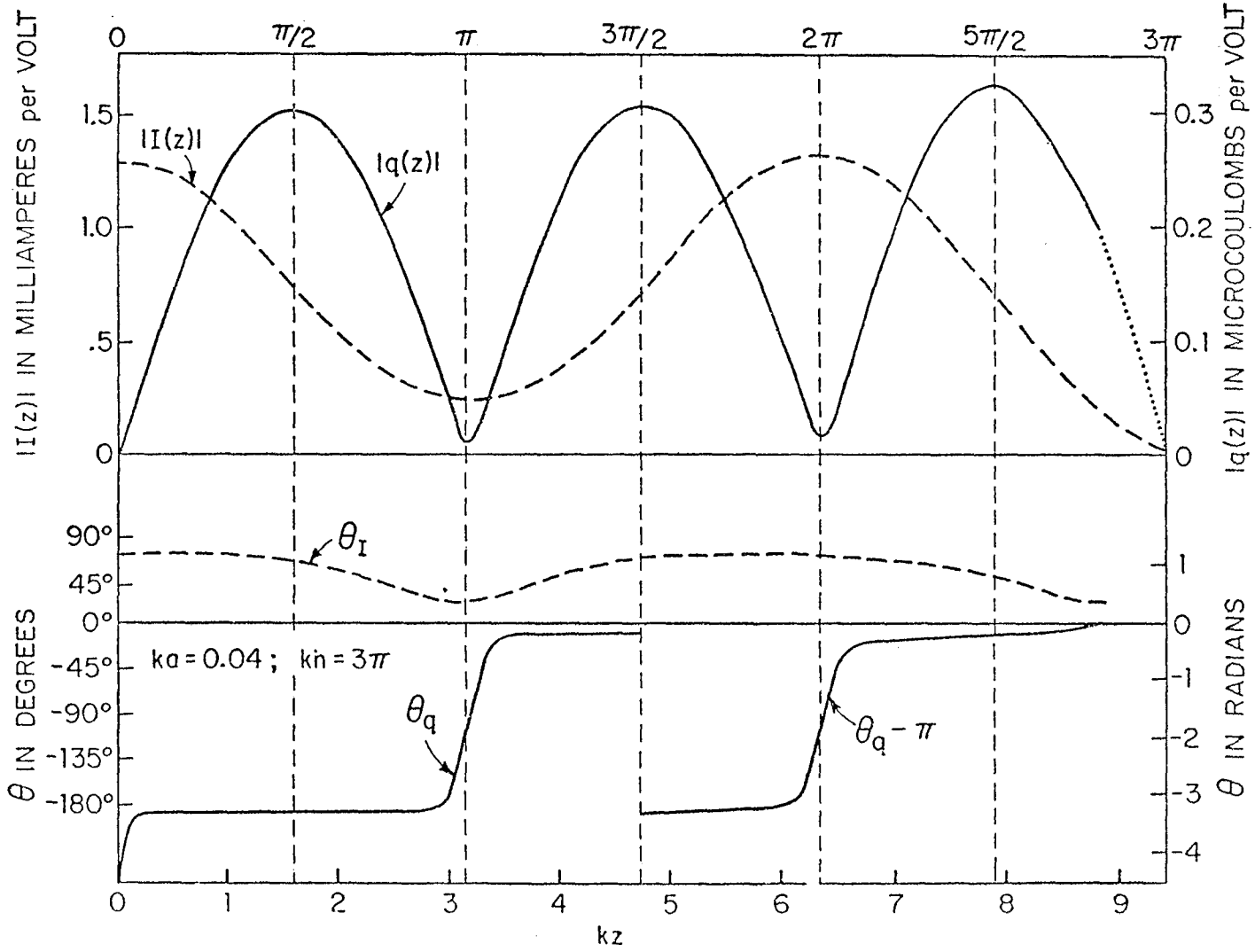

Fig. 5. Theoretical distributions of current and charge per unit length in parasitic antenna in normally incident, plane-wave field; h = 1.5λ.

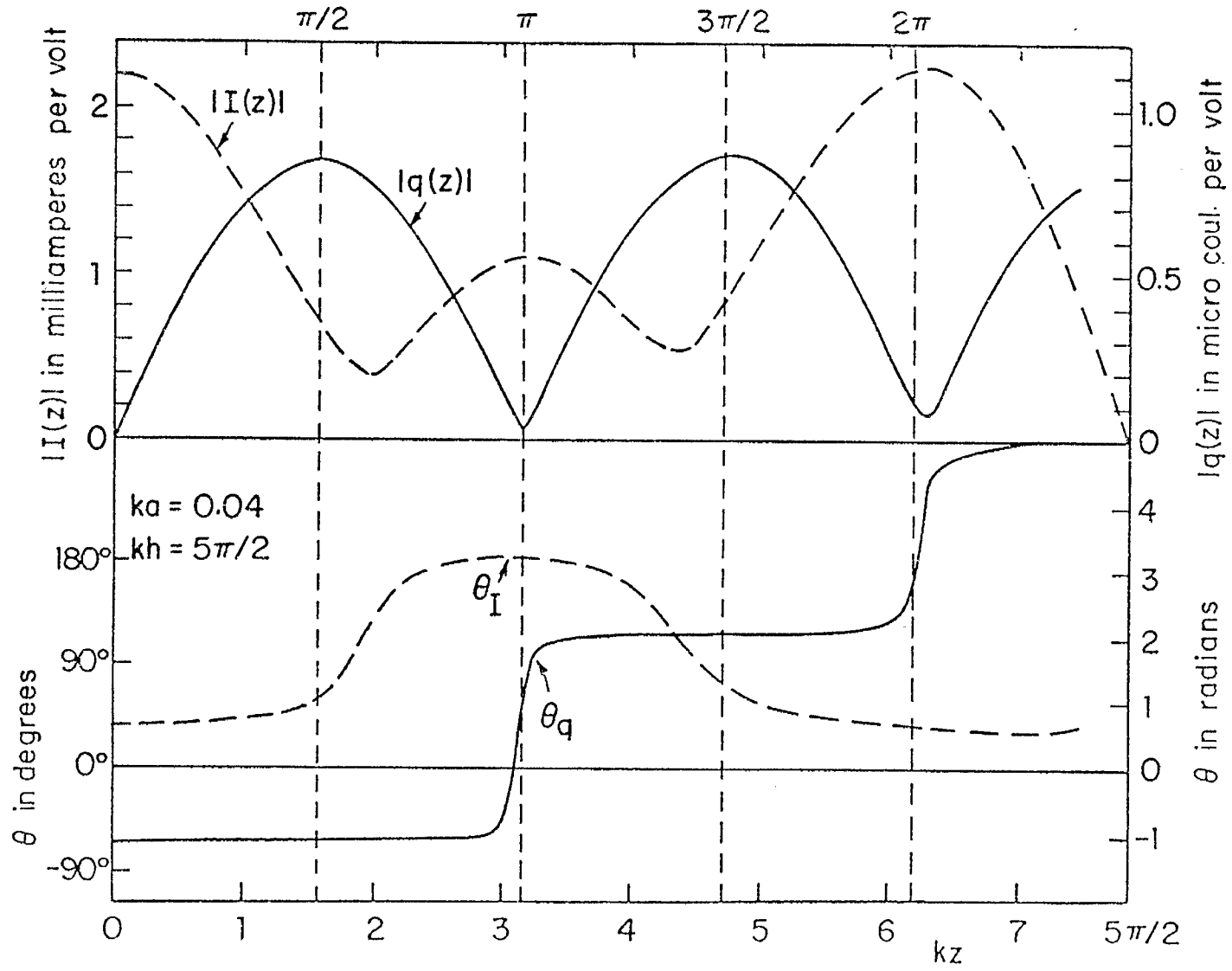

Fig. 6. Theoretical distributions of current and charge per unit length in parasitic antenna in normally incident, plane-wave field; h = 5λ/4.

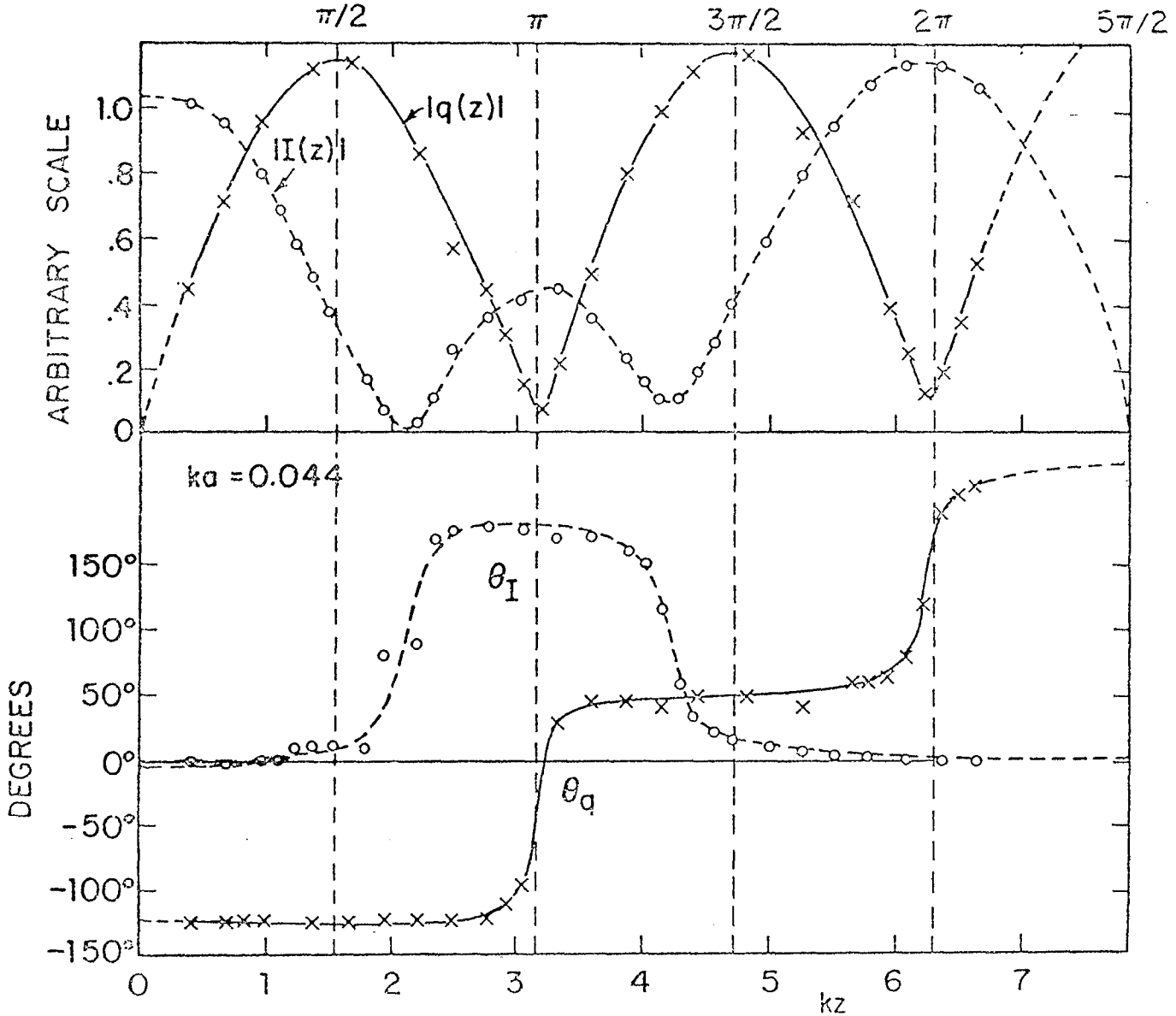

Fig. 7. Measured distributions of current and charge per unit length in parasitic antenna in normally incident, plane-wave field; h = 5λ/4.

shown in Fig. 8 for six lengths. They are seen to be essentially vertically displaced cosine curves. The constant value corresponding to the shift is the forced current, the superimposed oscillation is the resonant current. For the resonant lengths (kh = $5\pi/2$ and $7\pi/2$ in Fig. 8) a useful, very simple representation is

$$I(z)/\lambda E_z^{inc} \doteq Ae(kz) + A_r \cos kz \tag{3.7}$$

where $A = A_R + iA_I$ is approximately the complex amplitude of the current induced in the wire when infinitely long, and $A_r = A_{rR} + iA_{rI}$ is the complex amplitude of the resonant part of the current. The function e(kz) is shown graphically in Fig. 9. It is equal to one for all values of kz to within a quarter wavelength of each end where it decreases smoothly to zero. When multiplied by the appropriate complex amplitude, e(kz) represents the forced currents. An analytical representation is

$$e(kz) = U(kz + kh - \pi/2)[1 - U(kz - kh + \pi/2)] + U(kz - kh + \pi/2)$$

$$\times \sin k(h - z) + [1 - U(kz + kh - \pi/2)]\sin k(h + z) \tag{3.8}$$

where $U(t) = 1$ when $t \geq 0$, $U(t) = 0$ when $t < 0$.

With ka = 0.04 and kh = $5\pi/2$, the currents computed from (3.1) combined with the simple form (3.7) have the values: $I(0)/\lambda E_z^{inc} = 1.69 + i1.39 = A + A_R$, $I(\pi)/\lambda E_z^{inc} = -(1.10 + i0.09) = A - A_R$, $I(2\pi)/\lambda E_z^{inc} = 1.80 + i1.35 = A + A_R$. With the average values of I(0) and $I(2\pi)$, it follows that $A = 0.32 + i0.64$ (which differs somewhat from the value $A = 0.18 + i0.53$ given in (2.8) for the infinitely long wire) and $A_r = 1.42 + i0.72$. Accordingly, for kh = $5\pi/2$,

$$I(z)/\lambda E_z^{inc} \doteq (0.32 + i0.64)e(kz) + (1.42 + i0.72)\cos kz \quad mA/V \tag{3.9}$$

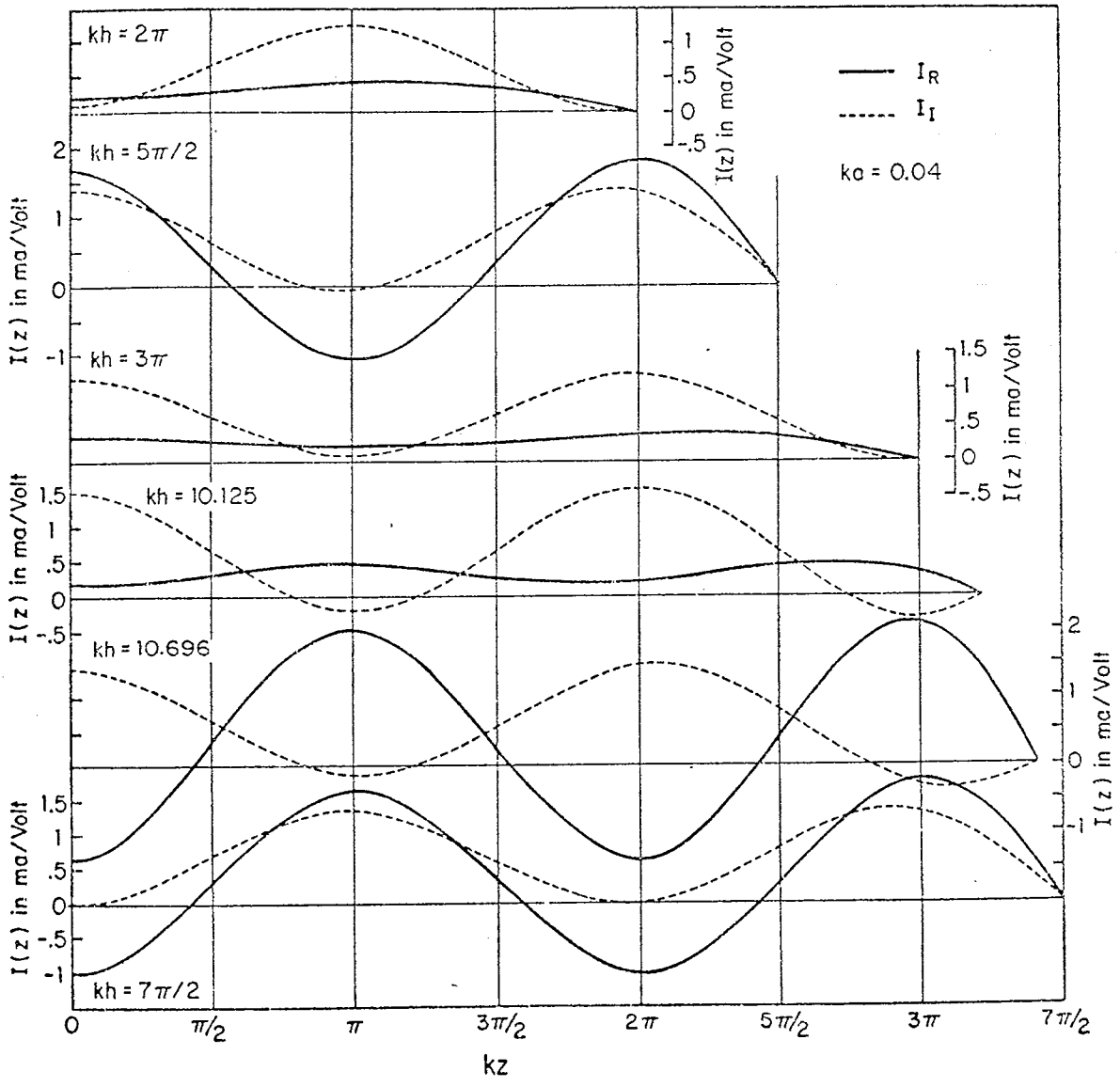

Fig. 8. Real and imaginary currents on parasitic antenna in normally incident, plane-wave field.

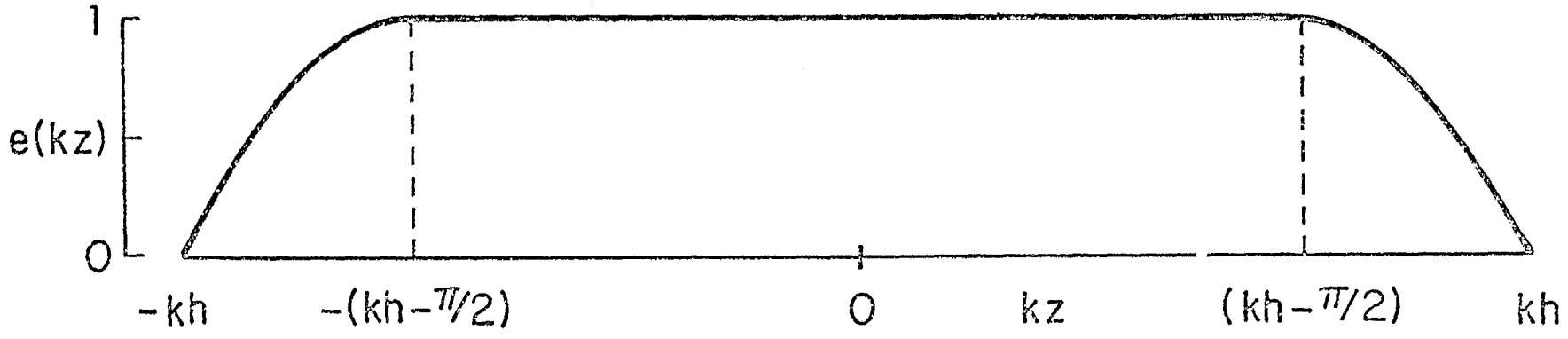

Fig. 9. The function e(kz).

The corresponding value for kh = $7\pi/2$ is

$$I(z)/\lambda E_z^{inc} \doteq (0.33 + i0.64)e(kz) - (1.36 + i0.67)\cos kz \quad mA/V \qquad (3.10)$$

The normalized associated charges per unit length are $cq(z)/\lambda E_z^{inc} \doteq -i[(0.32 + i0.64)e'(kz) + (1.42 + i0.72)\sin kz]$ for kh = $5\pi/2$ and $cq(z)/\lambda E_z^{inc} \doteq -i[(0.33 + i0.64)e'(kz) + (1.36 + i0.67)\sin kz]$ for kh = $7\pi/2$. In these formulas, $c = 3 \times 10^8$ m/sec.

The simple approximate representation (3.7) for resonant lengths is readily generalized to other lengths. The appropriate formula is

$$I(z)/\lambda E_z^{inc} = (A + A_r \cos kh)e(kz) + A_r(\cos kz - \cos kh) \qquad (3.11)$$

Thus, for the antiresonant length kh = 3π with ka = 0.04, the currents calculated from (3.1) at kz = 0, π, and 2π give: $A = 0.31 + i0.65$, $A_r = -0.10 + i0.56$ so that

$$I(z)/\lambda E_z^{inc} \doteq (0.21 + i0.09)e(kz) + (0.10 + i0.56)(\cos kz + 1) \text{ mA/V} \qquad (3.12)$$

Similarly for the general length kh = 10.696 with ka = 0.04, $A = 0.32 + i0.61$, $A_r = -1.70 + i0.83$ so that with cos kh = -0.295,

$$I(z)/\lambda E_z^{inc} \doteq (0.82 + i0.36)e(kz) - (1.70 - i0.83)(\cos kz + 0.295) \text{ mA/V} \qquad (3.13)$$

The simple approximate representations in the form (3.11) in terms of a shifted forced component $(A + A_r \cos kh)e(kz)$ and a shifted resonant component $A_r(\cos kz - \cos kh)$ are quite accurate and satisfactory for many purposes.

If the scattering wire lies in the plane of the incident plane electromagnetic wave but has its axis rotated through an angle ψ from the direction of the electric vector, the entire formulation in this section is valid if $E_z^{inc} \cos \psi$ is substituted for E_z^{inc}. On the other hand, when the wave normal

is at an arbitrary angle θ with respect to the axis of the wire (instead of at $\theta = 90°$ for normal incidence), the phase of the incident wave is not constant along the wire. This more difficult problem has been analyzed for shorter lengths by King [27] and King et al. [28] and for long wires by Chen [30]. Graphs showing the real and imaginary parts of the induced current with θ as the parameter are in Figs. 10 and 11 for $kh = 0.75\pi$ and 1.9π, respectively; the magnitude of the current induced in a long wire with $kh = 4\pi$ is in Fig. 12. It is seen that the distribution is very sensitive to the angle of incidence even in antennas that are not very long. A departure from normal incidence of as little as 2° is sufficient to change the current greatly when the wire is four wavelengths long.

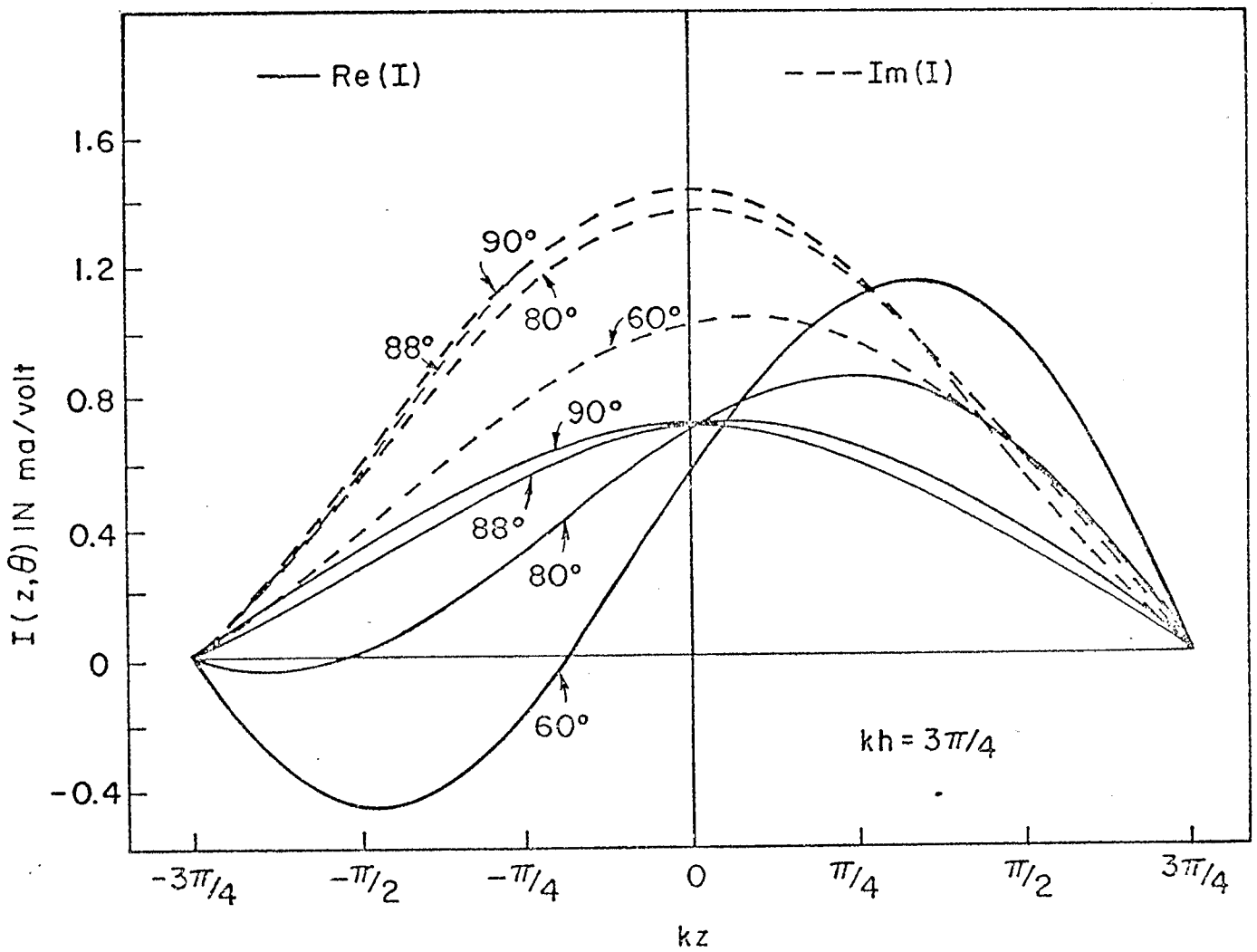

Fig. 10. Real and imaginary currents on parasitic antenna in normally incident, plane-wave field; kh = 3π/4.

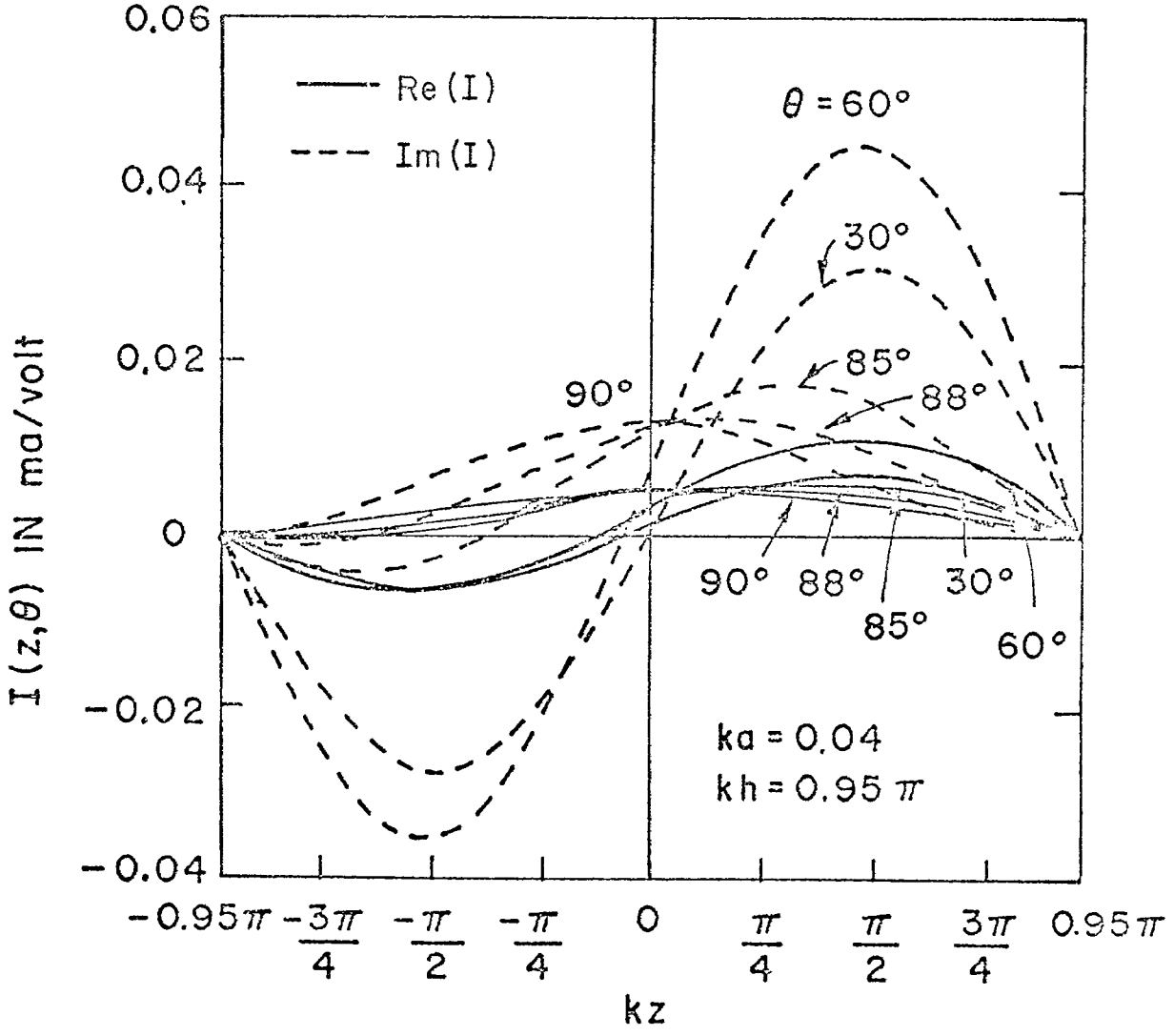

Fig. 11. Real and imaginary currents on parasitic antenna in normally incident, plane-wave field; kh = 0.95π.

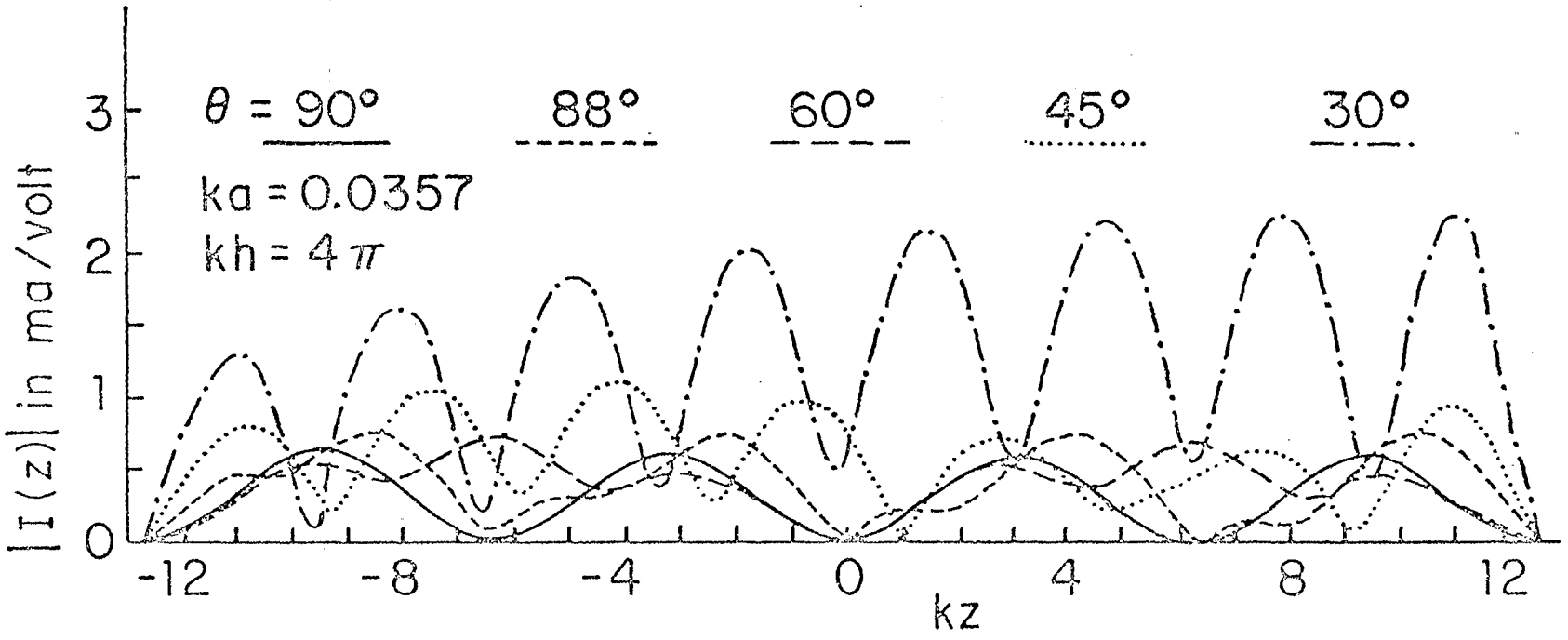

Fig. 12. Induced current in parasitic antenna. θ = 90° is normal incidence with E parallel to axis.

SECTION IV

CURRENTS AND CHARGES ON CROSSED THIN WIRES IN A PLANE-WAVE FIELD

A pair of crossed mutually perpendicular wires in a normally incident plane-wave field is shown in Fig. 13 when the incident electric field is parallel to one of the conductors. The solution when the electric vector is parallel to the other wire is obtained by a simple change in the notation. A superposition of the solutions for the two polarizations gives the solution for an arbitarily polarized, normally incident wave. The wires have equal radii a and extend from $x = -\ell_1$ to $x = \ell_2$ and from $z = -h_1$ to $z = h_2$ with the center of their junction at $x = y = z = 0$. The incident field is $E_z^{inc}(y) = E_z^{inc} e^{-jky}$ where E_z^{inc} is the value at $y = 0$ and the time dependence is $e^{j\omega t}$.

Under the action of the incident field, standing-wave distributions of charge and current are induced on the vertical conductor and these, in turn, induce distributions on the horizontal arms. Subject to the condition $ka << 1$, all transverse currents are negligible so that on the vertical conductor $\vec{K} = \hat{z}K_z$, on the horizontal conductor $\vec{K} = \hat{x}K_x$ Since the excitation is not rotationally symmetric, the induced axial surface currents and associated surface charges also depart from rotational symmetry. However, when $ka << 1$, the asymmetry is negligible and total currents and charges per unit length defined by $I_x(x) = 2\pi a K_x(x)$, $I_z(z) = 2\pi a K_z(z)$, $q(x) = 2\pi a \eta(x)$, and $q(z) = 2\pi a \eta(z)$ are good approximations. The currents and the charges per unit length are related by the equations of continuity: $\partial I_x(x)/\partial x + j\omega q(x) = 0$ and $\partial I_z(z)/\partial z + j\omega q(z) = 0$. The four sets of currents and charges per unit length are: $I_{1z}(z)$, $q_1(z)$ in the range $-h_1 \leq z \leq -a$; $I_{2z}(z)$, $q_2(z)$ in the range $a \leq z \leq h_2$; $I_{3x}(x)$, $q_3(x)$ in the range $-\ell_1 \leq x \leq -a$; and $I_{4x}(x)$, $q_4(x)$ in the range $a \leq x \leq \ell_2$. The following conditions defining electrical thinness are assumed:

$$ka << 1 \quad , \quad h_i/a >> 1 \quad , \quad \ell_i/a >> 1 \qquad i = 1, 2 \qquad (4.1)$$

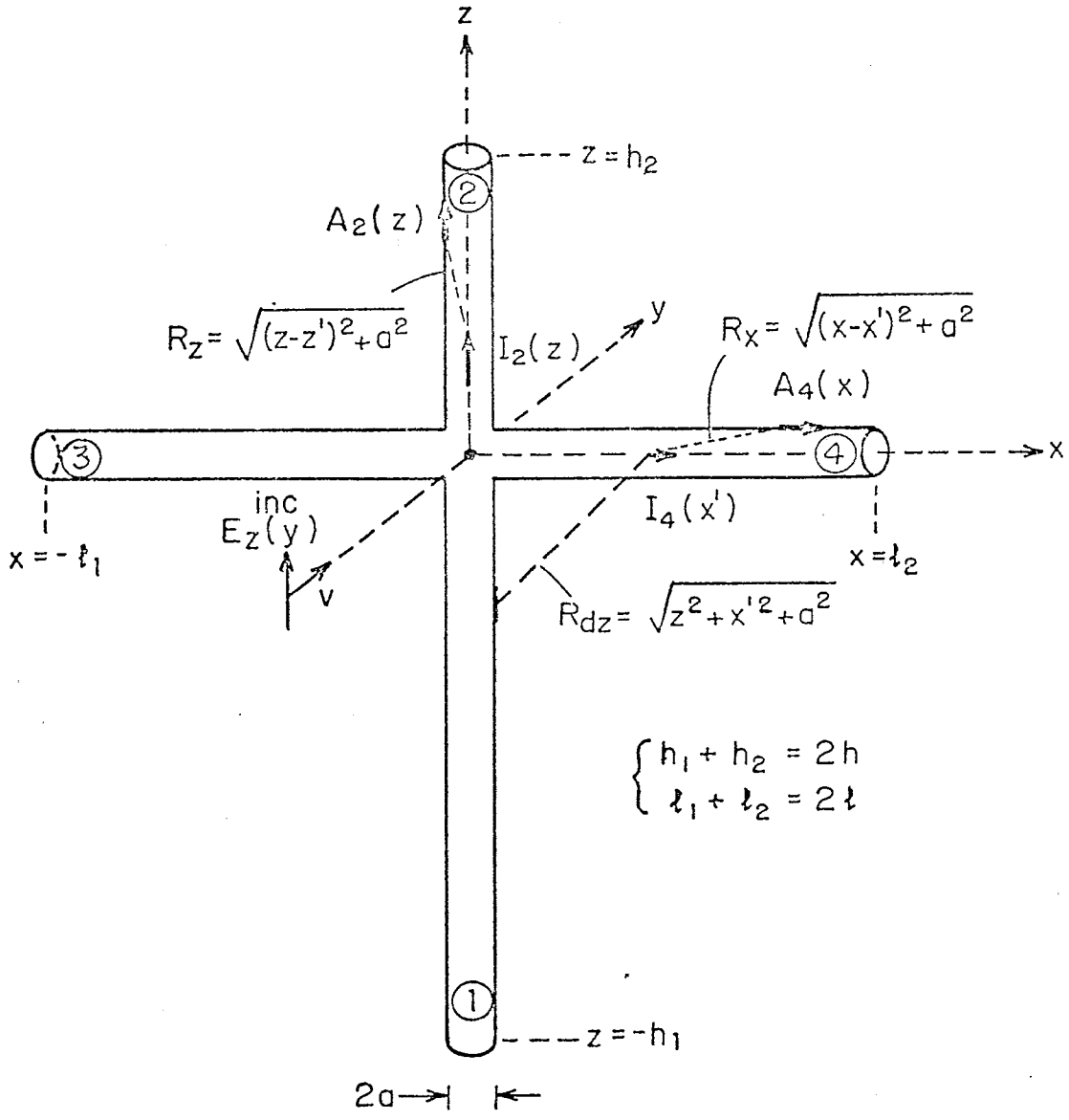

Fig. 13. Crossed wires in normally incident, plane-wave field.

At the open ends of the tubular conductors, the total currents vanish so that

$$I_{1z}(-h_1) = I_{2z}(h_2) = I_{3x}(-\ell_1) = I_{4x}(\ell_2) = 0 \tag{4.2}$$

If the boundary condition $\hat{n} \times \vec{E} = 0$ could be enforced accurately on the surfaces of the conductors including the junction region and the surface densities of current and charge determined from the conditions $\vec{K} = -\mu_0^{-1}\hat{n} \times \vec{E}$, $\eta = -\varepsilon_0 \hat{n} \cdot \vec{E}$, no additional conditions would have to be imposed. The cross would be treated as a single structure with mutual interactions correctly treated. In the approximations implicit in thin-wire theory, the condition $\hat{n} \times \vec{E} = 0$ is enforced only on the parts of the conductors that have rotationally symmetric surfaces and in a manner that assumes rotationally symmetric currents and charges. In effect, the cross is treated as four separate confluent conductors, each with two ends. The junction with its irregular surface is replaced by fictitious, rotationally symmetric extensions of the four conductors from $|x| = |z| = a$ to $|x| = |z| = 0$. These are physically unavailable since they necessarily overlap. However, the surface area of the junction region defined by $-a \leq x \leq a$, $-a \leq z \leq a$ is of the order a^2 and hence, with (4.1), electrically negligible as a chargeable surface. Thus, the substitution of the idealized extensions each of length a and with chargeable surface $2\pi a^2$ for the actual junction surface involves a negligible error and the ranges of the four conductors may be taken as $-h_1 \leq z \leq 0$, $0 \leq z \leq h_2$, $-\ell_1 \leq x \leq 0$, $0 \leq x \leq \ell_2$ in which approximately rotationally symmetric total currents and charges per unit length are defined. Thus, in conductor 1 are the current $I_1(z)$ and charge per unit length $q_1(z) = (j/\omega)[\partial I_1(z)/\partial z]$ with the condition $I_1(-h_1) = 0$. An additional condition on $I_1(z)$ as $z \to 0$ is required in order to bound $I_1(z)$. Similar conditions obtain for $I_2(z)$, $I_3(x)$,

and $I_4(x)$. The required four conditions are:

$$I_{1z}(0) - I_{2z}(0) + I_{3x}(0) - I_{4x}(0) = 0 \tag{4.3}$$

and

$$[\partial I_{1z}(z)/\partial z]_{z=0} = [\partial I_{2z}(z)/\partial z]_{z=0} = [\partial I_{3x}(x)/\partial x]_{x=0} = [\partial I_{4x}(x)/\partial x]_{x=0} \tag{4.4}$$

With the equations of continuity, (4.4) is equivalent to:

$$q_1(0) = q_2(0) = q_3(0) = q_4(0) \tag{4.5}$$

Condition (4.3) is Kirchhoff's current law. Since the junction contains no charge-separating generator and has a surface too small to permit the accumulation of significant charges, the charges per unit length on the four confluent conductors must be equal where they join. This is true when the four conductors have equal radii. The generalization of (4.5) to conductors with different radii is considered later.

Integral equations for the currents in the four conductors can be derived in the manner familiar in thin-wire theory by the imposition of the boundary conditions in terms of the scalar and vector potentials ϕ and $\vec{A}$, viz.,

$$E_z(z) = E_z^{inc} - \frac{\partial \phi(z)}{\partial z} - j\omega A_z(z) = 0 \quad ; \quad -h_1 \leq z \leq h_2 \tag{4.6}$$

$$E_x(x) = - \frac{\partial \phi(x)}{\partial x} - j\omega A_x(x) = 0 \quad ; \quad -\ell_1 \leq x \leq \ell_2 \tag{4.7}$$

on the surfaces of the crossed conductors. When the explicit integrals [10] are inserted in (4.6) and (4.7), the following simultaneous integral equations are obtained for the currents [10]:

$$\int_{-h_1}^{h_2} I(z')K(z,z')dz' - \frac{j\omega}{k^2}\frac{\partial}{\partial z}\left[\int_{-h_1}^{h_2} q(z')K(z,z')dz' + \int_{-\ell_1}^{\ell_2} q(x')K(z,x')dx'\right]$$

[continued]

$$= -\frac{j4\pi}{\omega\mu} E_z^{inc} \tag{4.8}$$

$$\int_{-\ell_1}^{\ell_2} I(x')K(x,x')dx' - \frac{j\omega}{k^2}\frac{\partial}{\partial x}\left[\int_{-\ell_1}^{\ell_2} q(x')K(x,x')dx' + \int_{-h_1}^{h_2} q(z')K(x,z')dz'\right] = 0 \tag{4.9}$$

where $K(z,z') = \exp(-jkR_z)/R_z$ with $R_z = [(z - z')^2 + a^2]^{1/2}$ and $K(z,x') = \exp(-jkR_{cz})/R_{cz}$ with $R_{cz} = [z^2 + x'^2 + a^2]^{1/2}$. These equations have been solved by iteration for the four currents subject to the conditions (4.3) and (4.4) and the four distributions of charge per unit length have been obtained with the equations of continuity. Explicit formulas are available [10] in zero- and first-order approximations. Graphs of first-order currents and charges per unit length have been computed for numerous special cases [10].

In the simplest special case, the junction is at the center of the vertical element so that $h_1 = h_2 = h/2$, the horizontal element is in the neutral plane, and no currents or charges are induced in it. The currents and charges on the vertical conductor are the same as in the absence of the horizontal member. The theoretically determined currents are illustrated in Fig. 14 for the antiresonant length $h_1 + h_2 = h = \lambda$. They have the typical antiresonant form with the resonant components only slightly greater than the forced ones. A comparison with the top graph in Fig. 8 shows agreement between the two quite different mathematical formulations.

In order to understand the distributions of current and charge per unit length on crossed thin wires with different lengths and locations of the junction, it is useful to take note of the forces acting on the charges in the several members. The primary exciting force is the incident electric field which acts uniformly along the vertical conductor to excite the forced part of $I_z(z)$. Since the conductor is finite in length, the alternating induced current locates periodically reversing charges near the ends which, in

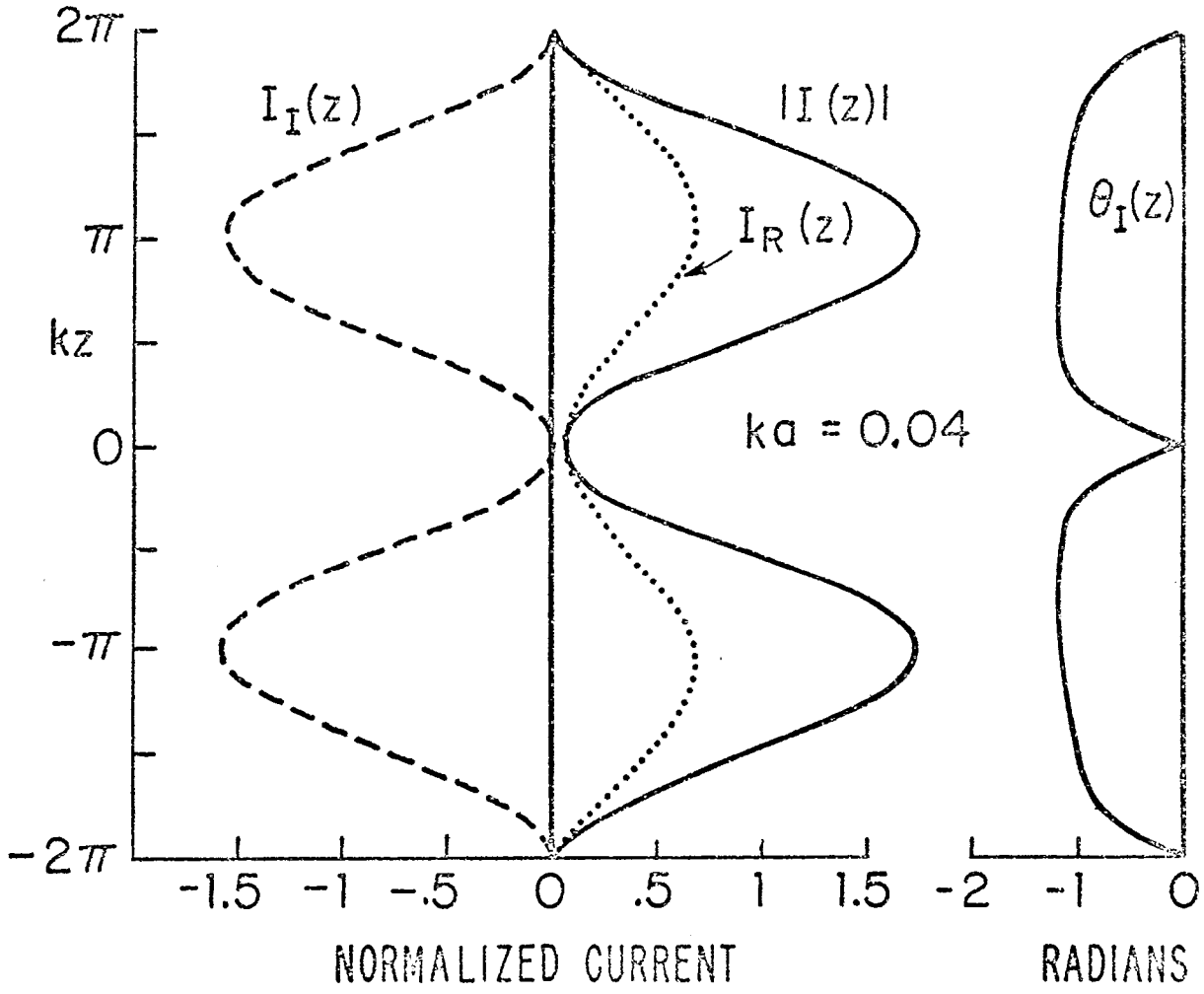

Fig. 14. Current on parasitic antenna (King-Wu theory).

turn, excite resonant currents in varying proportions that depend on the length of the several possible circuits. Since the horizontal members are perpendicular to the vertical ones, there is no inductive coupling between them. On the other hand, there is capacitive coupling among the confluent conductors near the junction and this is greatest when the standing-wave patterns on the vertical and horizontal wires locate charge maxima at the junction. It is smallest when there is a charge minimum at the junction. A standing-wave pattern in the vertical conductor that locates a maximum of $q(z)$ near the junction excites a corresponding $q(x)$ in the horizontal members. Note that, whereas E_z^{inc} acts equally and instantaneously unidirectionally along the vertical conductor, the electric fields due to a positive charge near the junction are directed outward along all four conductors. Thus, the currents induced in the two horizontal members must always be oppositely directed. There are six distinct circuits with possibly different resonant frequencies. These have the following, generally different lengths: $h_1 + h_2$, $h_1 + \ell_1$, $h_1 + \ell_2$, $\ell_1 + \ell_2$, $\ell_1 + h_2$ and $\ell_2 + h_2$. The degree in which a resonant current is excited in any one of these circuits depends on the amplitude of the exciting field and the tuning of the circuit. Forced currents are excited by the incident field only in the vertical members. Possible, theoretically evaluated distributions are shown in Figs. 15 through 17. Other examples are in the literature [11].

In Fig. 15 are shown the currents and charges per unit length on the four arms of a cross in which the six possible circuits have the following lengths: $h_1 + h_2 = h_1 + \ell_1 = h_1 + \ell_2 = 3\lambda/2$, $\ell_1 + \ell_2 = \ell_1 + h_2 = h_2 + \ell_2 = \lambda/2$. In the E-polarized, normally incident field all the circuits except $\ell_1 + \ell_2$ are resonant. This last is not excited because of symmetry - the currents in ℓ_1 and ℓ_2 must be equal and opposite. Furthermore, the junction is located

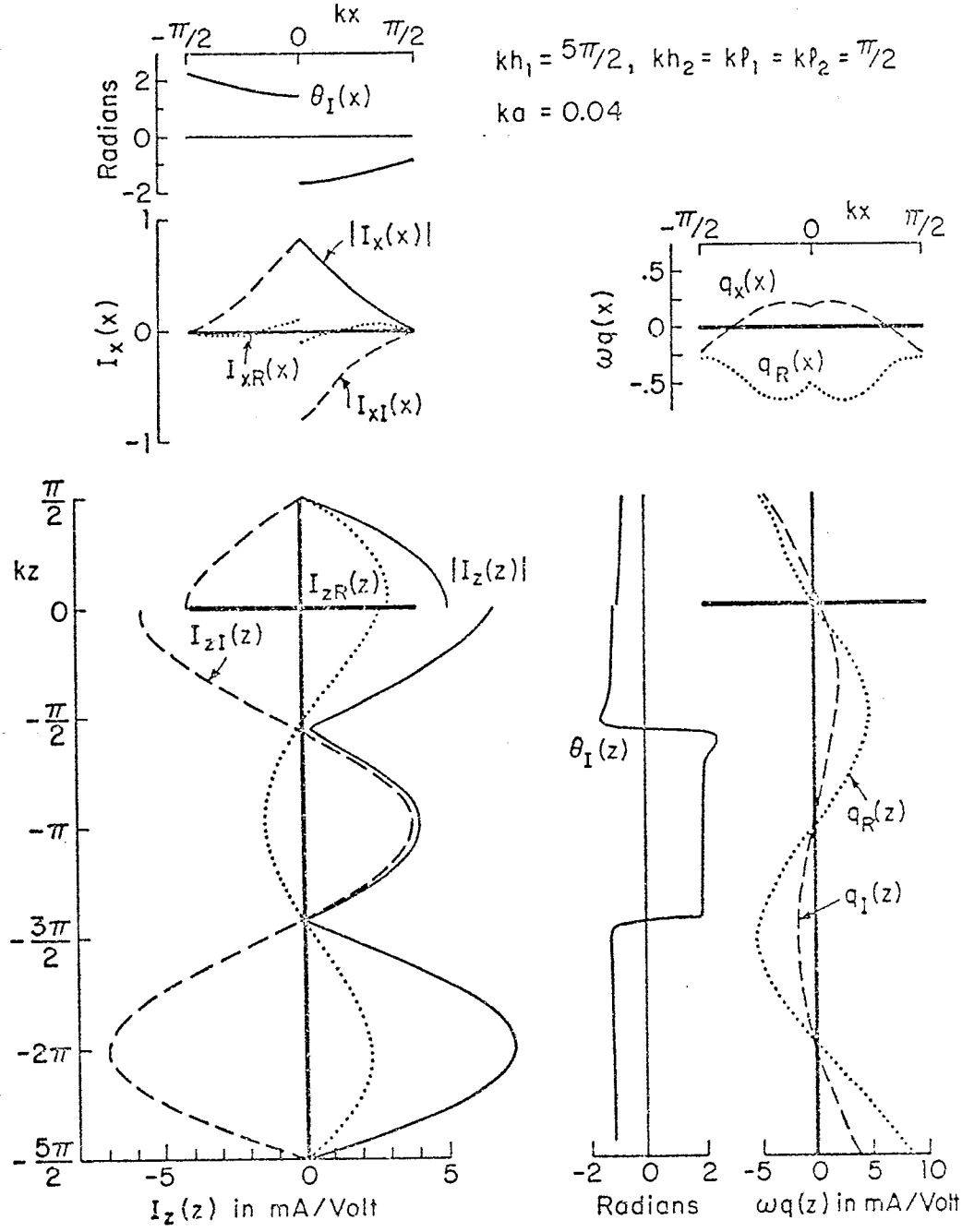

Fig. 15. Theoretical distributions of current and charge per unit length on crossed antenna in normally incident, plane-wave field; $kh_1 = 5\pi/2$, $kh_2 = k\ell_1 = k\ell_2 = \pi/2$.

at a current maximum and charge minimum in each of the five possible standing-wave patterns. The calculated current in the vertical sections is seen to be similar to the current in the absence of the horizontal arms (see Fig. 1 in [19]), i.e., a forced component of the type shown in Fig. 14 with a superimposed resonant current with approximately equal amplitude. In this case there is a discontinuity at the junction where the current from the lower member entering the upper member is reduced by an amount equal to the sum of the currents entering the horizontal arms. However, these last are relatively small since there is no inductive coupling between the mutually perpendicular elements and capacitive coupling among the four ends at and near the junction is small with a charge minimum in all of the standing-wave patterns located at the junction.

In Fig. 16 the six circuits have the following lengths: $h_1 + h_2 = h_1 + \ell_1 = h_1 + \ell_2 = 2\lambda$, $\ell_1 + \ell_2 = \ell_1 + h_2 = h_2 + \ell_2 = \lambda$. The circuit $h_1 + h_2$ is antiresonant in the normally incident field with a maximum of current and a minimum of the associated charge per unit length at the junction. The circuits $\ell_1 + \ell_2$, $\ell_1 + h_2$, $h_2 + \ell_2$, $h_1 + \ell_1$ and $h_1 + \ell_2$ are individually resonant with equal and opposite currents in ℓ_1 and ℓ_2. These have minima at the junction. The associated charges per unit length have maxima at the junction. In Fig. 17 the lengths of the circuits are: $h_1 + h_2 = 3\lambda$, $h_1 + \ell_1 = h_1 + \ell_2 = 5\lambda/2$, $\ell_1 + \ell_2 = \ell_1 + h_2 = h_2 + \ell_2 = \lambda$. The length $h_1 + h_2$ is again antiresonant but this time with a minimum of current at the junction. Nevertheless, the associated charge per unit length also has a minimum at the junction. The circuit $\ell_1 + \ell_2$ is again resonant with equal and opposite currents in ℓ_1 and ℓ_2 and a maximum of associated charge per unit length at the junction. The circuits $\ell_1 + h_2$, $h_2 + \ell_2$, $h_1 + \ell_1$ and $h_1 + \ell_2$ combine antiresonant properties in the vertical member with respect to the normally incident field and

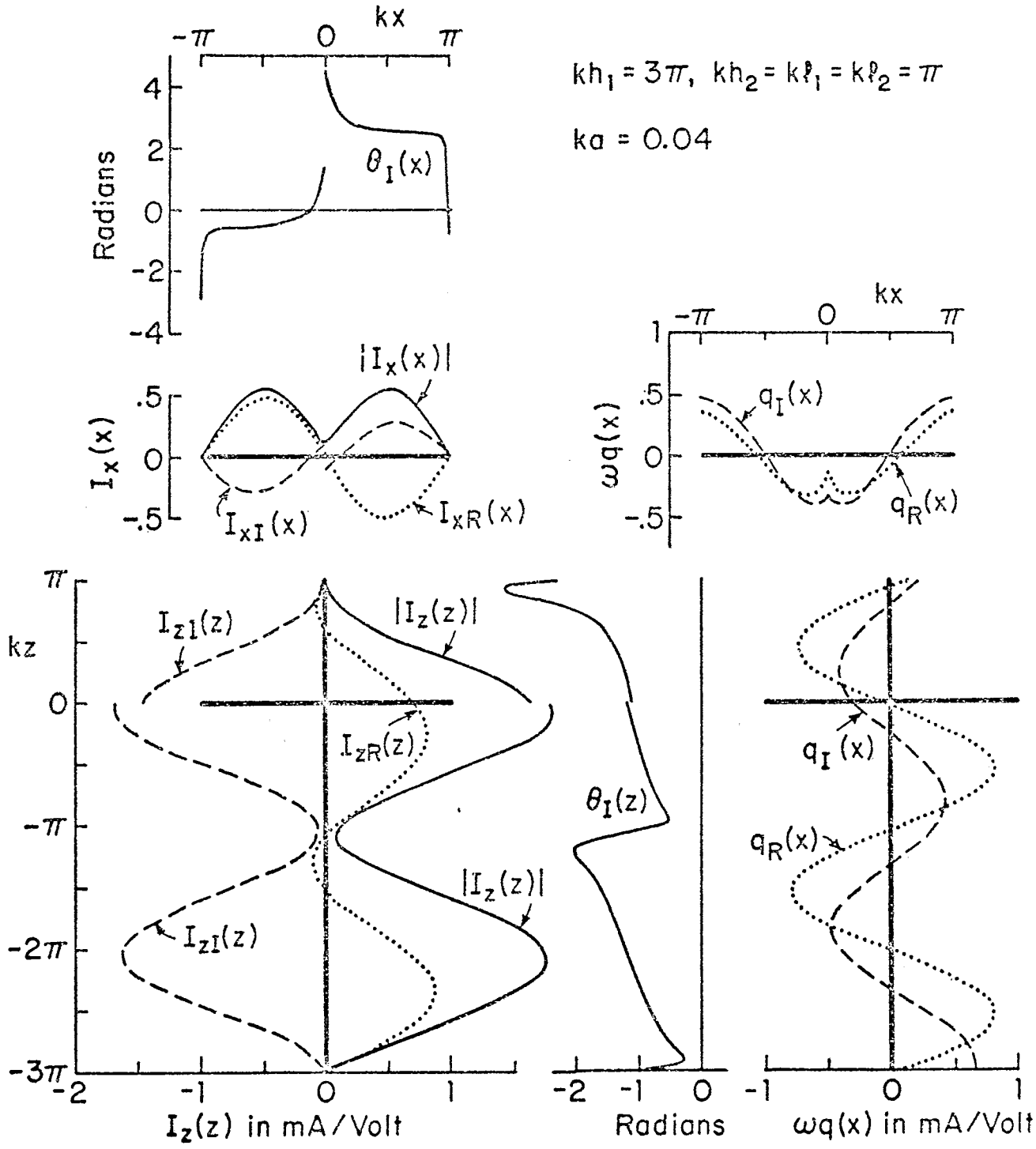

Fig. 16. Theoretical distributions of current and charge per unit length on crossed antenna in normally incident, plane-wave field; $kh_1 = 3\pi$, $kh_2 = k\ell_1 = k\ell_2 = \pi$.

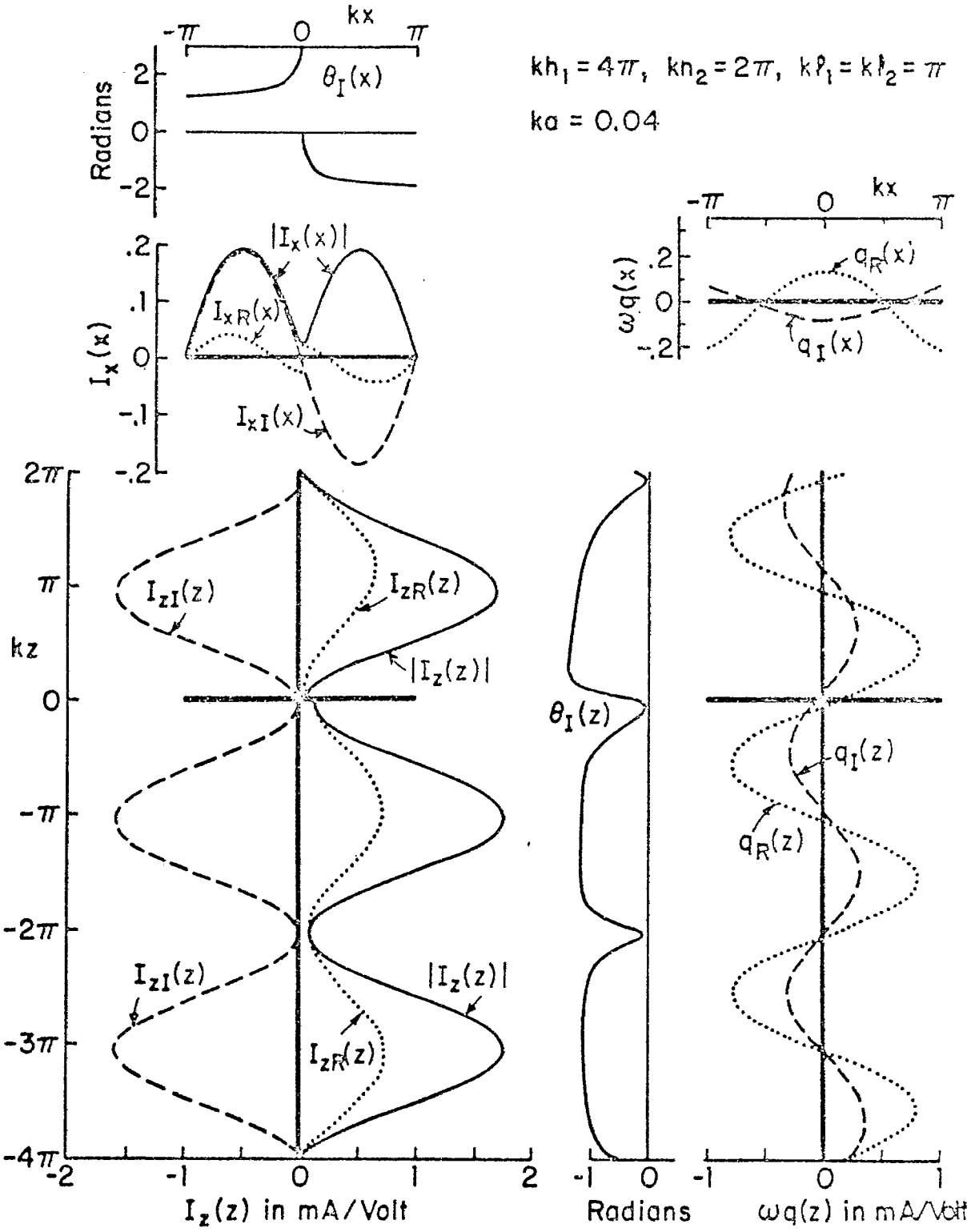

Fig. 17. Theoretical distributions of current and charge per unit length on crossed antenna in normally incident, plane-wave field; $kh_1 = 4\pi$, $kh_2 = 2\pi$, $k\ell_1 = k\ell_2 = \pi$.

resonant properties in the horizontal members with respect to the capacitive coupling near the junction. The currents in the horizontal members are relatively small because the primary oscillation in the vertical conductors (with the typical antiresonant current with nearly equal forced and resonant components) has a minimum of charge at the junction with a correspondingly small excitation of all modes that are related to the equal and opposite currents in the horizontal members.

In Fig. 18 the circuits have the lengths: $h_1 + h_2 = h_1 + \ell_1 = h_1 + \ell_2 = 5\lambda/2$, $\ell_1 + \ell_2 = \ell_1 + h_2 = h_2 + \ell_2 = \lambda$. The circuit $h_1 + h_2$ is resonant in the normally incident field. The current consists of a resonant part approximately equal to the forced component in amplitude. It has a minimum at the junction while the associated charge per unit length has a maximum there. The circuit $\ell_1 + \ell_2$ is resonant with equal and opposite currents in ℓ_1 and ℓ_2 and a maximum of the associated charges per unit length at the junction. The circuits $\ell_1 + h_2$, $h_2 + \ell_2$, $h_1 + \ell_1$ and $h_1 + \ell_2$ combine antiresonant properties in the vertical conductors with respect to the normally incident field and resonant properties in the horizontal members with respect to the capacitive coupling near the junction. Since the oscillations in both $h_1 + h_2$ and $\ell_1 + \ell_2$ locate maxima of charges per unit length at the junction, the two modes are closely coupled and the currents in the horizontal arms are comparable in magnitude with those in the vertical sections. The currents in the vertical members are superpositions of comparable resonant and antiresonant distributions. The real parts have relatively large resonant components, the imaginary parts only small resonant components superimposed on the forced currents.

It is seen from these relatively simple crossed wires that the distributions of current and charge are quite complicated. This complication in-

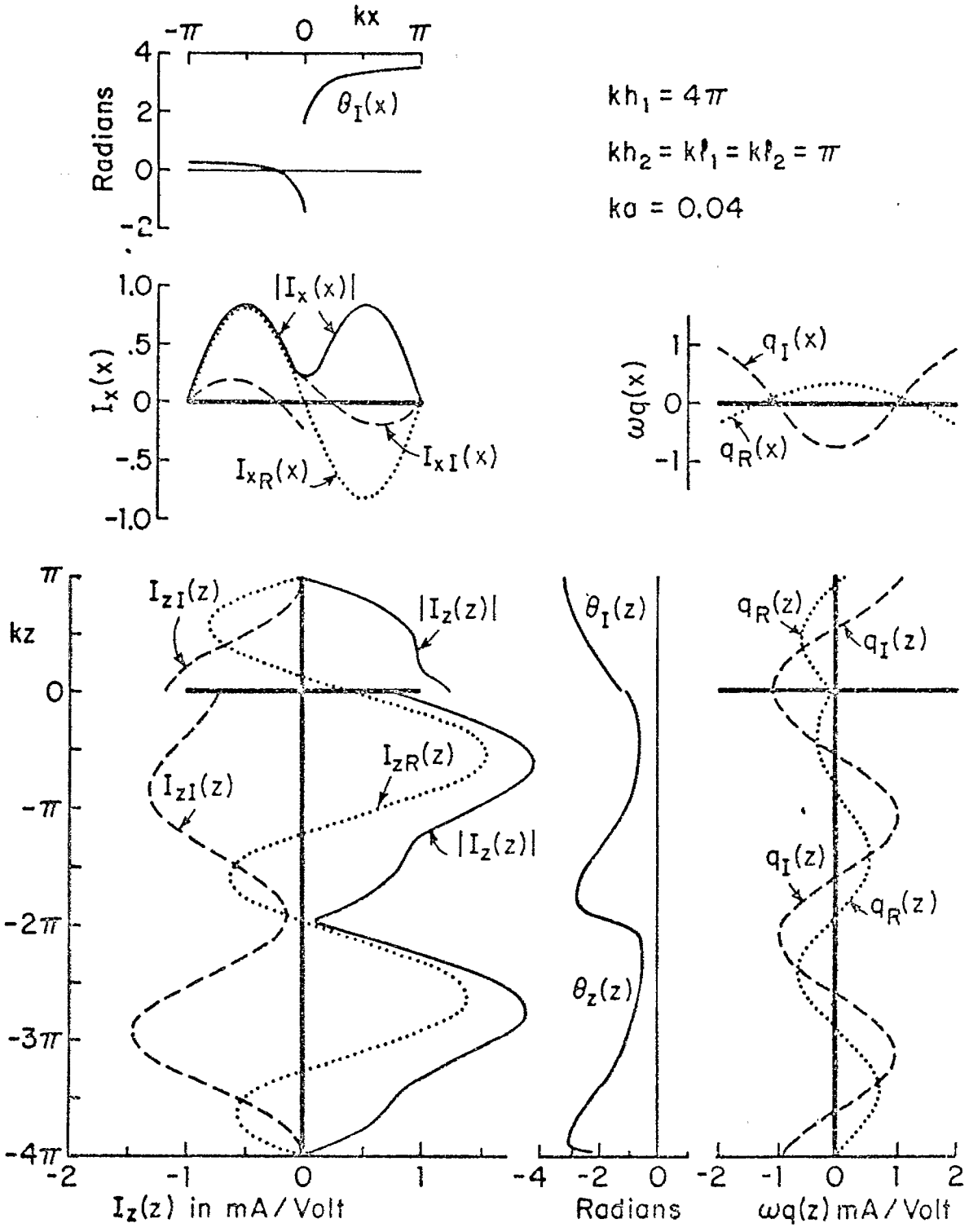

Fig. 18. Theoretical distributions of current and charge per unit length on crossed antenna in normally incident, plane-wave field; $kh_1 = 4\pi$, $kh_2 = k\ell_1 = k\ell_2 = \pi$.

creases when the lengths of the four arms are all different and not simple multiples of a quarter wavelength. An example is in Fig. 7 of [19].

Direct experimental confirmation of the theoretically evaluated currents and charges on the thin-wire cross has not been carried out because intricate movable probes without external cables are required. However, closely related measurements have been made on crossed wires erected on a metal ground plane [20] with a probe system controlled from below through the lower vertical member. With the associated image these crossed wires correspond to an isolated structure with a vertical section of double length, $2(h_1 + h_2)$, and two identical horizontal sections each with arms of length ℓ_1 and ℓ_2 located at equal distances h_2 from the ends of the vertical conductor. This is a more complicated structure than the single cross since it involves two junctions and the coupling between the two horizontal members. It provides nine possible resonant circuits instead of six and correspondingly more intricate superpositions of currents. These circuits have the following, generally different lengths: $h_2 + \ell_1$, $h_2 + \ell_2$, $h_2 + 2h_1 + \ell_1$, $h_2 + 2h_1 + \ell_2$, $2(h_2 + h_1)$, $2(\ell_1 + h_1)$, $2(\ell_2 + h_1)$, $\ell_1 + 2h_1 + \ell_2$ and $\ell_1 + \ell_2$. However, under special conditions the currents in the upper half of the symmetrical double cross can be made to resemble those in the single cross. Specifically, with $2(h_1 + h_2) = h_2 + 2h_1 + \ell_1 = h_2 + 2h_1 + \ell_2 = 3\lambda/2$, $\ell_1 + \ell_2 = \ell_1 + h_2 = h_2 + \ell_2 = \lambda/2$, conditions resembling those in Fig. 15 are obtained. Except for the presence of the lower (image) cross, the circuits are the same. The measured currents and charges per unit length on the half above the ground plane are shown in Fig. 19. They are seen to agree quite well with the currents and charges on the section of Fig. 15 above the center of the vertical conductor. Similarly with $2(h_1 + h_2) = h_2 + 2h_1 + \ell_1 = h_2 + 2h_1 + \ell_2 = 5\lambda/2$, $\ell_1 + \ell_2 = \ell_1 + h_2 = h_2 + \ell_2 = \lambda$, the measured currents and charges per unit length above the

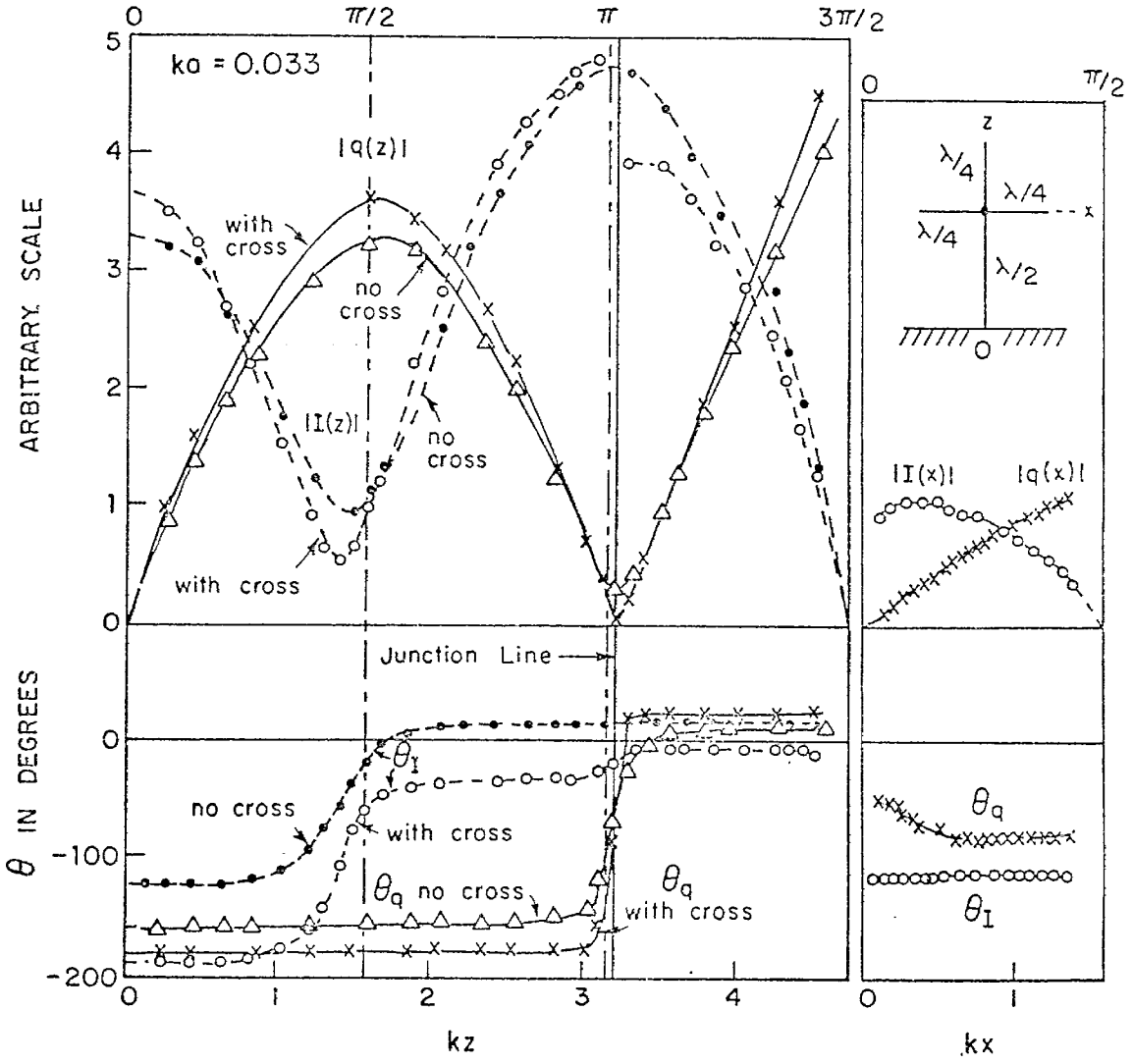

Fig. 19. Measured distributions of current and charge per unit length on antenna with and without cross in normally incident, plane-wave field. Junction at maximum current, minimum charge.

ground plane are those shown in Fig. 20. These are in good general agreement with those in Fig. 18 above the center of the vertical conductor. Note that the measured charges on the four conductors in Figs. 19 and 20 approach the same values at the common junction in agreement with the boundary condition (4.5) and the theoretical graphs. The condition (4.2) on the currents is also satisfied.

The extension of the theory to crossed electrically thin conductors when these lie in the same plane but the angles at the junction are not all 90° is straightforward but has not been carried out. In general, there is both inductive and capacitive coupling between each pair of confluent elements and the simultaneous integral equations involve more complicated kernels. The condition at the junction remains the same so long as the angle θ between any pair of elements is not too small; the condition $ka \ll 1$ must be generalized to $|ka \sin(\theta/2)| \ll 1$.

When the conductors do not have a common radius a, the condition (4.5) at the junction must be replaced with [11]

$$q_1(0)\psi_1 = q_2(0)\psi_2 = q_3(0)\psi_3 = q_4(0)\psi_4 \tag{4.10}$$

where

$$\psi_i = 2[\ell n(2/ka_i) - c] \quad , \quad s_i \geq \lambda/4 \tag{4.11}$$

$$\psi_i = 2\ \ell n(2s_i/a_i) \quad , \quad s_i < \lambda/4 \tag{4.12}$$

and where s stands for h or ℓ, i = 1, 2, 3 or 4, and $c = \ell n\ \gamma = 0.577$ is Euler's constant. The integral equations also become more involved since different values of a occur in the different ranges of integration. Specifically, $a = a_1$ in the range from $z = 0$ to $z = -h_1$, etc.

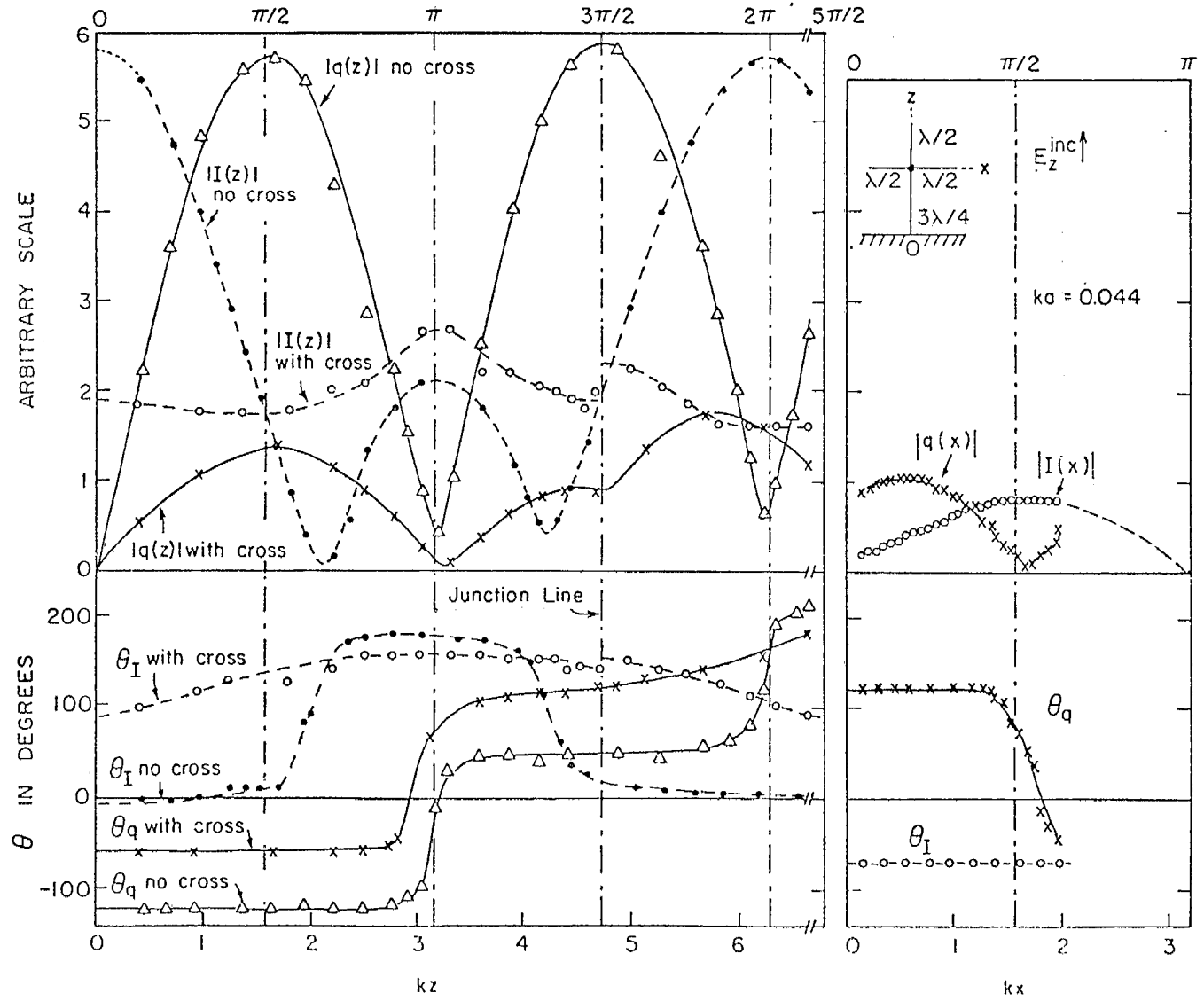

Fig. 20. Measured distributions of current and charge per unit length on antenna with and without cross in normally incident, plane-wave field. Junction at maximum of charge.

SECTION V

THEORY OF THE TUBULAR CYLINDER OF FINITE LENGTH

When the circular cylinder shown in Fig. 1 is finite in length and unrestricted in radius, the analytical determination of the distributions of current and charge induced on its surface by an incident plane wave is three-dimensional. In order to simplify the analysis the cylinder is idealized to be an infinitely thin-walled, perfectly conducting tube extending from $z = -h$ to $z = h$ with the inside radius a_- and the outside radius a_+, both sensibly equal to a. The induced currents and charges are, therefore, in a single thin layer at $\rho = a$. When the field is normally incident and E-polarized, the forced currents are axially directed as when the cylinder is infinitely long. In reversing their direction periodically they must satisfy the condition $K_z(\theta,z) = 0$ at $z = \pm h$. This requires the presence of concentrations of surface charge $\eta(\theta,z)$ with periodically reversing sign at and near the edges at $|z| = h$. The sign of the charge density near $z = h$ is opposite to that near $z = -h$. These charges act to excite standing-wave distributions of current and charge between them. Since the induced forced current and the associated charge concentrations near the ends are not rotationally symmetric, the currents they excite must have both axial and transverse components. Unlike the infinite cylinder which has only z-directed currents and remains uncharged in an E-polarized field, the finite cylinder supports surface densities of both charge and transverse current in addition to the axial current. Similarly, in an H-polarized field the axial distribution of charge associated with the forced transverse currents is not uniform near the ends of the tube so that axially directed currents are generated and combined with the transverse currents induced by the incident field. Thus, on a finite cylinder there are distributions of $K_z(\theta,z)$, $K_\theta(\theta,z)$ and $\eta(\theta,z)$ with either E- or H-polarization.

The determination of these currents and charges by Kao [14]-[17] involves the solution of integral equations obtained from the boundary condition $E_{tang} = 0$ on the surface of the cylinder. The first step in the formulation is the expansion of the incident field in a Fourier series of the form

$$E_p^{inc}(\rho,\theta) = \sum_{n=0}^{\infty} E_p^{inc}(\rho|n)\cos n\theta \tag{5.1}$$

where $p = z$ for the E-polarization, and $p = \theta$ for the H-polarization. The n^{th}-order Fourier coefficients in (5.1) are

$$E_z^{inc}(\rho|n) = \epsilon_n i^n J_n(k\rho) \quad ; \quad E_\theta^{inc}(\rho|n) = \epsilon_n i^{n-1} J_n'(k\rho) \tag{5.2}$$

where $\epsilon_n = 1$ for $n = 0$ and $\epsilon_n = 2$ for $n > 0$; $J_n(k\rho)$ is the Bessel function and $J_n'(k\rho)$ its derivative with respect to the argument. Further steps in the analysis include the expansion of all functions of θ in Fourier series and the separate treatment of each Fourier component as due to an incident wave of the form $e^{in\theta}$. The formation of Fourier transforms with respect to the axial variable z permits the expression of both the ρ and θ components of the electromagnetic field in terms of the axially directed components $\bar{E}_z$ and $\bar{B}_z$. These, in turn, satisfy the Bessel equation in the radial variable ρ, viz.,

$$[(\partial^2/\partial\rho^2) + \rho^{-1}(\partial/\partial\rho) - (n^2/\rho^2) + \xi^2]\bar{f}(\rho,\zeta|n) = 0 \tag{5.3}$$

where $\xi^2 = k^2 - \zeta^2$, ζ is the transform variable, and $\bar{f}(\rho,\zeta|n)$ is the Fourier transform of the axial components of the scattered field $\bar{E}_z^s(\rho,\zeta|n)$ or $\bar{B}_z^s(\rho,\zeta|n)$. In order to express them in terms of the current on the tube, use is made of the following boundary conditions which require the continuity of the tangential electric field and the discontinuity of the tangential magnetic field:

$$\bar{E}_p^s(a_+,\zeta|n) = \bar{E}_p^s(a_-,\zeta|n) \tag{5.4a}$$

$$\bar{B}_p^s(a_+,\zeta|n) - \bar{B}_p^s(a_-,\zeta|n) = \pm\mu_0\bar{K}_p(\zeta|n) \tag{5.4b}$$

where p = z with the upper sign and p = θ with the lower sign. $\bar{K}_p(\zeta|n)$ is the transform of the current density in the tube. Since $\bar{E}_z^{inc}$ and $\bar{B}_z^{inc}$ are both continuous at ρ = a, it is correct to impose the boundary conditions (5.4a,b) on the scattered field. The expressions for $\bar{E}_z^s(\rho,\zeta|n)$ and $\bar{B}_z^s(\rho,\zeta|n)$ can be used to obtain formulas for $\bar{E}_z^s(a,\zeta|n)$ and $\bar{E}_\theta^s(a,\zeta|n)$ on the surface of the cylinder, ρ = a, $|z| \leq h$. With $\zeta = i\partial/\partial z$, the inverse Fourier transforms of $\bar{E}_z^s(a,\zeta|n)$ and $\bar{B}_z^s(a,\zeta|n)$ lead to two differential equations with respect to z. With the help of a common factor, the solutions of these equations can be combined and used to satisfy the boundary condition requiring the vanishing of the tangential component of the total electric field on the surface of the cylinder. This results in two integral equations for the Fourier components $K_\theta(z|n)$ and $K_z(z|n)$ of the transverse and axial currents. For normal incidence with E-polarization they are:

$$2\int_0^{kh} G_\theta(u,u'|n)K_\theta(u'|n)du' = \pm ink^{-1}a^{-1}C\sin u + C_\theta(n) \tag{5.5}$$

$$2\int_0^{kh} G_z(u,u'|n)K_z(u'|n)du' + 2nk^{-1}a^{-1}\int_0^{kh} G_{z\theta}(u,u'|n)K_\theta(u'|n)du' = C\cos u + C_z(n) \tag{5.6}$$

(The equations for H-polarization are the same but with sin u replaced by $-\cos u$ and cos u replaced by sin u.) The constant C is determined from the condition $K_z(u|n) = 0$ at u = kh. For E-polarization, $C_z(n) = -4\varepsilon_n i^n(\zeta_0 ka)^{-1} \times J_n(ka)$, $C_\theta(n) = 0$; for H-polarization $C_z(n) = 0$, $C_\theta(n) = -4\varepsilon_n i^{n-1}(\zeta_0 ka)^{-1} \times J_n'(ka)$. The kernels are $G_\theta(u,u'|n) = 2(\zeta_0 k^2 a)^{-1}[M_\theta(u-u'|n) \mp M_\theta(u+u'|n)$, $G_z(u,u'|n) = 2(\zeta_0 a)^{-1}[M_z(u-u'|n) \pm M_z(u+u'|n)]$, $G_{z\theta}(u,u'|n) = 2k(n\zeta_0)^{-1} \times$

$[M_{z\theta}(u - u'|n) \mp M_{z\theta}(u + u'|n)]$ where the upper signs are for E-polarization, the lower signs for H-polarization. The M's are the inverse Fourier transforms of $\bar{M}_\theta(\zeta|n) = -(\pi\omega\mu_0 a/2)J'_{|n|}(a\xi)H^{(1)'}_{|n|}(a\xi)$, $\bar{M}_z(\zeta|n) = -(\pi a/2\omega\epsilon_0)J_{|n|}(a\xi) \times H^{(1)}_{|n|}(a\xi)$, $\bar{M}_{z\theta}(\zeta|n) = (n\pi\zeta/2\omega\epsilon_0\xi^2)J_{|n|}(a\xi)H^{(1)}_{|n|}(a\xi)$ with $\xi^2 = k^2 - \zeta^2$. The n^{th}-order Fourier component of the total current was calculated by first determining $K_\theta(u|n)$ from (5.5) and using this value in (5.6) to obtain $K_z(u|n)$. The total currents for E-polarization are:

$$K_z(\theta,z) = \sum_{n=0}^{\infty} C_z(n)K_z(z|n)\cos n\theta \tag{5.7a}$$

$$K_\theta(\theta,z) = i\sum_{n=0}^{\infty} C_z(n)K_\theta(z|n)\sin n\theta \tag{5.7b}$$

For H-polarization:

$$K_z(\theta,z) = i\sum_{n=1}^{\infty} C_\theta(n)K_z(z|n)\sin n\theta \tag{5.8a}$$

$$K_\theta(\theta,z) = \sum_{n=1}^{\infty} C_\theta(n)K_\theta(z|n)\cos n\theta \tag{5.8b}$$

These series have been summed using numerically obtained solutions of (5.5) and (5.6) for the Fourier coefficients $K_\theta(u|n)$ and $K_z(u|n)$. Graphs and tables were constructed by Kao [14], [15] for ka = 1, 2 and 3, kh = 0.5π, π, and 1.5π. Kao's computer program for $K_z(\theta,z)$ and $K_\theta(\theta,z)$ has been expanded by B. Sandler to include the surface density of charge defined by

$$\eta(\theta,z) = -\frac{i}{c}\left[\frac{\partial K_z(\theta,z)}{k\,\partial z} + \frac{1}{ka}\frac{\partial K_\theta(\theta,z)}{\partial\theta}\right] \tag{5.9}$$

where $c = 3 \times 10^8$ m/sec.

With ka = 1 only a small number of terms in (5.7a,b) need be retained. Specifically, for E-polarization,

$$K_z(\theta,z) \doteq A(kz) + B(kz)\cos\theta + C(kz)\cos 2\theta + D(kz)\cos 3\theta + E(kz)\cos 4\theta + F(kz)\cos 5\theta \qquad (5.10)$$

$$K_\theta(\theta,z) \doteq i[B'(kz)\sin\theta + C'(kz)\sin 2\theta + D'(kz)\sin 3\theta] \qquad (5.11)$$

where the coefficients are given in Tables 2 and 3 for kh = 1.5π and in Tables 4 and 5 for kh = 3π. Comparison with the corresponding coefficients for the infinitely long cylinder reveals that C(kz) through F(kz) are sensibly constant at the values C through F given in Table 1 except within a quarter wavelength of the end where they decrease smoothly to zero at z = h. It is seen that E(kz), F(kz) and D'(kz) are small.

In practice, infinitely thin-walled, perfectly conducting cylinders are not available. The walls of metal tubes useful in an experiment are much thicker than the skin depth and separate currents can be identified on the outer and inner surfaces of the tube. Measurements made with probes traveling along the outside surface measure only this part of the current which does not vanish at the open ends of the tube but continues over the edge to become the entering inside current. This decays rapidly as the tube is entered if the cross-sectional size is small enough to cut off wave-guide modes as when ka = 1. Although the current density $\vec{K}(\theta,z)$ and charge density $\eta(\theta,z)$ on an infinitely thin-walled, perfectly conducting tube are not physically separable into inside and outside parts, it is possible to associate parts of the currents and charges with the fields outside and inside the walls. Specifically,

$$\vec{K}(\theta,z) = -\mu_0^{-1}\hat{\rho} \times [\vec{E}(a_+,\theta,z) - \vec{E}(a_-,\theta,z)] \equiv \vec{K}_+(\theta,z) + \vec{K}_-(\theta,z) \qquad (5.12a)$$

TABLE 2

FOURIER COEFFICIENTS IN mA/V FOR $K_z(\theta,z)$ FOR TUBULAR CYLINDER, E-POLARIZATION, kh = 1.5π, ka = 1

kz	A(kz)	B(kz)	C(kz)	D(kz)	E(kz)	F(kz)
0	0.50 + i0.20	-4.83 + i1.76	-0.17 - i2.04	0.58 - i2.13	0.00 + i0.10	0.01 + i0.00
.25π	1.02 + i0.11	-4.44 + i1.90	-0.17 - i2.04	0.58 - i2.09	0.00 + i0.10	0.01 + i0.00
.50π	2.28 - i0.13	-3.45 + i2.22	-0.16 - i2.02	0.58 - i1.97	0.00 + i0.10	0.01 + i0.00
.75π	3.52 - i0.48	-2.23 + i2.43	-0.14 - i1.99	0.58 - i1.76	0.00 + i0.10	0.01 + i0.00
1.00π	3.94 - i0.84	-1.24 + i2.26	-0.12 - i1.94	0.58 - i1.49	0.00 + i0.10	0.01 + i0.00
1.25π	3.02 - i0.96	-0.66 + i1.54	-0.08 - i1.75	0.53 - i1.12	0.00 + i0.09	0.01 + i0.00
1.50π	0	0	0	0	0	0

TABLE 3

FOURIER COEFFICIENTS IN mA/V FOR $K_\theta(\theta,z)$ FOR TUBULAR CYLINDER, E-POLARIZATION, kh = 1.5π, ka = 1

kz	B'(kz)	C'(kz)	D'(kz)
0	0.00 + i0.00	0.00 + i0.00	0.00 + i0.00
.25π	0.18 - i0.15	0.00 + i0.00	0.00 + i0.00
.50π	0.24 - i0.30	0.01 + i0.00	0.00 + i0.00
.75π	0.06 - i0.45	0.02 - i0.02	0.00 + i0.00
1.00π	-0.56 - i0.61	0.02 - i0.08	0.00 + i0.00
1.25π	-2.32 - i0.81	0.02 - i0.33	0.03 + i0.00
1.30π	-3.04 - i0.88	0.01 - i0.47	0.05 + i0.01
1.40π	-5.57 - i1.09	0.01 - i1.18	0.16 + i0.05
1.50π	∞	∞	∞

TABLE 4

FOURIER COEFFICIENTS IN mA/V FOR $K_z(\theta,z)$ FOR TUBULAR CYLINDER, E-POLARIZATION, kh = 3π, ka = 1

kz	A(kz)	B(kz)	C(kz)	D(kz)	E(kz)
0	2.89 + i0.93	-3.26 + i2.66	-0.14 - i2.03	0.58 + i0.00	0.00 + i0.10
.25π	2.70 + i0.57	-3.22 + i2.44	-0.14 - i2.03	0.58 + i0.00	0.00 + i0.10
.50π	2.21 - i0.30	-3.15 + i1.88	-0.14 - i2.03	0.58 + i0.00	0.00 + i0.10
.75π	1.70 - i1.14	-3.14 + i1.28	-0.14 - i2.04	0.58 + i0.00	0.00 + i0.10
1.00π	1.44 - i1.45	-3.26 + i0.96	-0.14 - i2.05	0.58 + i0.00	0.00 + i0.10
1.25π	1.58 - i1.01	-3.49 + i1.12	-0.15 - i2.05	0.58 + i0.00	0.00 + i0.10
1.50π	2.06 - i0.09	-3.71 + i1.70	-0.15 - i2.04	0.58 + i0.00	0.00 + i0.10
1.75π	2.65 + i0.76	-3.75 + i2.45	-0.16 - i2.03	0.58 + i0.00	0.00 + i0.10
2.00π	3.03 + i0.99	-3.48 + i3.00	-0.16 - i2.01	0.58 + i0.00	0.00 + i0.10
2.25π	2.96 + i0.40	-2.90 + i3.03	-0.15 - i1.99	0.58 + i0.00	0.00 + i0.10
2.50π	2.38 - i0.68	-2.15 + i2.44	-0.12 - i1.94	0.57 + i0.00	0.00 + i0.10
2.75π	1.42 - i1.45	-1.32 + i1.39	-0.08 - i1.75	0.53 + i0.00	0.00 + i0.09
3.00π	0	0	0	0	0

TABLE 5

FOURIER COEFFICIENTS IN mA/V FOR $K_\theta(\theta,z)$ FOR TUBULAR CYLINDER, E-POLARIZATION, kh = 3π, ka = 1

kz	B'(kz)	C'(kz)
0	0.00 + i0.00	0.00 + i0.00
.25π	-0.03 + i0.07	0.00 + i0.00
.50π	-0.04 + i0.11	0.00 + i0.00
.75π	-0.00 + i0.11	0.00 + i0.00
1.00π	0.06 + i0.05	0.00 + i0.00
1.25π	0.11 - i0.04	0.00 + i0.00
1.50π	0.11 - i0.14	0.00 + i0.00
1.75π	0.03 - i0.21	0.00 + i0.00
2.00π	-0.14 - i0.20	0.00 - i0.01
2.25π	-0.37 - i0.01	-0.02 - i0.02
2.50π	-0.65 + i0.54	-0.08 - i0.02
2.75π	-1.04 + i2.10	-0.33 - i0.03
3.00π	∞	∞

$$\eta(\theta,z) = -\varepsilon_0^{-1}\hat{\rho} \cdot [\vec{E}(a_+,\theta,z) - \vec{E}(a_-,\theta,z)] \equiv \eta_+(\theta,z) + \eta_-(\theta,z) \qquad (5.12b)$$

where the identity on the right defines the outside and inside surface densities of current and charge with subscripts + and -, respectively. The currents and charges measured on the outside surface of a metal tube with walls that are many skin depths thick must be identified with the fields outside the tube and compared with $\vec{K}_+(\theta,z)$ and $\eta_+(\theta,z)$ near the open ends where they differ significantly from $\vec{K}(\theta,z)$ and $\eta(\theta,z)$.

The numerical evaluation of the outside and inside currents was carried out by first calculating the difference current $\vec{K}_+(\theta,z) - \vec{K}_-(\theta,z)$. From this and $\vec{K}(\theta,z) = \vec{K}_+(\theta,z) + \vec{K}_-(\theta,z)$, the outside and inside currents $\vec{K}_+(\theta,z)$ and $\vec{K}_-(\theta,z)$ were obtained.

SECTION VI

THEORETICAL CURRENTS AND CHARGES ON A TUBULAR CYLINDER

Extensive computations and graphical representations of $K_z(\theta,z)$, $K_\theta(\theta,z)$ and $\eta(\theta,z)$ have been carried out by King et al. [18] in order to gain insight into the physical phenomena and provide a foundation for measurements designed to develop and test experimental procedures and techniques. For this purpose tubular cylinders with ka = 1 were selected since a circumference of one wavelength is large enough to involve most of the characteristics of electrically thick tubes and small enough to avoid the complications of higher-order transverse resonances. Later studies will include ka = 2 and ka = 3. The initial computations and measurements were made with kh = 1.5π. Later, in anticipation of crossed cylinders, kh = 3π and 3.5π were also studied.

Consider first a cylinder with ka = 1 and kh = 1.5π. The axial distribution of $K_z(\theta,z) = |K_z(\theta,z)|\exp \theta_z = K_{zR}(\theta,z) + iK_{zI}(\theta,z)$ is shown in Figs. 21a,b,c as a function of kz. At θ = 0° (shadow), $|K_z(\theta,z)|$ and θ_z have strongly resonant forms with a high standing-wave ratio and a 180° phase change, whereas at θ = 180° (illuminated region) they have the nearly constant values characteristic of predominantly forced distributions. At intermediate angles a gradual transition takes place. In Figs. 22a,b,c are shown graphs of the transverse distributions of $K_z(\theta,z)$ which are seen to be quite different from one another at various values of kz. They are reasonably like those along an infinitely long cylinder with the same radius (shown by crosses in Fig. 22c) only when kz is near 0.5π where resonant currents have a minimum. This is easily understood if it is recalled that there are no resonant currents on the infinitely long cylinder. It is evident from Figs. 21a,b,c and 22a,b,c as well as Fig. 1 in [19] that the distribution of $K_z(\theta,z)$ on an electrically thick cylinder cannot be constructed as a simple combination of the axial distribution along an electrically thin cylinder of

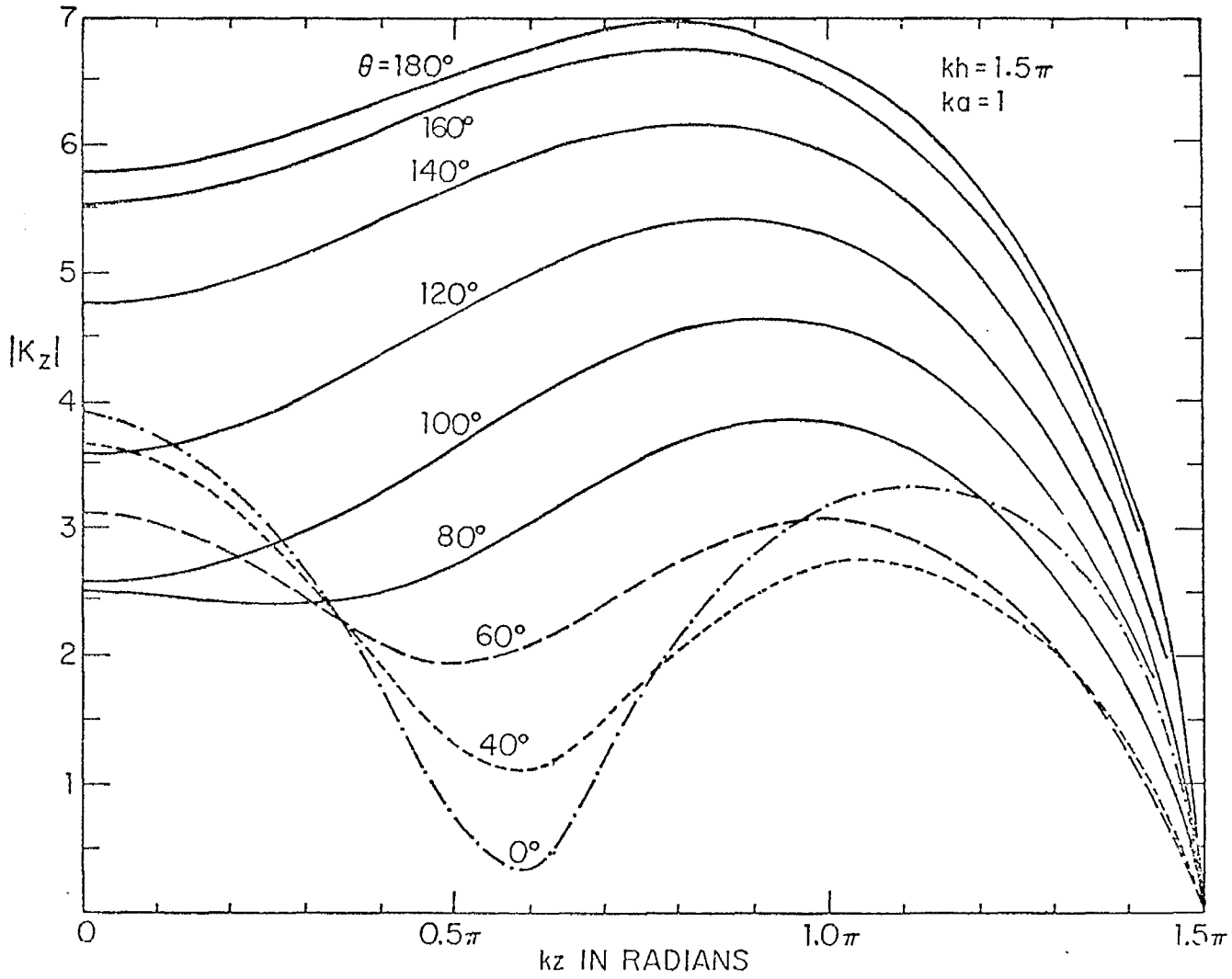

Fig. 21a. Theoretical amplitude of surface density of total axial current on tubular cylinder; E-polarization, normal incidence.

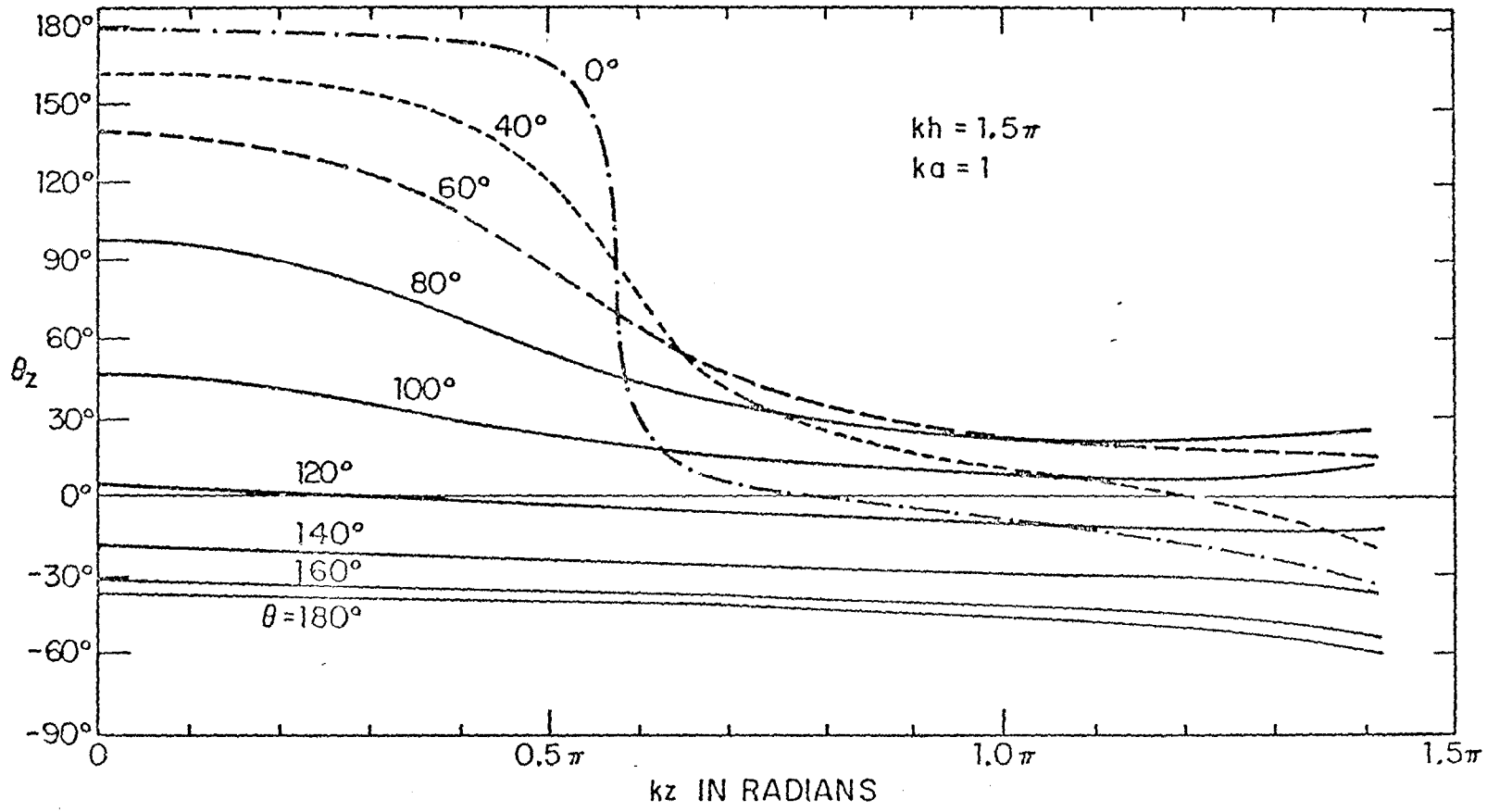

Fig. 21b. Theoretical phase of surface density of total axial current on tubular cylinder; E-polarization, normal incidence.

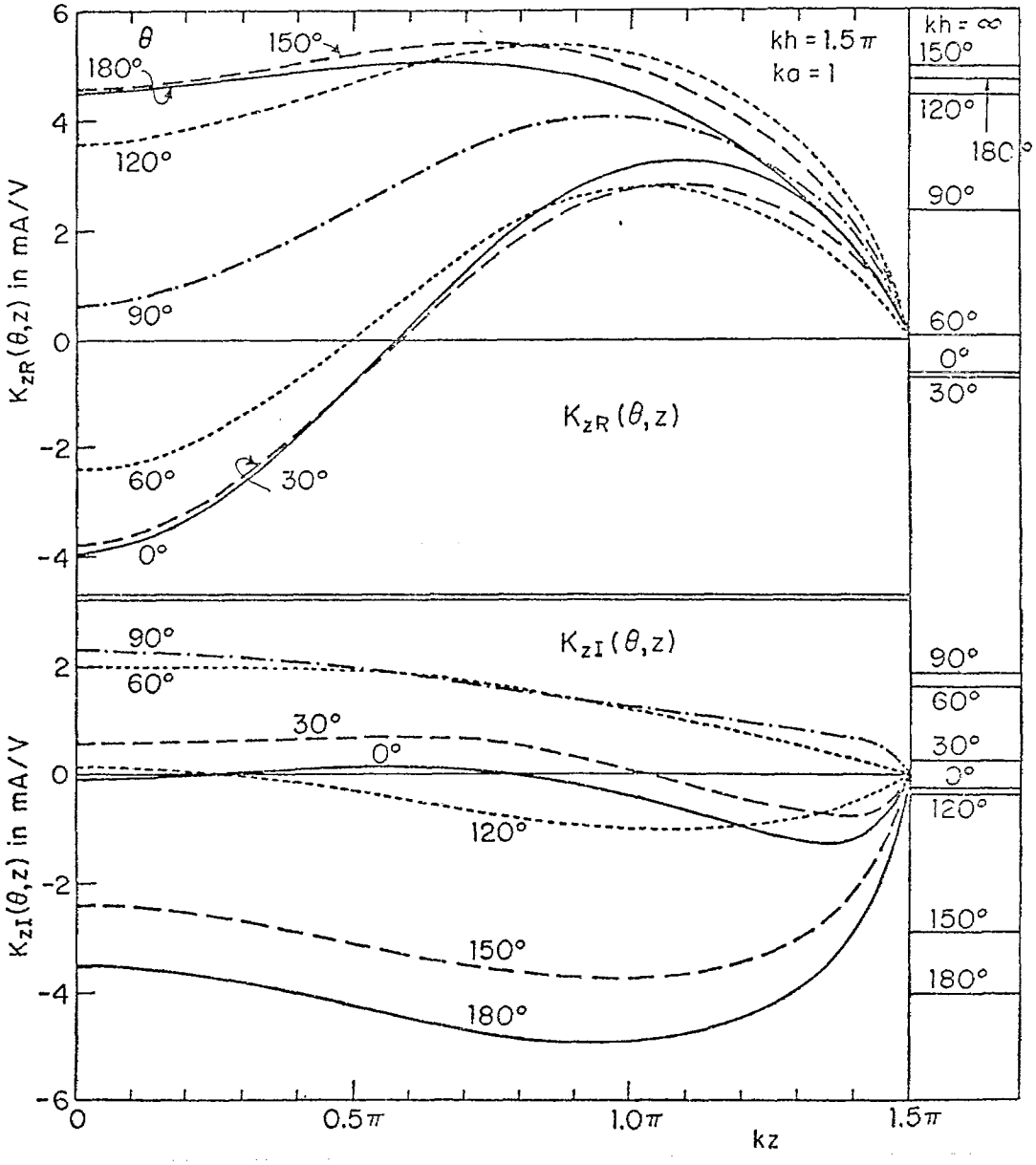

Fig. 21c. Real and imaginary parts of $K_z(\theta,z)$ on tubular cylinder; E-polarization, normal incidence.

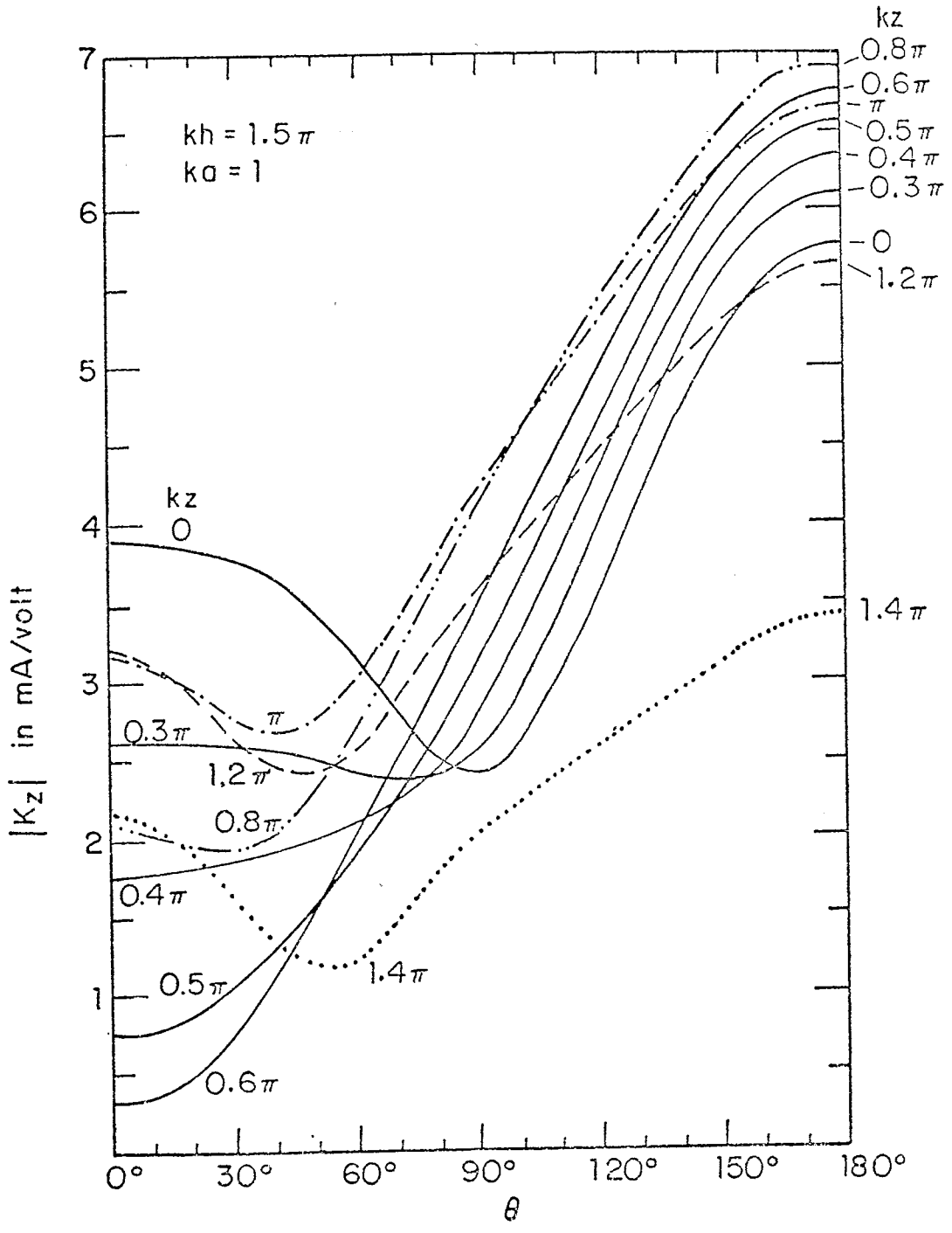

Fig. 22a. Theoretical amplitude of surface density of total axial current on tubular cylinder; E-polarization, normal incidence.

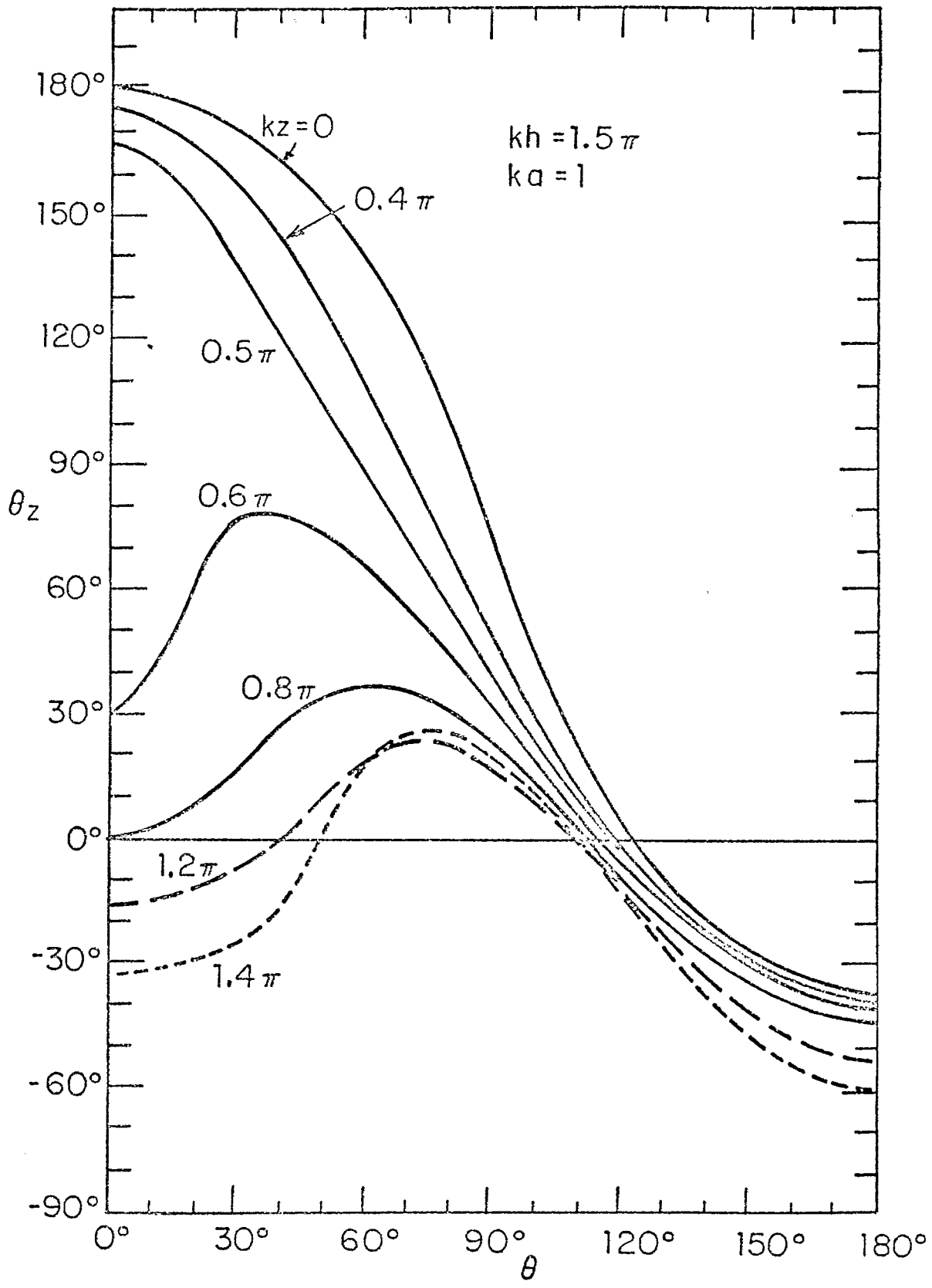

Fig. 22b. Theoretical phase of surface density of total axial current on tubular cylinder; E-polarization, normal incidence.

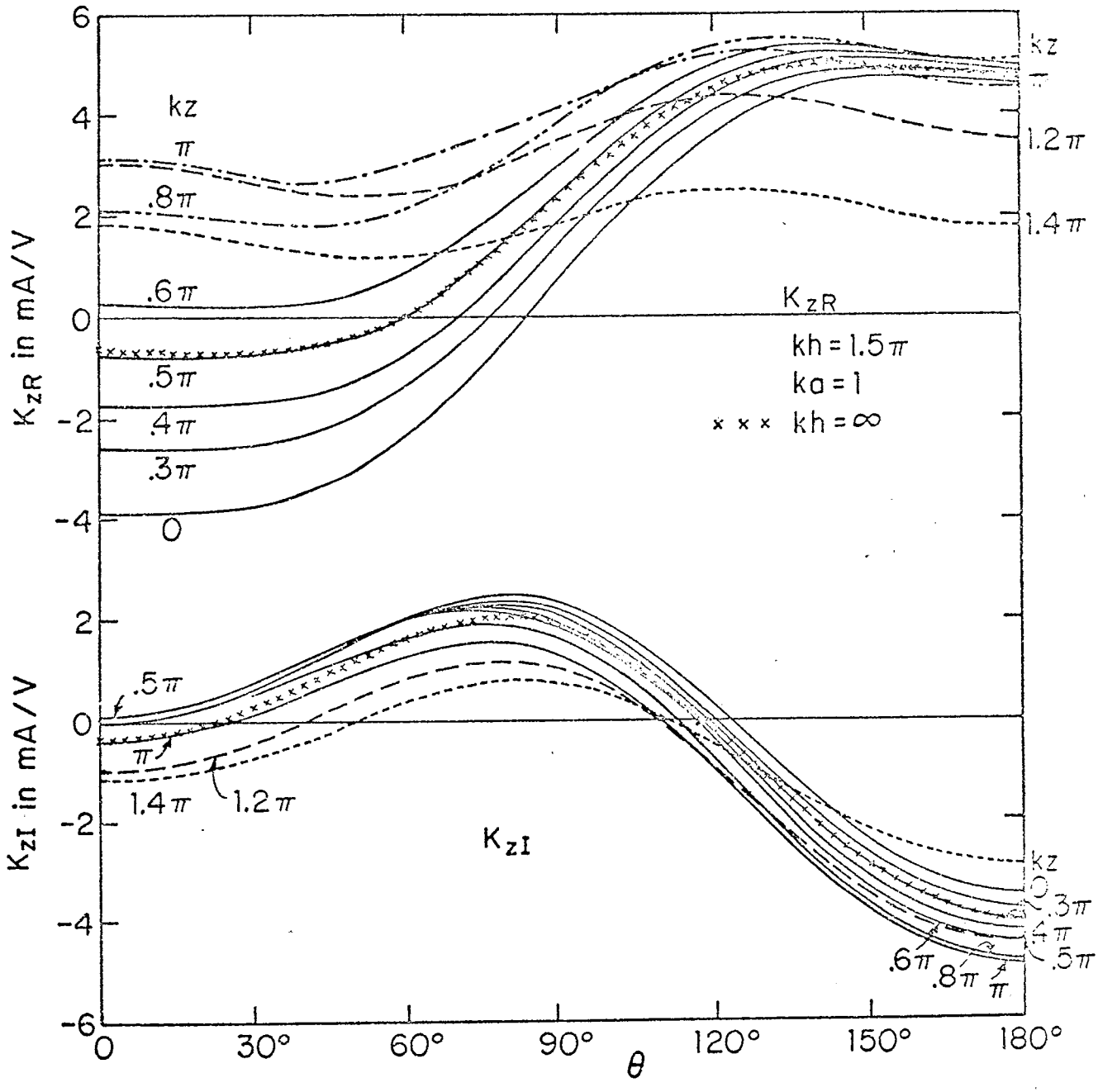

Fig. 22c. Real and imaginary parts of $K_z(\theta,z)$ on tubular cylinder; E-polarization, normal incidence. $K_z(\theta)$ with kh = ∞.

the same length with the transverse distribution around an infinitely long cylinder with the same radius.

On an electrically thick cylinder of finite length a very significant transverse component of current $K_\theta(\theta,z) = |K_\theta(\theta,z)| \exp \theta_t = K_{\theta R}(\theta,z) + iK_{\theta I}(\theta,z)$ is excited by the periodically varying, non-rotationally symmetric charge distributions at the ends. $|K_\theta(\theta,z)|$ is shown in Fig. 23a, θ_t in Fig. 23b, and $K_{\theta R}(\theta,z)$ and $K_{\theta I}(\theta,z)$ in Fig. 23c. Note that $|K_\theta(\theta,z)|$ vanishes at $\theta = 0°$ and 180° and has a maximum near $\theta = 90°$ for all values of kz. $K_\theta(\theta,z)$ is very small compared with $K_z(\theta,z)$ except near the open ends where it rises steeply to very large values - infinity for the idealized infinitely thin-walled tube.

Both $K_\theta(\theta,z)$ and $K_z(\theta,z)$ are complex so that at each point (a,θ,z) on the cylinder $\vec{K}(\theta,z) = \vec{K}_R(\theta,z) + i\vec{K}_I(\theta,z)$ where $\vec{K}_R(\theta,z) = \hat{\theta}K_{\theta R}(\theta,z) + \hat{z}K_{zR}(\theta,z)$ and $\vec{K}_I(\theta,z) = \hat{\theta}K_{\theta I}(\theta,z) + \hat{z}K_{zI}(\theta,z)$. The real vectors $\vec{K}_R(\theta,z)$ and $\vec{K}_I(\theta,z)$ at uniformly spaced points on the surface of the cylinder are shown drawn to scale in Fig. 24. At each point the length of the vector is proportional to $|\vec{K}_R(\theta,z)|$ on the left, $|\vec{K}_I(\theta,z)|$ on the right; the direction of the vector gives the direction of $\vec{K}_R(\theta,z)$ or $\vec{K}_I(\theta,z)$. The general direction of flow and the standing-wave pattern in the shadow are evident.

The real instantaneous current $\vec{K}(\theta,z;t) = \hat{\theta}K_\theta(\theta,z;t) + \hat{z}K_z(\theta,z;t)$ has the components $K_\theta(\theta,z;t) = K_{\theta R}(\theta,z)\cos \omega t + K_{\theta I}(\theta,z)\sin \omega t$ and $K_z(\theta,z;t) = K_{zR}(\theta,z)\cos \omega t + K_{zI}(\theta,z)\sin \omega t$. It is easily shown that $\vec{K}(\theta,z;t)$ is elliptically polarized as shown in Fig. 25.

An important aspect of a standing wave of current on a conducting surface consists of the associated standing-wave concentrations of charge. The surface density of charge $\eta(\theta,z) = |\eta(\theta,z)| \exp \theta_\eta$ is related to the rates of change of both $K_z(\theta,z)$ and $K_\theta(\theta,z)$ as given by (5.9). Graphs of $|\eta(\theta,z)|$ and θ_η are shown in Figs. 26a,b. The charge density is seen to have a simple

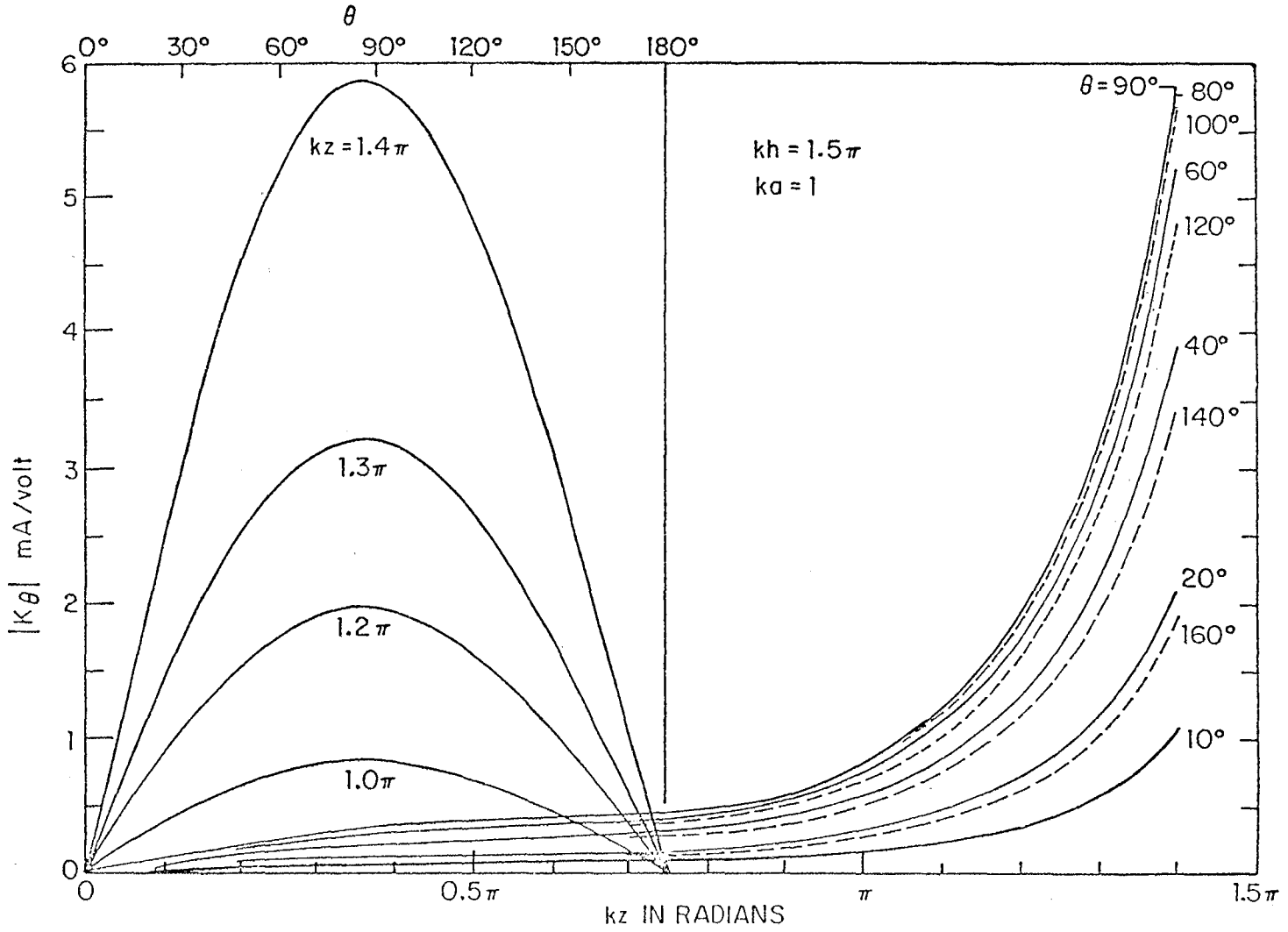

Fig. 23a. Theoretical amplitude of surface density of transverse current on tubular cylinder; E-polarization, normal incidence.

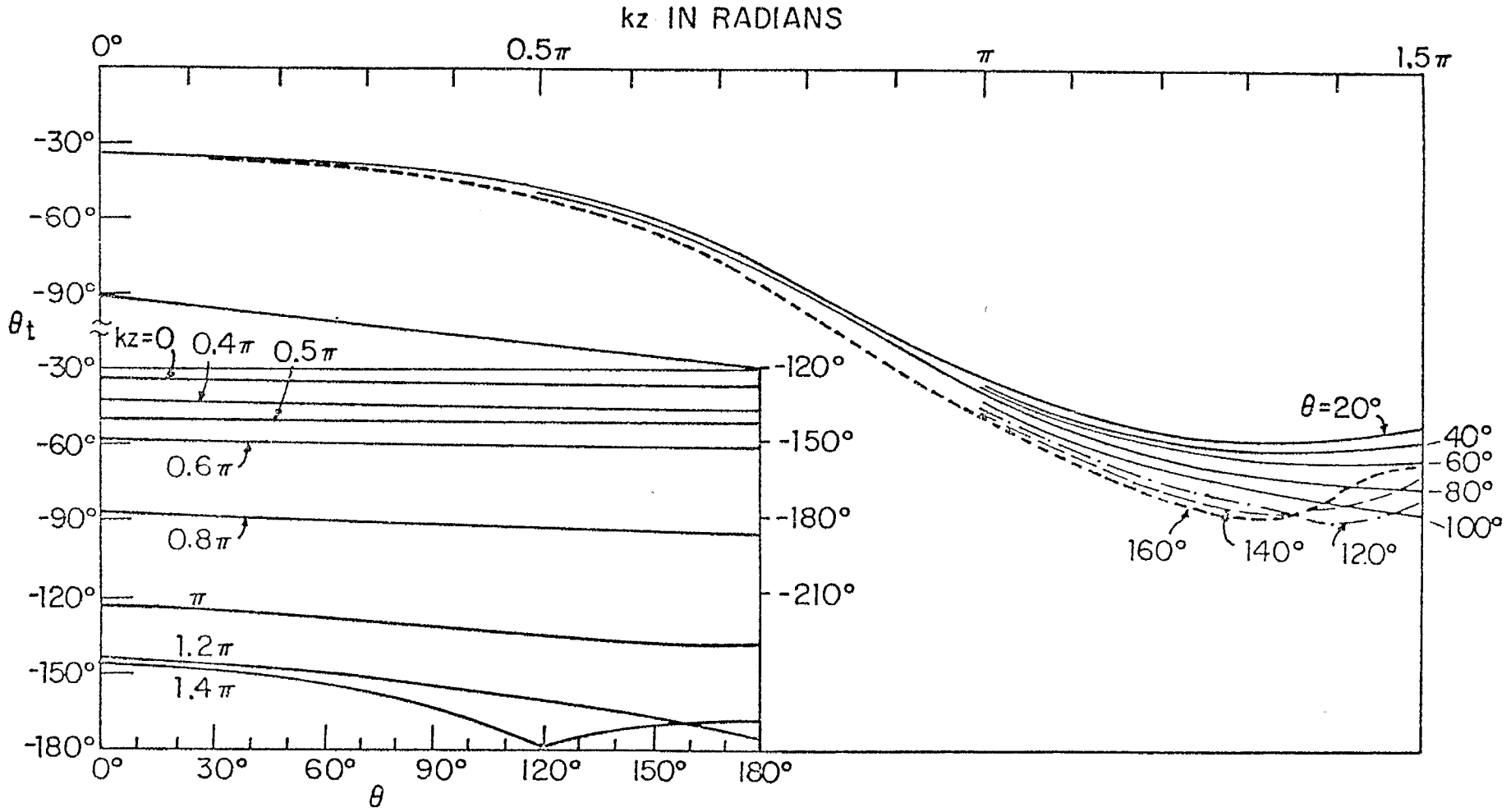

Fig. 23b. Theoretical phase of surface density of transverse current on tubular cylinder; E-polarization, normal incidence.

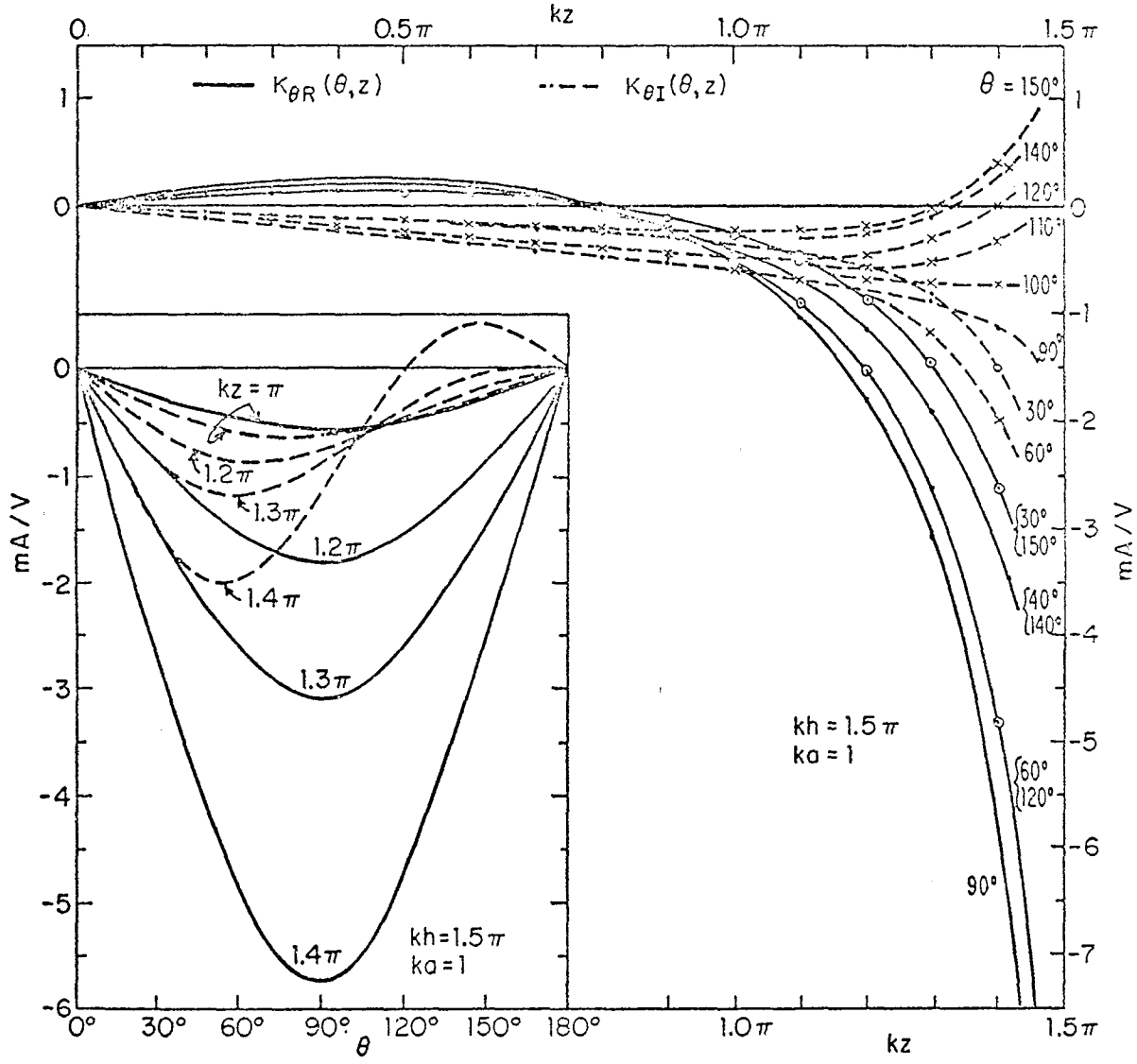

Fig. 23c. Real and imaginary parts of $K_\theta(\theta,z)$ on tubular cylinder; E-polarization, normal incidence.

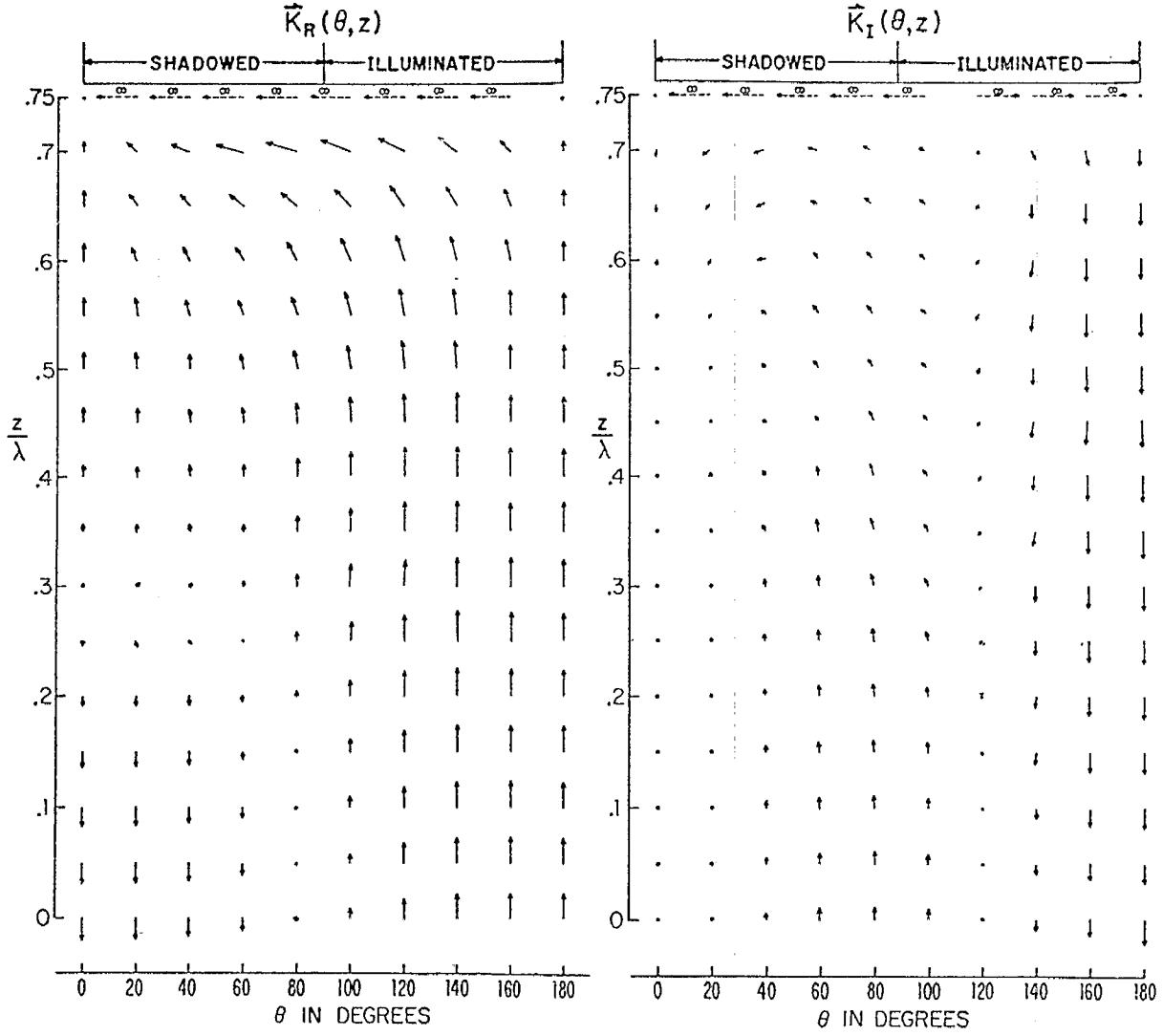

Fig. 24. $\vec{K}_R(\theta,z)$ and $\vec{K}_I(\theta,z)$ on tubular cylinder; E-polarization, normal incidence; $kh = 1.5\pi$, $ka = 1$.

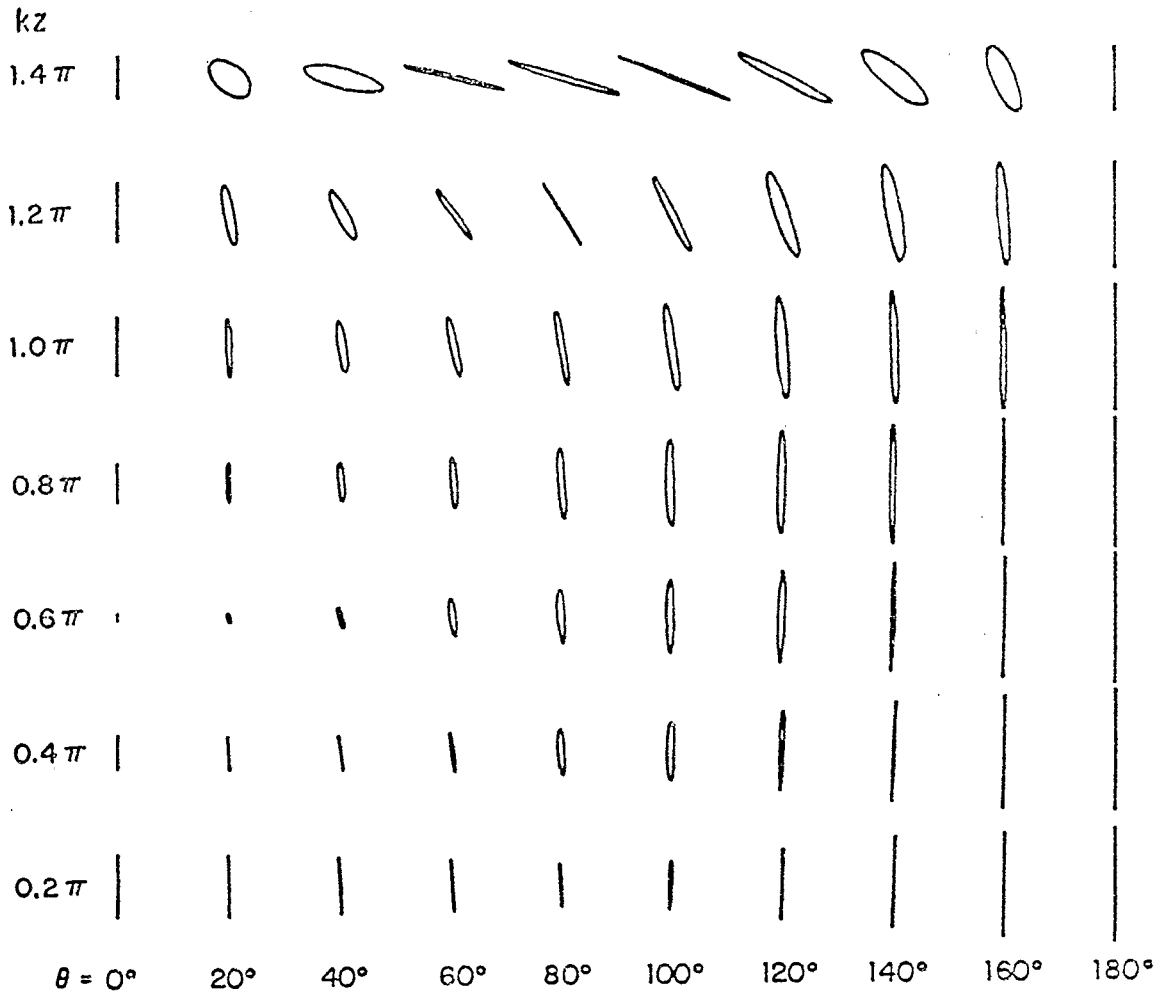

Fig. 25. Theoretical polarization ellipses of $\vec{K}(\theta,z)$ on tubular cylinder; E-polarization, normal incidence; kh = 1.5π, ka = 1.

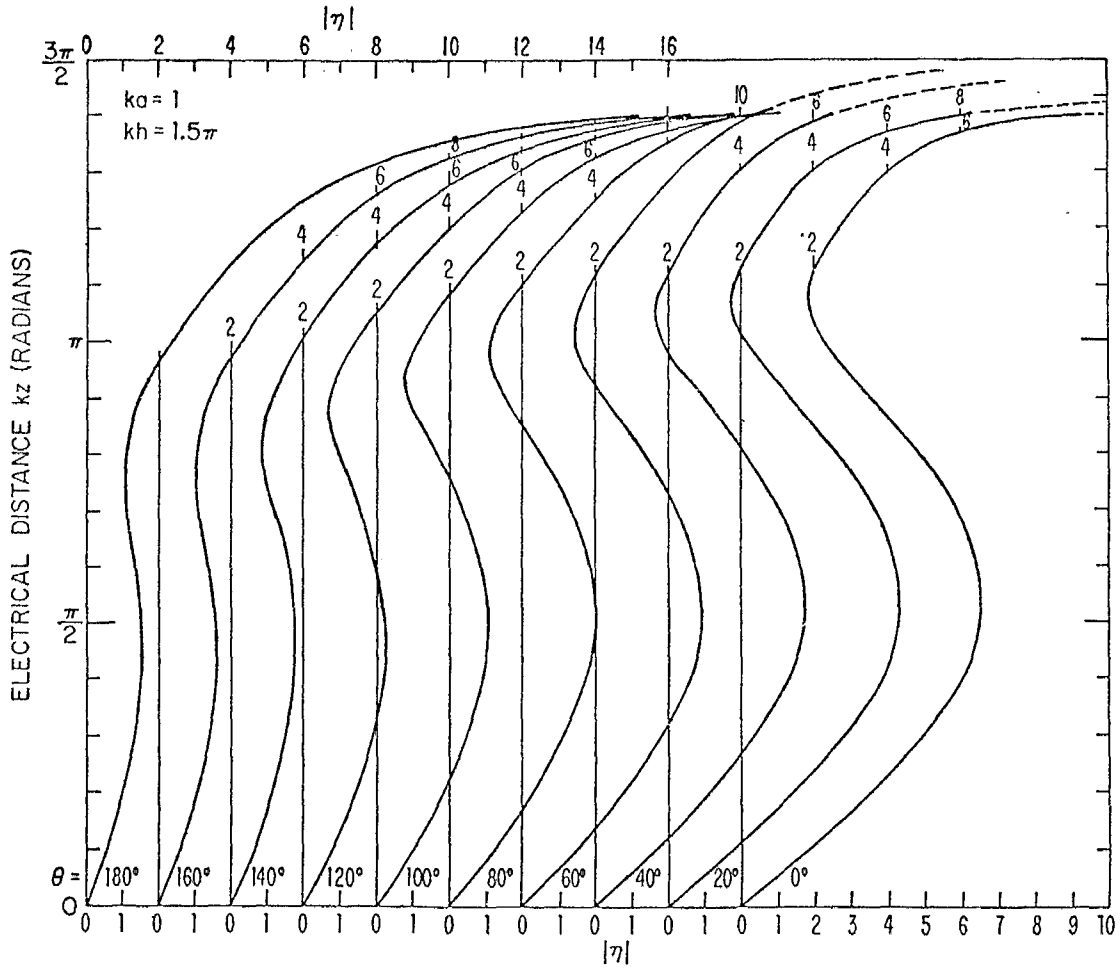

Fig. 26a. Theoretical magnitude of surface density of charge on tubular cylinder, $\eta = |\eta| e^{i\theta_\eta}$; E-polarization, normal incidence.

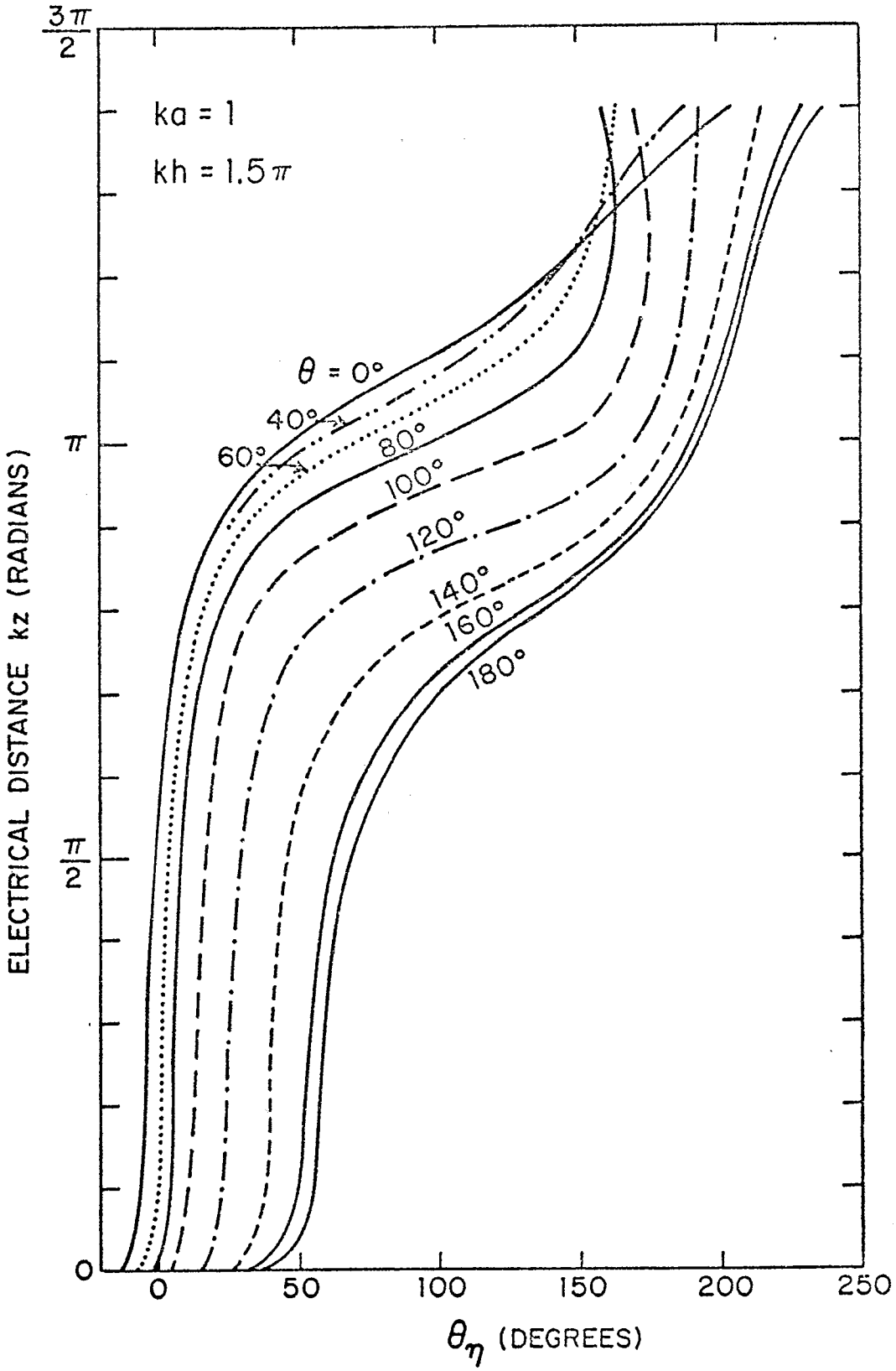

Fig. 26b. Theoretical phase of surface density of charge on tubular cylinder, $\eta = |\eta| e^{i\theta_\eta}$; E-polarization, normal incidence.

standing-wave pattern with zero amplitude at $kz = 0$, a maximum near $kz = \pi/2$, a minimum near $kz = \pi$, and a high maximum at $kz = kh = 3\pi/2$. The standing-wave ratio is much lower in the illuminated region than in the shadow. A clear picture of the overall distribution of charge density is obtainable from Figs. 27a,b which show contours of constant $|\eta(\theta,z)|$ and θ_η, respectively. The important characteristics in Fig. 27a are the very high maximum at the open end, the secondary maximum in the shadow near $kz = 0.5\pi$, $\theta = 0°$, and a deep valley between the contours marked 1.5. Fig. 27b suggests a phase front diverging from $kz = 1.5\pi$, $\theta = 180°$ and converging toward $kz = 0$, $\theta = 0°$.

The distributions of axial current on cylinders with $ka = 1$ and lengths other than $kh = 1.5\pi$ are shown in Fig. 28 for a range of electrical half-lengths extending from $kh = 1.4\pi$ to 3π in steps of 0.2π. The graphs reveal the significant fact that the distributions are virtually identical when $kh = kh_1$ and $kh = kh_1 + n\pi$ in the ranges $0 \leq kz \leq kh_1$ and $n\pi \leq kz \leq kh_1 + n\pi$. Specifically, all curves for $kh = 2\pi$ virtually coincide with those for $kh = 3\pi$ in the range $\pi \leq kz \leq 2\pi$. The same is true for the lengths $kh = 1.8\pi$ and 2.8π, 1.6π and 2.6π, etc.

In view of this periodic behavior of the currents, it is sufficient to examine the associated distributions of charge density for only selected lengths. The most interesting are the resonant lengths like $kh = 1.5\pi$ (Figs. 26a,b and 27a,b) and $kh = 3.5\pi$ (Figs. 38 and 40) and the antiresonant lengths like $kh = 3\pi$. The axial distributions of $|\eta(\theta,z)|$ for $kh = 3\pi$ are shown in Fig. 29 for $\theta = 0°$ to $180°$ in steps of $20°$. The associated contour diagram is in Fig. 30. The corresponding representations when $kh = 3.5\pi$ are in Figs. 38 and 40. They are seen to be substantially the same in the range $0 \leq kz \leq 2\pi$. The graphs in the range $2\pi \leq kz \leq 3.5\pi$ in Figs. 38 and 40 are squeezed together axially into the range $2\pi \leq kz \leq 3\pi$ in Figs. 29 and 30. The boundary

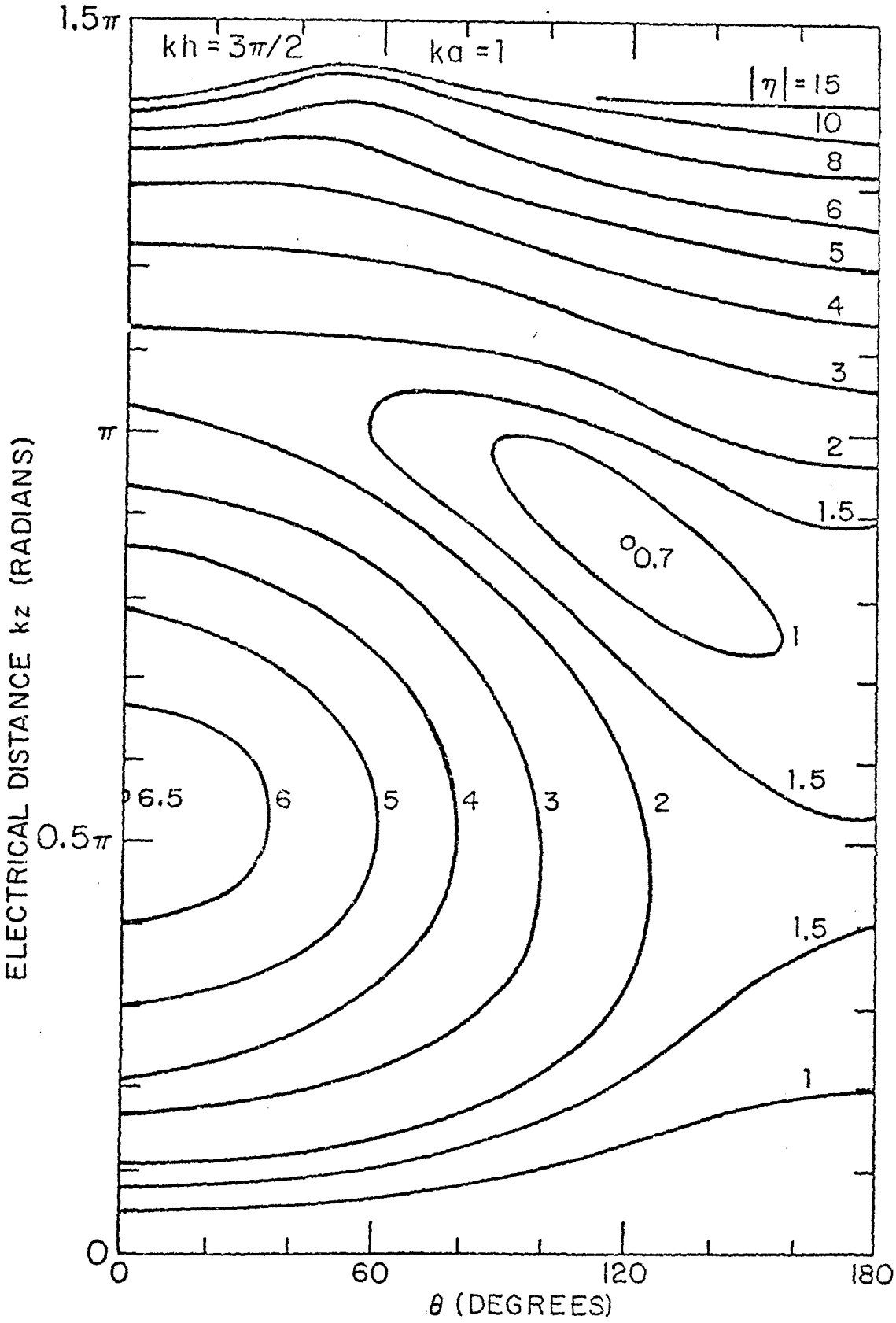

Fig. 27a. Theoretical contours of magnitude of surface density of charge on tubular cylinder; E-polarization, normal incidence.

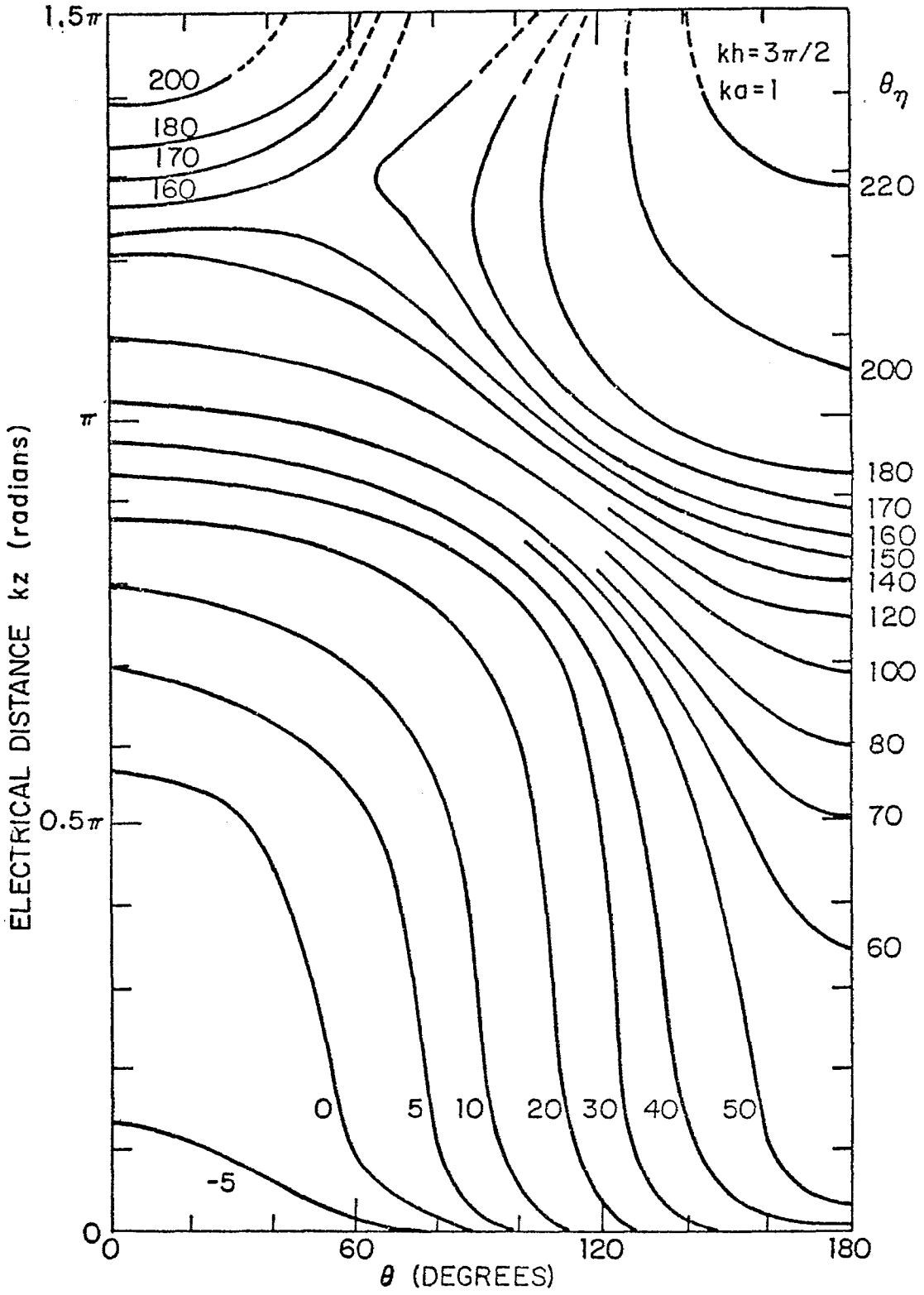

Fig. 27b. Theoretical contours of constant phase of surface density of charge on tubular cylinder; E-polarization, normal incidence.

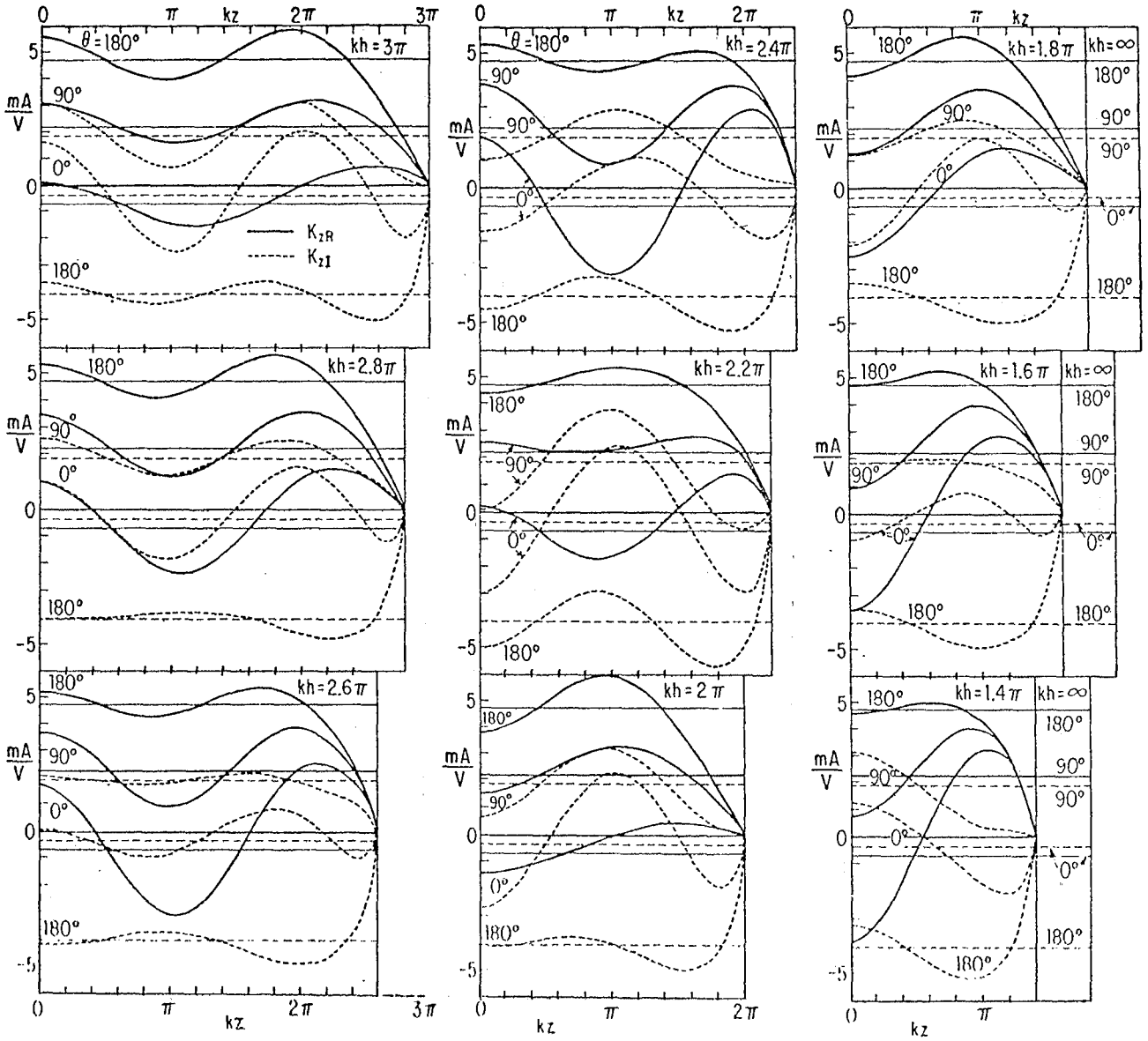

Fig. 28. Surface density of axial current on tubular cylinder, $K_z(\theta,z) = K_{zR} + iK_{zI}$; E-polarization, normal incidence; ka = 1.

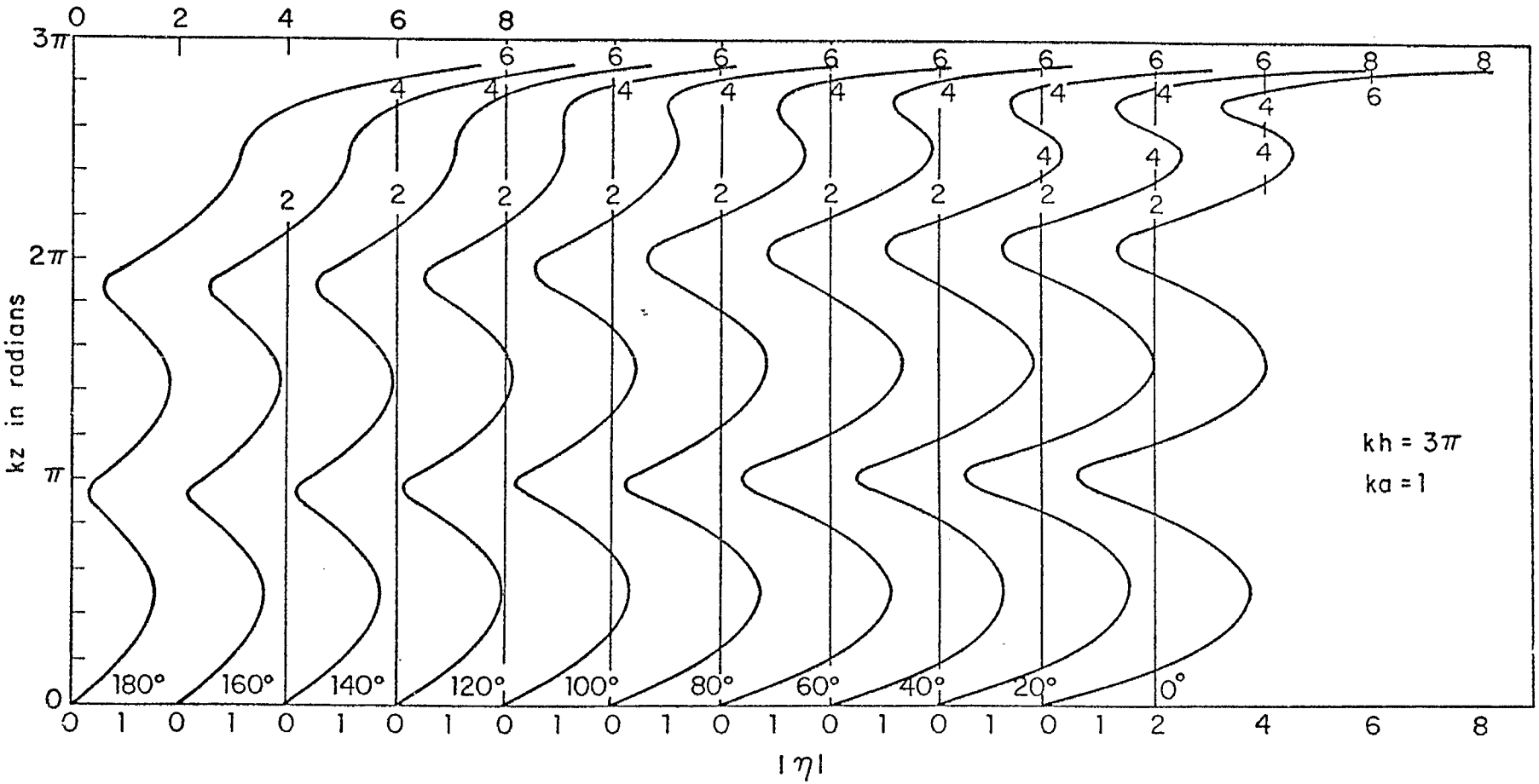

Fig. 29. Theoretical magnitude of surface density of outside charge on tubular cylinder; E-polarization, normal incidence.

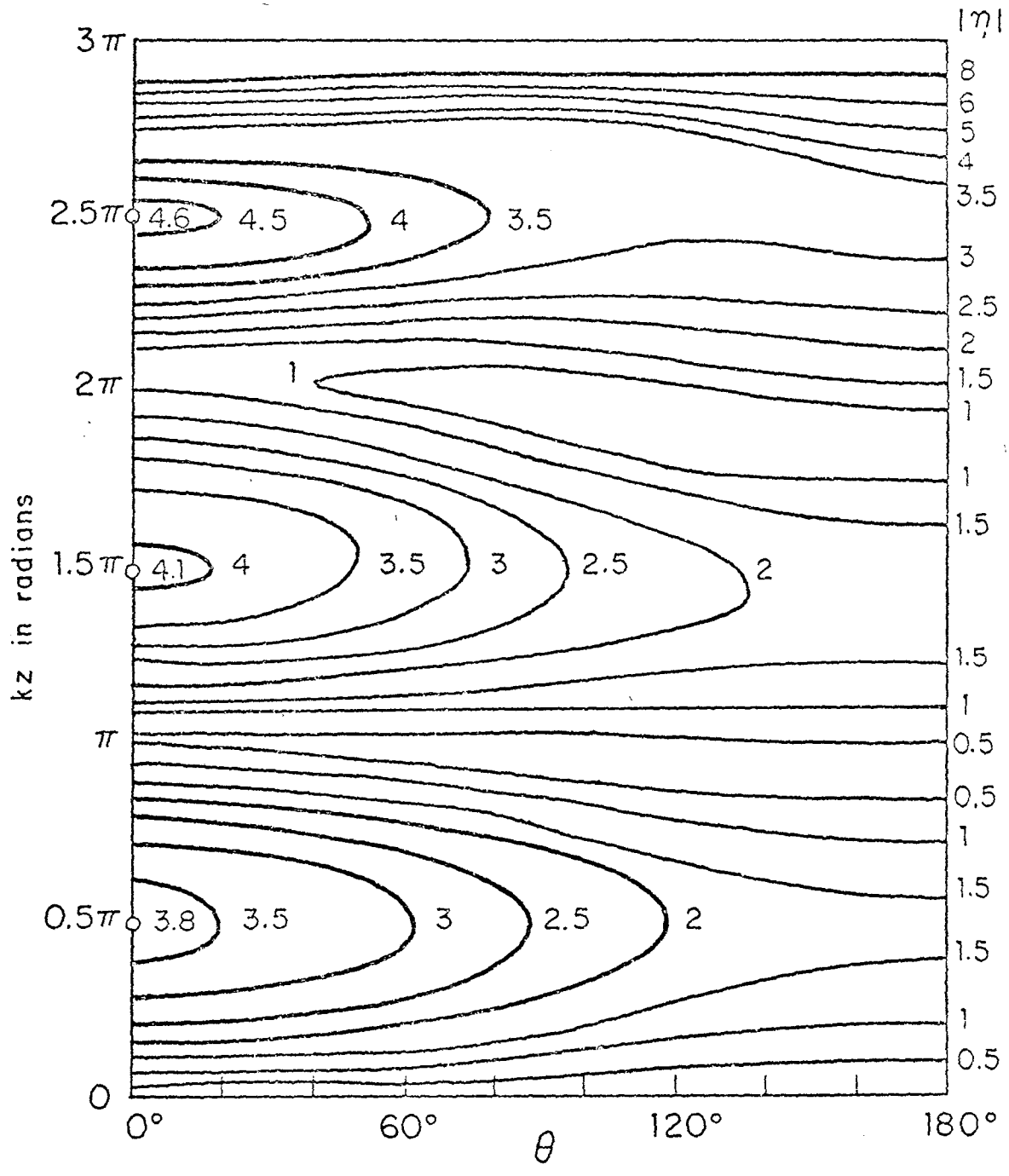

Fig. 30. Contour diagram of theoretical surface density of outside charge on tubular cylinder; E-polarization, normal incidence; kh = 3π, ka = 1.

condition $\eta(\theta,0) = .0$ dominates and the distribution is substantially like $\eta(\theta,z) \sim \sin kz$ for all lengths - resonant, antiresonant, and in between - with suitable modifications within a half wavelength of the open end. Thus, the contour diagrams in Figs. 30 and 40 have three maxima in the shadow region near $kz \doteq (2n + 1)\pi/2$. When $kh = 3\pi$, the charge maximum is superimposed on the steeper rise in charge density at a quarter wavelength from the open end instead of on the slower increase at a half wavelength from the end when $kh = 3.5\pi$.

SECTION VII

EXPERIMENTAL VERIFICATION; CYLINDER WITH ka = 1, kh = 3.5π

In order to develop and test apparatus and techniques for measuring distributions of surface charges and elliptically polarized surface currents, extensive measurements were made on cylinders with ka = 1 and kh = 1.5π [22]. The apparatus and movable probes are shown schematically in Fig. 31. Two ground planes of very different size (6.3 × 4.2 and 30.5 × 15.25 wavelengths) and distances ($\rho_0 = 4\lambda$ and 10λ) from the axis of the 6 in. diameter cylinder to the monopole source in a corner reflector were used successively. Generally very good agreement with theory was obtained with both ground planes. Differences were observed in the phases of the transverse currents where these were very small and accurate measurements difficult and in the amplitudes of the charge densities in parts of the illuminated region. These latter changed in a systematic manner as the distance between the cylinder and the source was increased from $\rho_0 = 4\lambda$ to $\rho_0 = 10\lambda$ to $\rho_0 = \infty$ (theory), and were presumed due to the progressive change from an incident spherical wave to an incident plane wave. Since the distance $\rho_0 = 4\lambda$ from the axis of the cylinder to the dipole source is greater than required for a line source to induce currents like those of a plane wave [as discussed following eq. (2.16)], it is likely that it is the spherical curvature of the wave front in the vertical plane along the length of the cylinder that is responsible for the observed, relatively small differences.

In anticipation of measurements on the surfaces of crossed cylinders and as a final check on the accuracy of the apparatus, distributions of <u>outside</u> surface current and charge density were computed and measured for a cylinder with ka = 1, kh = 3.5π with the dipole source 7.5λ from the axis of the cylinder. The theoretical values of $|K_z(\theta,z)|$ and θ_z are shown in Fig. 32, the corresponding measured ones in Fig. 33. The agreement is seen to be good.

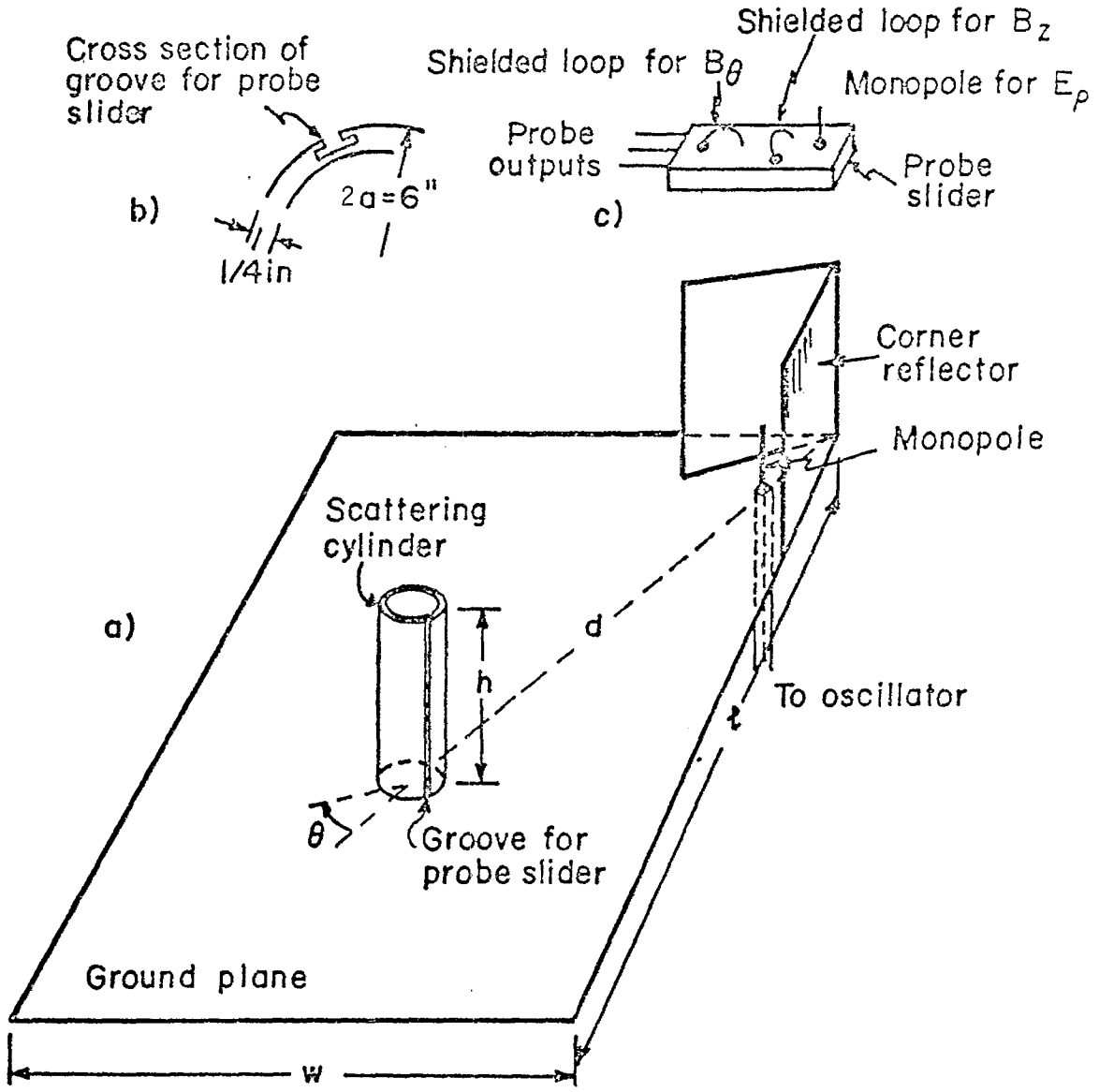

Fig. 31. Schematic diagrams of (a) scattering cylinder on ground plane, (b) cross section of groove in cylinder, and (c) probes on slider.

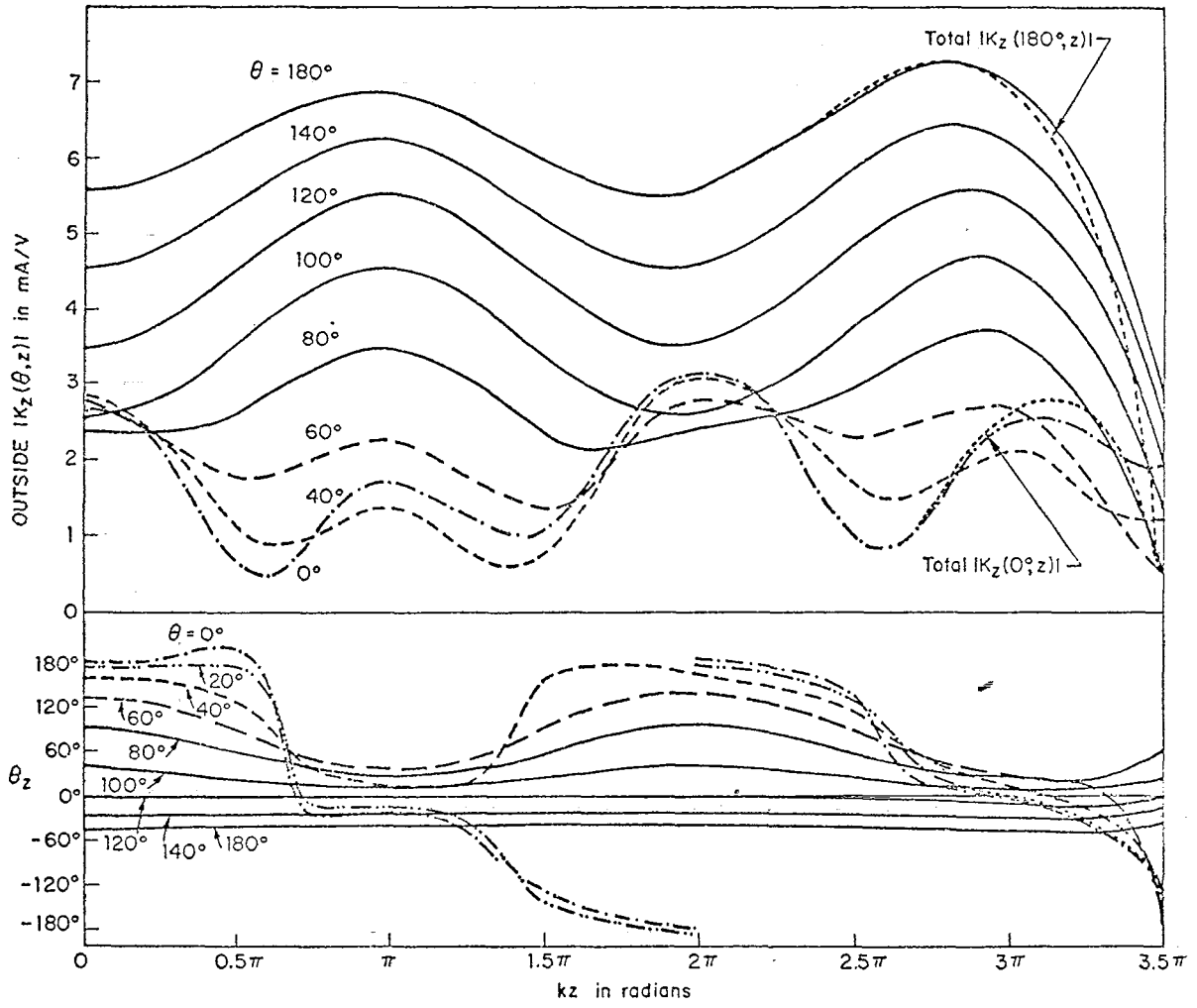

Fig. 32. Theoretical magnitude and phase of surface density of outside axial current on tubular cylinder; E-polarization, normal incidence; kh = 3.5π, ka = 1.

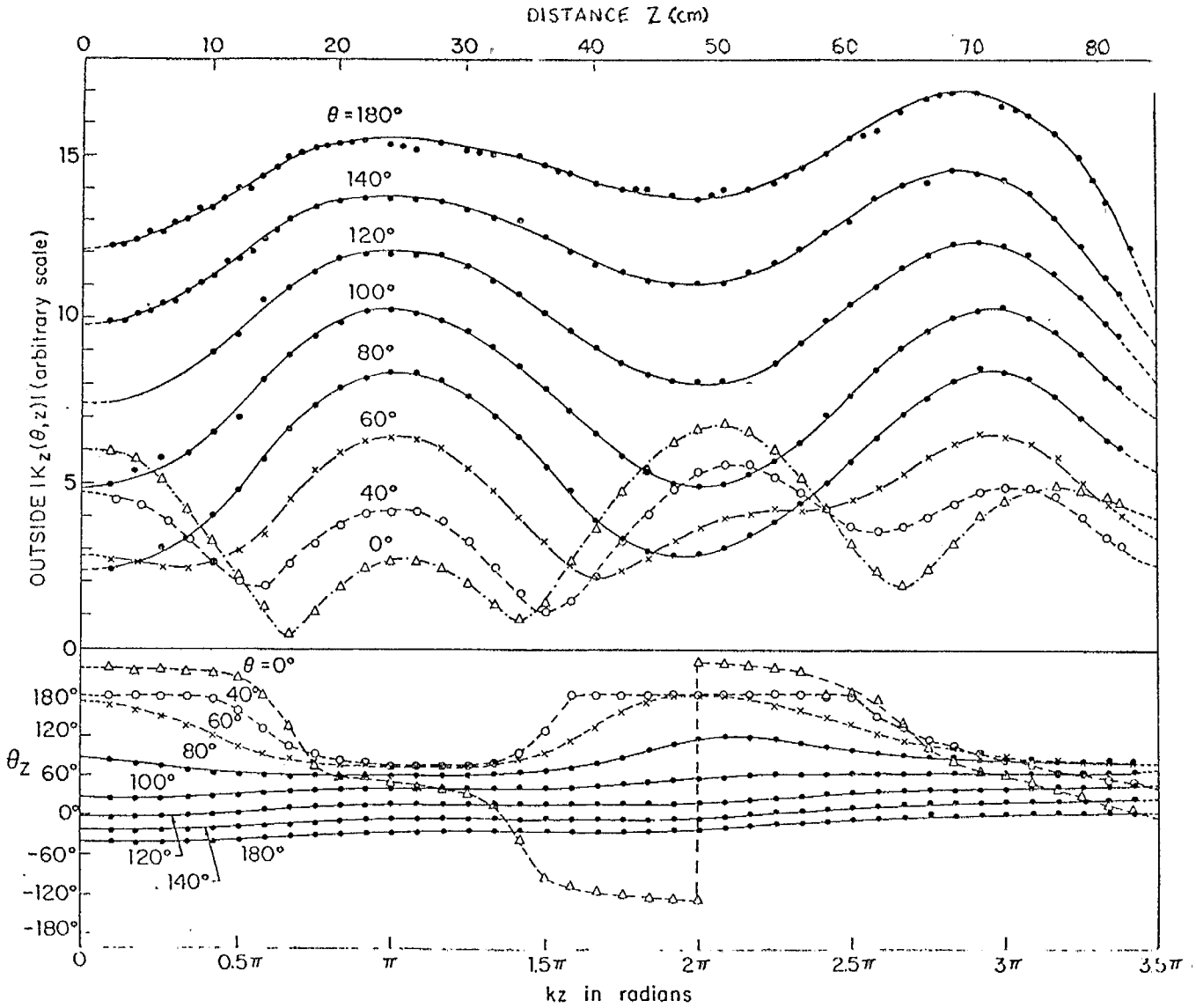

Fig. 33. Measured magnitude and phase of surface density of outside axial current on tubular cylinder; E-polarization, normal incidence; kh = 3.5π, ka = 1, λ = 48.0 cm.

The transverse outside currents are very small except near the ends of the cylinder. The theoretical graphs are in Fig. 34. The current vectors for the $\vec{K}_R(\theta,z)$ and $\vec{K}_I(\theta,z)$ are shown in Fig. 35, and the associated polarization ellipses in Fig. 36. The corresponding measured ellipses are shown in Fig. 37. The evident departure from linear polarization along the lines $\theta = 0°$ and $\theta = 180°$ in the measurements was found to be due to a very small misalignment of the two mutually perpendicular loop probes. This was corrected but the original results are shown in order to emphasize the sensitivity of the measurements. The theoretical and measured distributions of charge density are in Figs. 38 and 39. In the shadow region the agreement is excellent. As the illuminated region is approached, the middle one of the three measured maxima begins to shrink until it disappears when $\theta = 0°$. This does not occur in the theoretical graphs where the relative magnitudes of the three charge maxima are maintained for all values of θ. The same effect is shown in a different manner in the theoretical and measured contour diagrams in Figs. 40 and 41. A reduced version of this effect was observed [18] for the cylinder with $ka = 1$ and $kh = 1.5\pi$ and, as discussed earlier in this section, was attributed to the spherical shape of the incident wave front. This effect can be expected to increase with the length of the cylinder and become more and more significant as the diameter of the cylinder is reduced. A verification with the use of an incident cylindrical wave is planned.

It may be concluded that the probes and techniques developed for measuring surface densities of charge and vector current are accurate and appropriate for use with crossed cylinders for which no theoretical results are available.

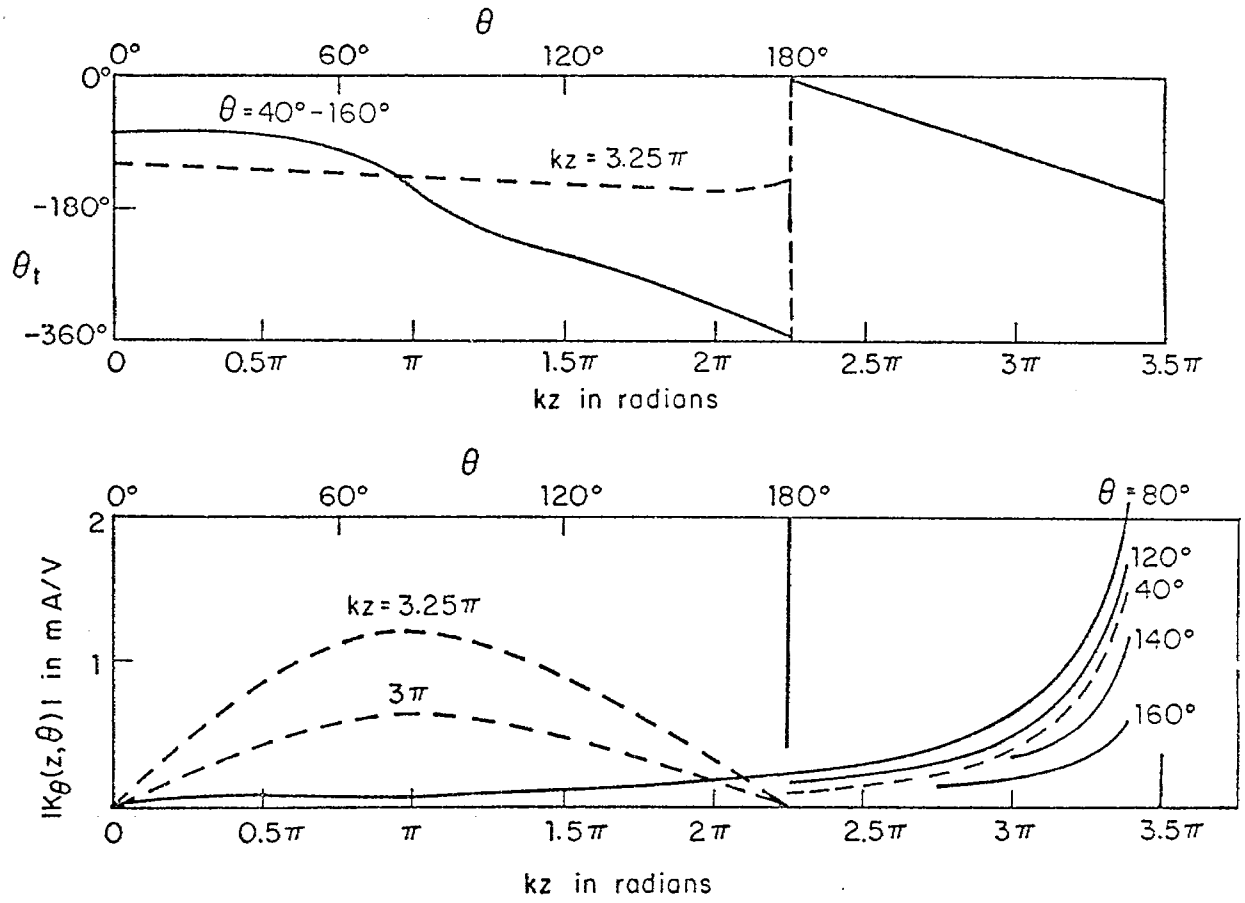

Fig. 34. Theoretical amplitude and phase of surface density of outside transverse current on tubular cylinder; E-polarization, normal incidence; kh = 3.5π, ka = 1.

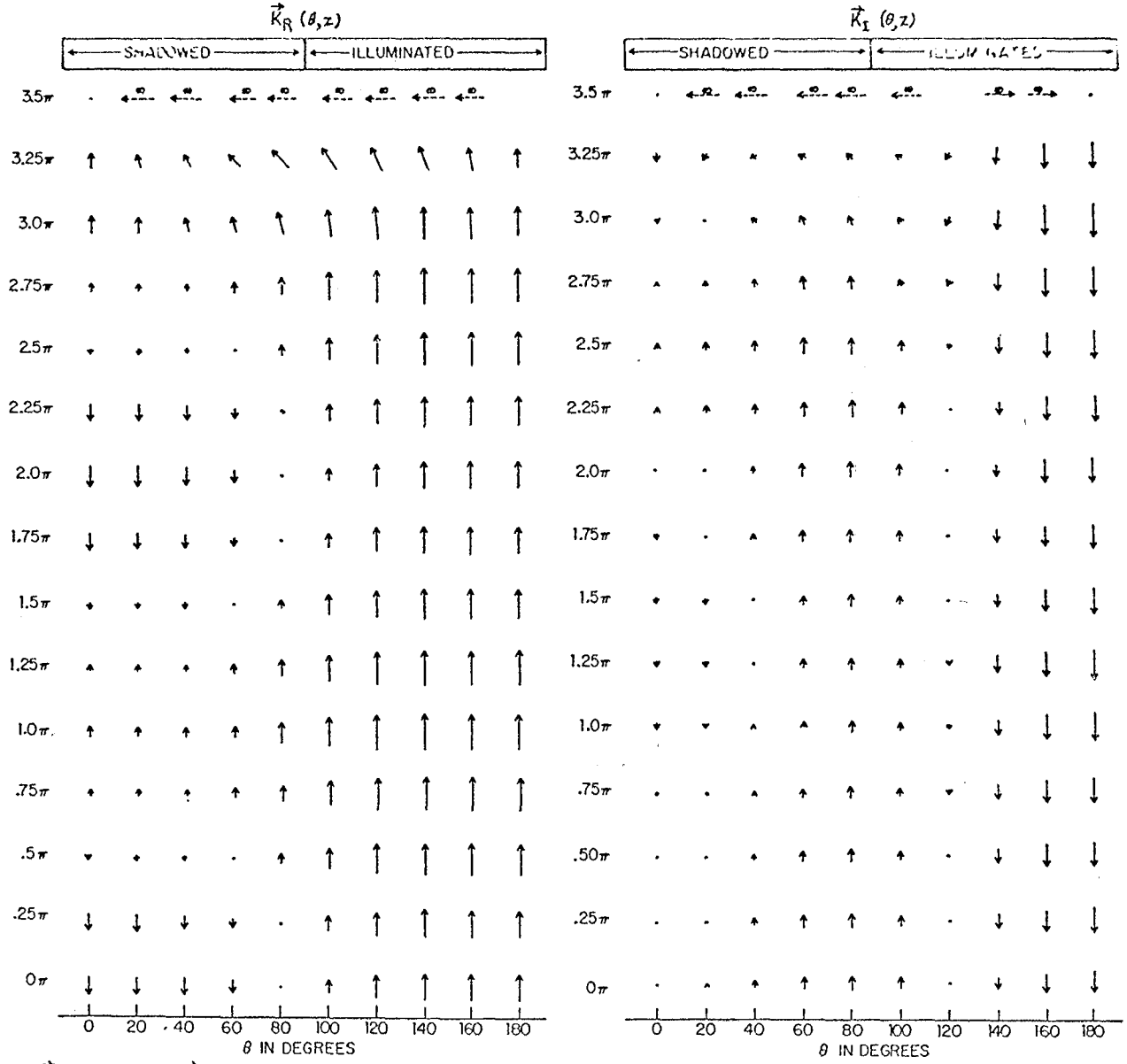

Fig. 35. $\vec{K}_R(\theta,z)$ and $\vec{K}_I(\theta,z)$ on tubular cylinder; E-polarization, normal incidence; kh = 3.5π, ka = 1.

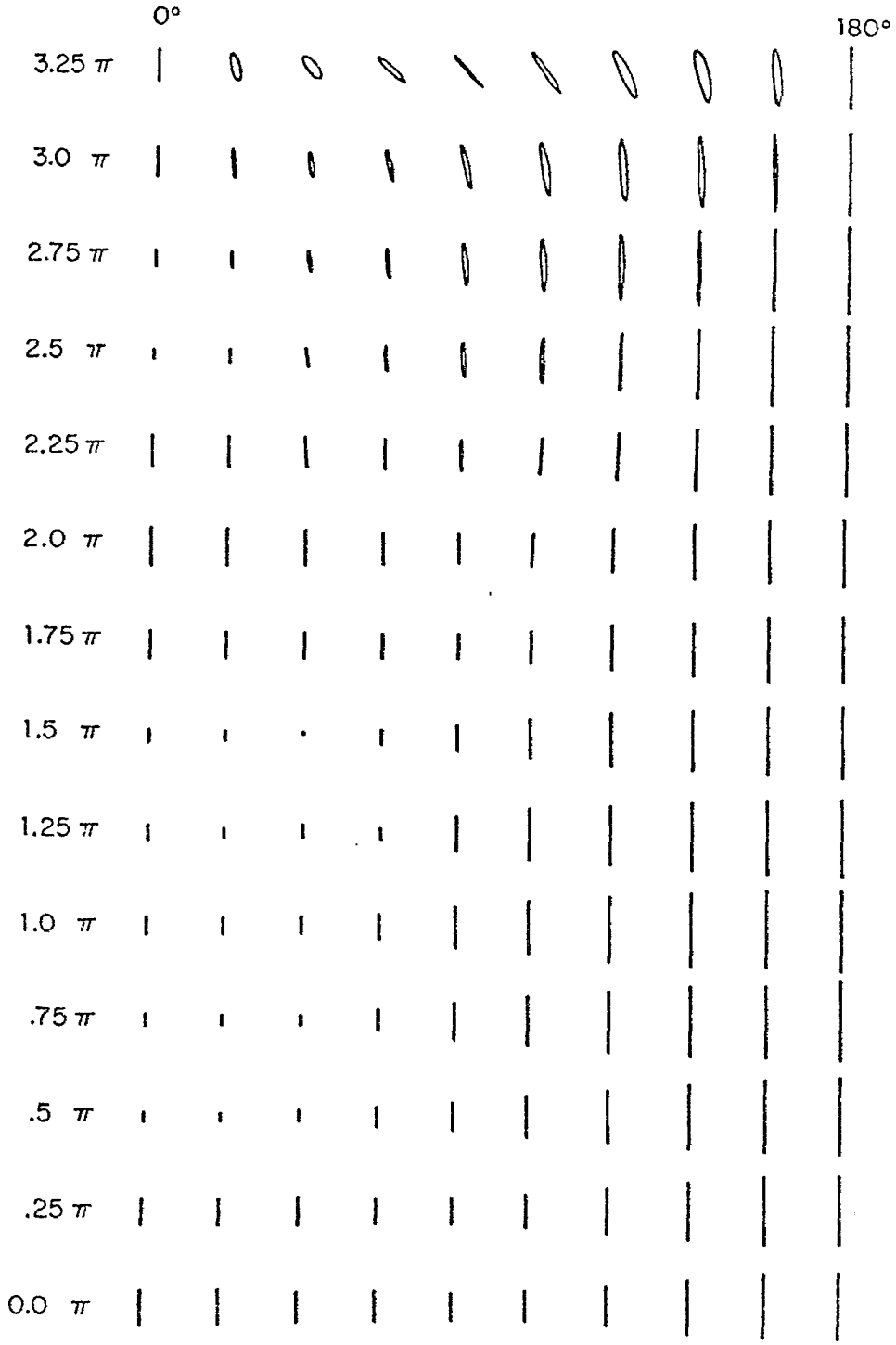

Fig. 36. Theoretical polarization ellipses of $\vec{K}(\theta,z)$ on tubular cylinder; E-polarization, normal incidence; kh = 3.5π, ka = 1.

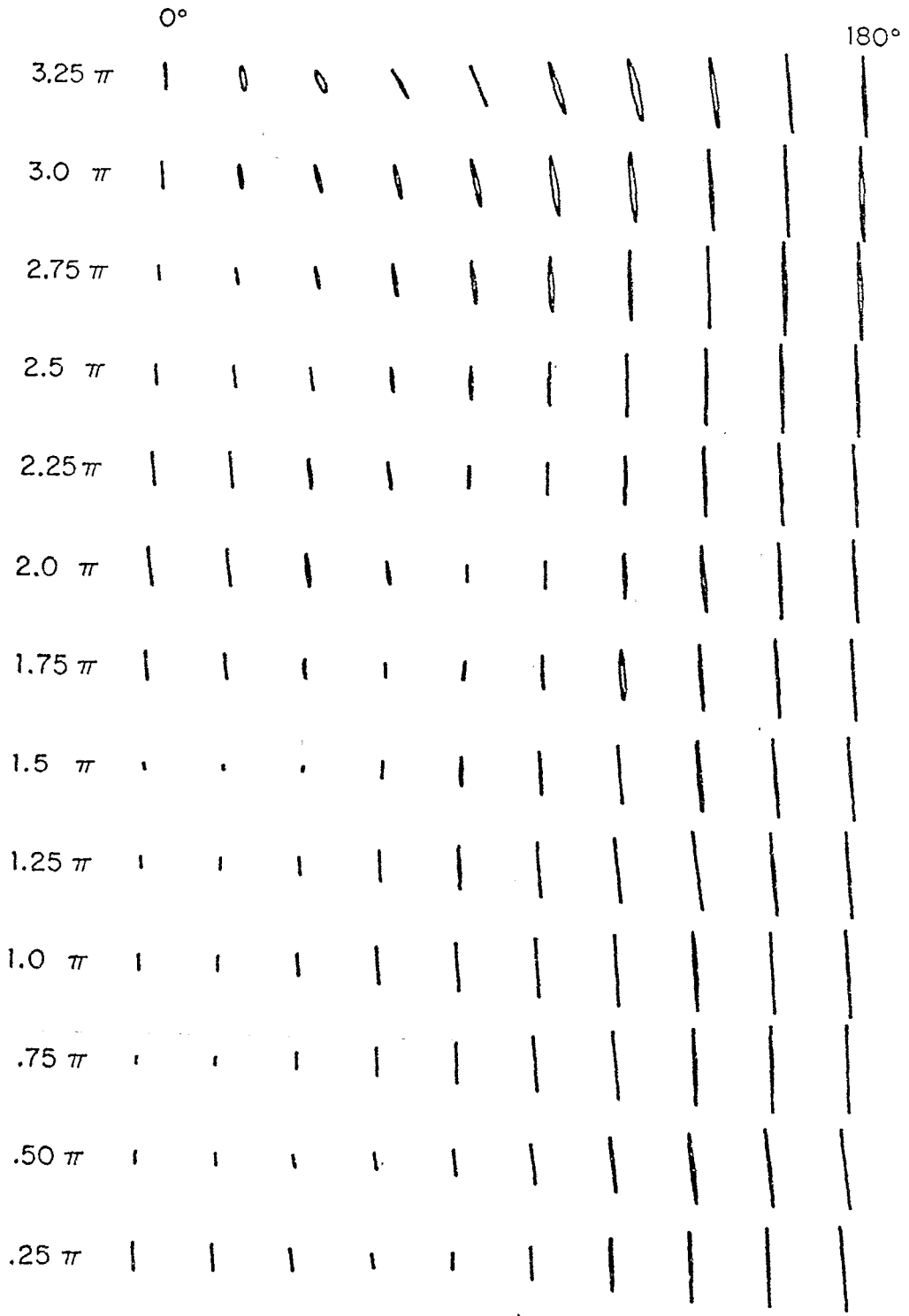

Fig. 37. Measured polarization ellipses of $\vec{K}(\theta,z)$ on tubular cylinder; E-polarization, normal incidence; kh = 3.5π, ka = 1.

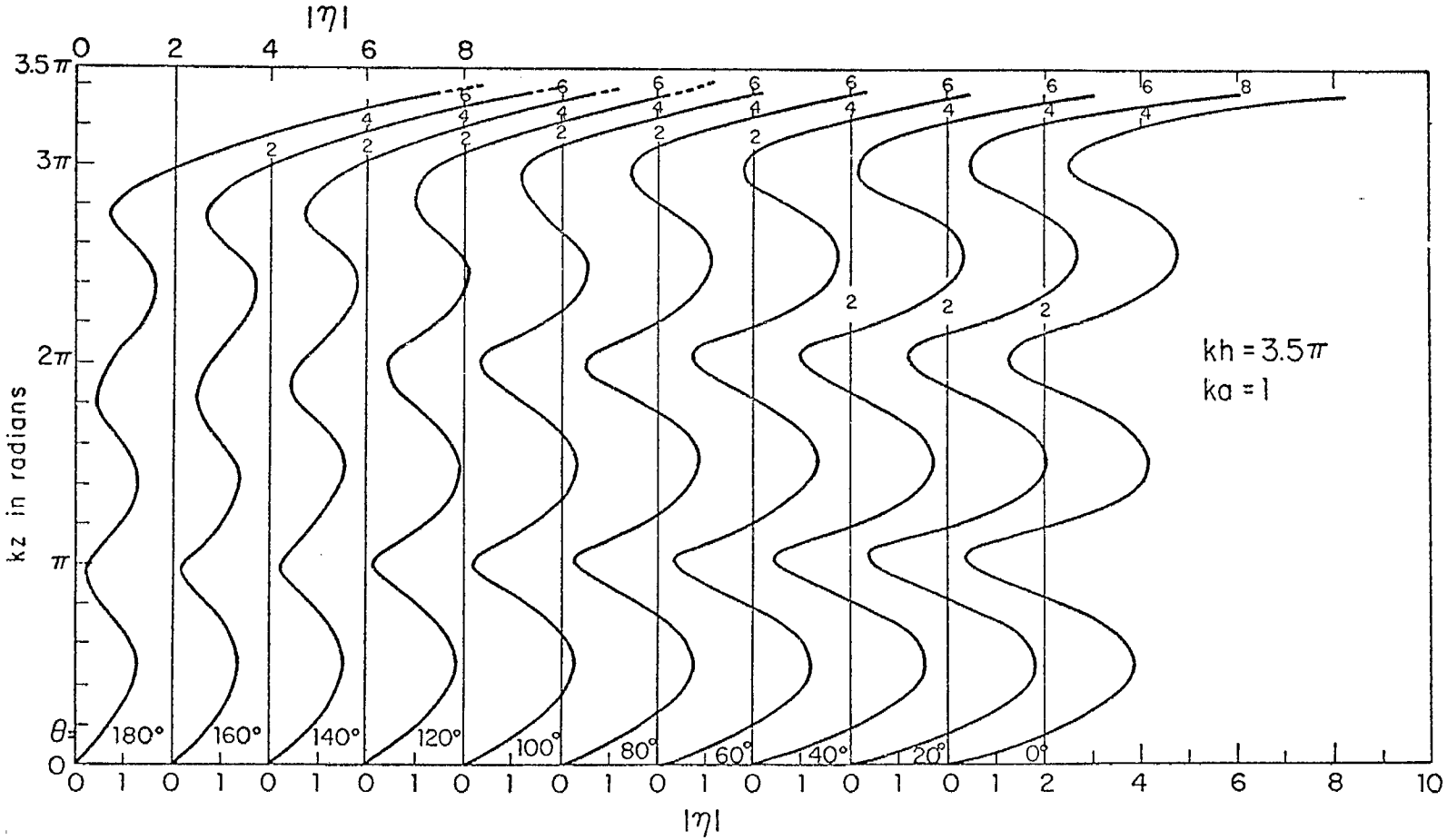

Fig. 38. Theoretical magnitude of surface density of outside charge on tubular cylinder; E-polarization, normal incidence.

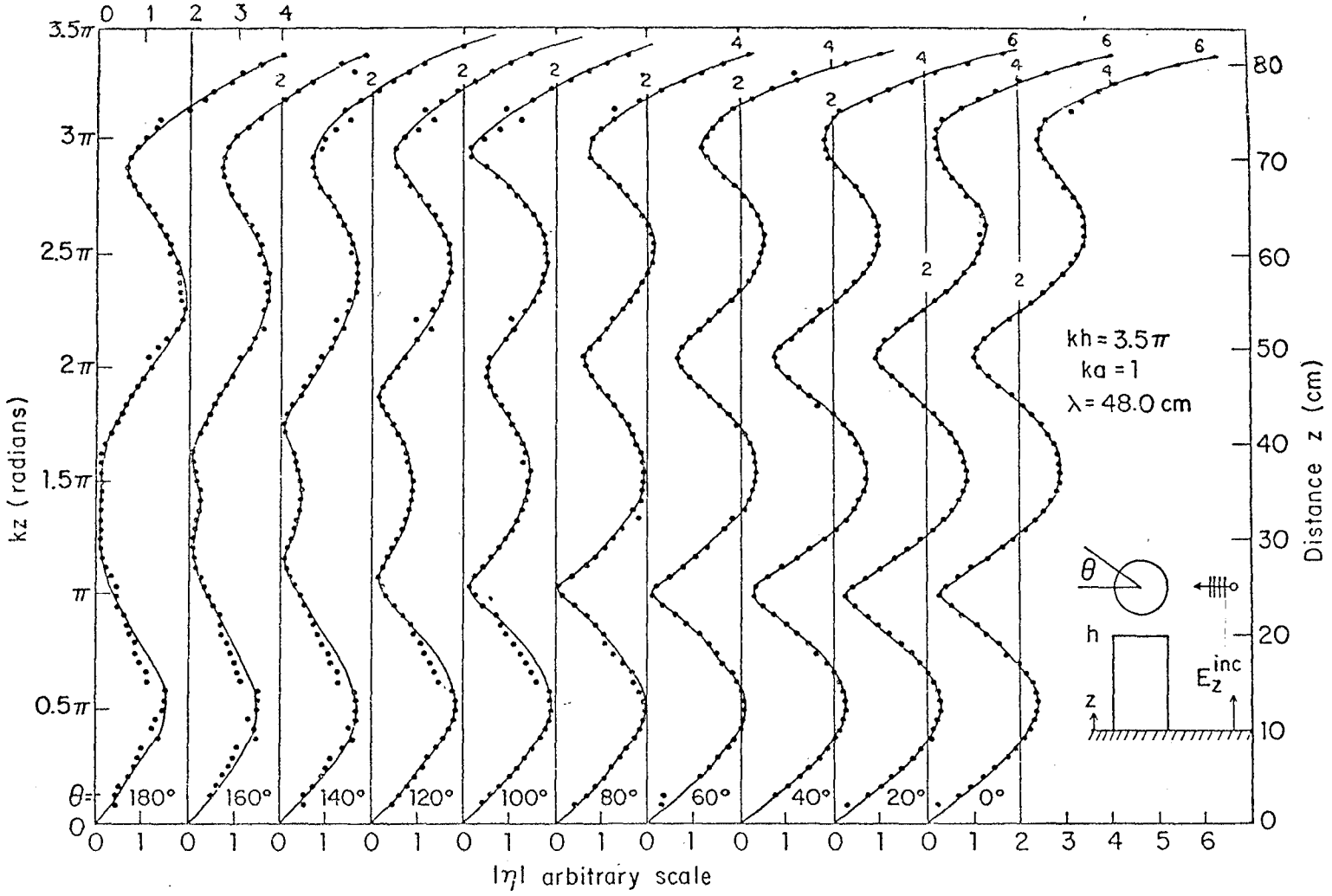

Fig. 39. Measured magnitude of surface density of outside charge on tubular cylinder; E-polarization, normal incidence.

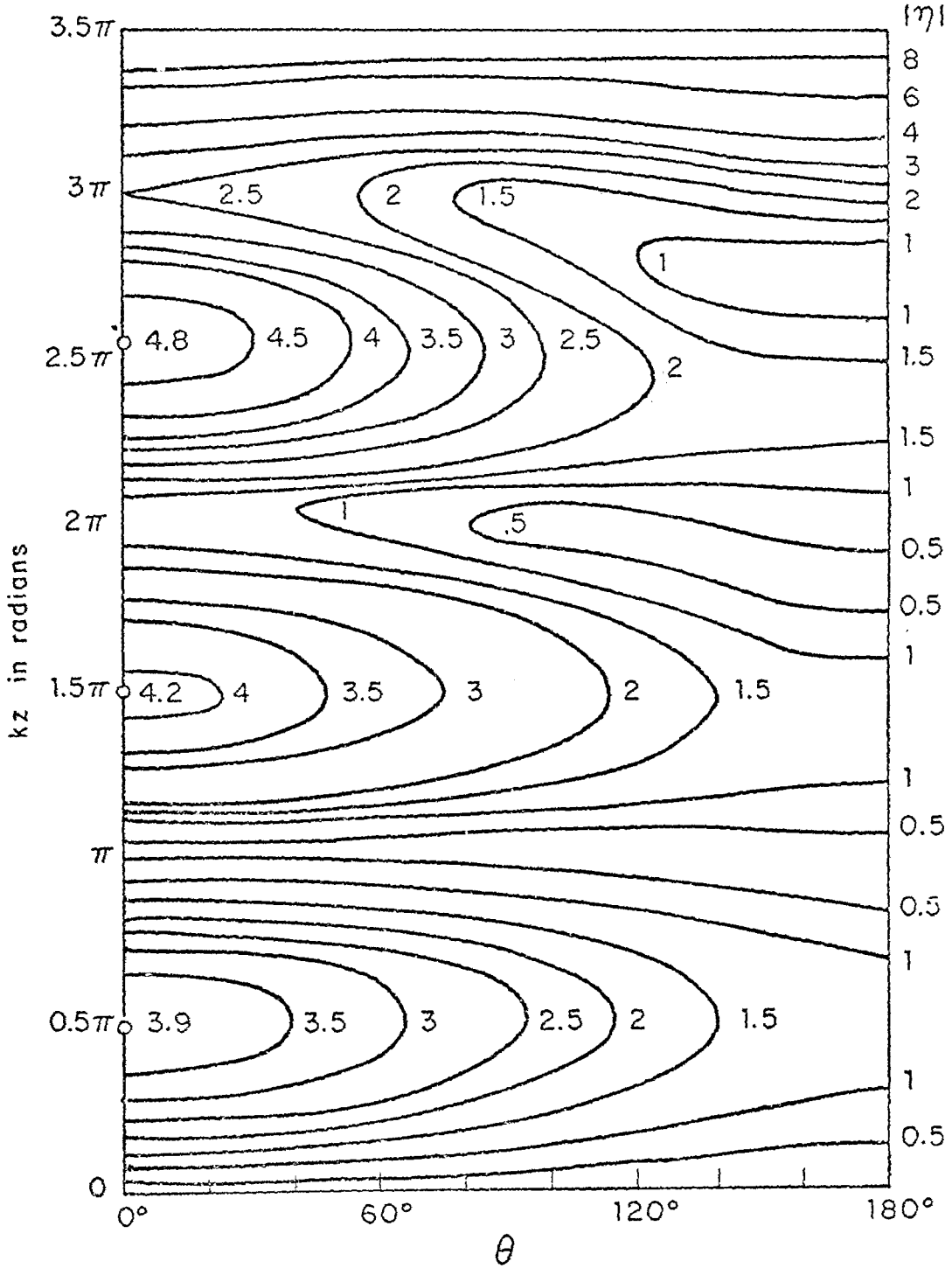

Fig. 40. Contour diagram of theoretical surface density of outside charge on tubular cylinder; E-polarization, normal incidence; kh = 3.5π, ka = 1.

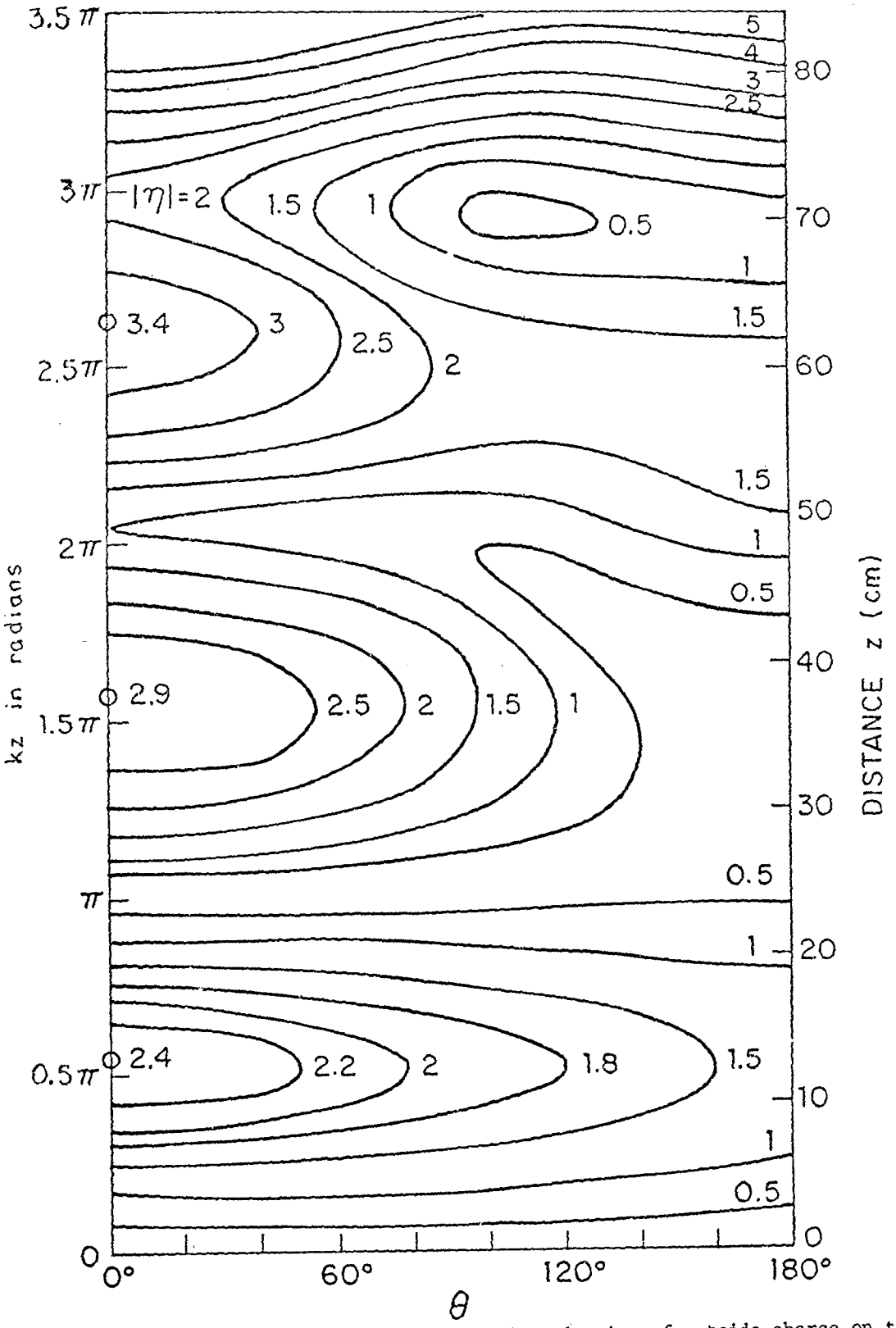

Fig. 41. Contour diagram of measured surface density of outside charge on tubular cylinder; E-polarization, normal incidence; kh = 3.5π, ka = 1, λ = 48.0 cm.

SECTION VIII

FOURIER COMPONENTS OF THE TOTAL CURRENT

In the interpretation of the distributions of current and charge on a conducting tube, the properties of the individual transverse Fourier components are useful since they are individually one-dimensional. Graphs of the coefficients $A(kz) = A_R(kz) + iA_I(kz)$ through $D(kz) = D_R(kz) + iD_I(kz)$ of $K_z(0,z)$ as given by (5.10) are shown in Fig. 42 for three resonant lengths, viz., $kh = 1.5\pi$, 2.5π and 3.5π, and in Fig. 43 for lengths between $kh = 2\pi$ and 3π in steps of 0.2π. The coefficients $E(kz)$ and $F(kz)$ are negligibly small. The constant coefficients $A = A_R + iA_I$ through $D = D_R + iD_I$ for the infinitely long tube with the same radius are shown on the right in the figures. It is seen that both the real and imaginary parts of $C(kz)$ and $D(kz)$ differ negligibly from C and D, respectively, except within about a quarter wavelength of the end where they decrease smoothly to zero. This type of distribution has already been encountered in Sec. III and approximated by the function $e(kz)$ defined in (3.8) and shown in Fig. 9. With it

$$C(kz) \doteq Ce(kz) \quad , \quad D(kz) \doteq De(kz) \tag{8.1}$$

The first two coefficients include both forced and resonant components in the manner of (3.7). Thus, for resonant lengths

$$A(kz) = A_f(kz) + A_r(kz)\cos kz \doteq Ae(kz) + A_r(kz)\cos kz \tag{8.2}$$

$$B(kz) = B_f(kz) + B_r(kz)\cos kz \doteq Be(kz) + B_r(kz)\cos kz \tag{8.3}$$

The amplitudes $A_r(kz)$ and $B_r(kz)$ can be determined in each case by noting that $A_{rR}(kz)$, $A_{rI}(kz)$, $B_{rR}(kz)$ and $B_{rI}(kz)$ must each vanish at $kz = \pi/2$. Graphs of these resonant components and of the forced components $A_{fR}(kz) \doteq A_Re(kz)$, $A_{fI}(kz) \doteq A_Ie(kz)$, $B_{fR}(kz) \doteq B_Re(kz)$ and $B_{fI}(kz) \doteq B_Ie(kz)$ are in

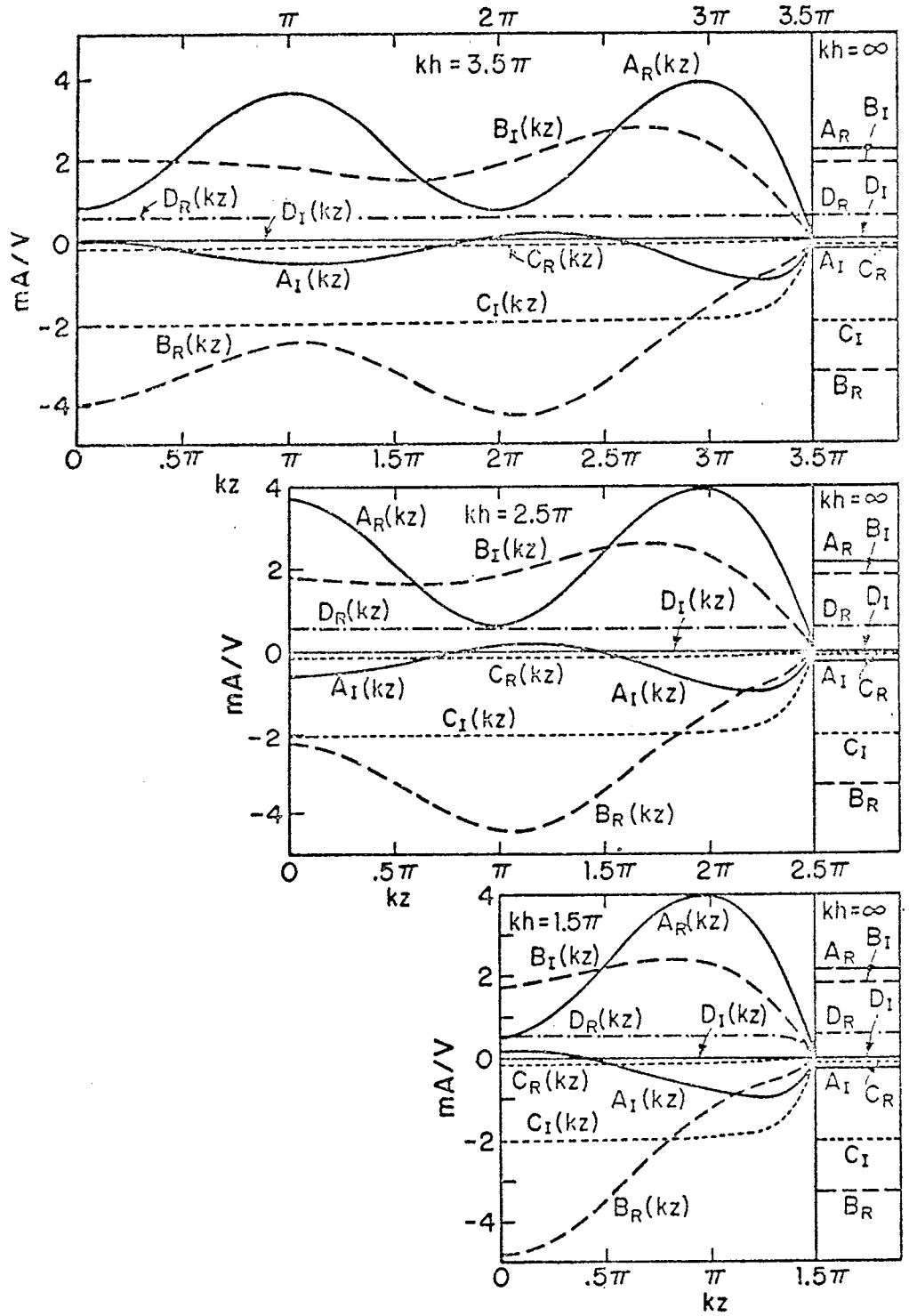

Fig. 42. Fourier coefficients of surface density of axial current on tubular cylinder, $K_z(\theta,z) = A(kz) + B(kz)\cos\theta + C(kz)\cos 2\theta + D(kz)\cos 3\theta$; E-polarization, normal incidence; ka = 1.

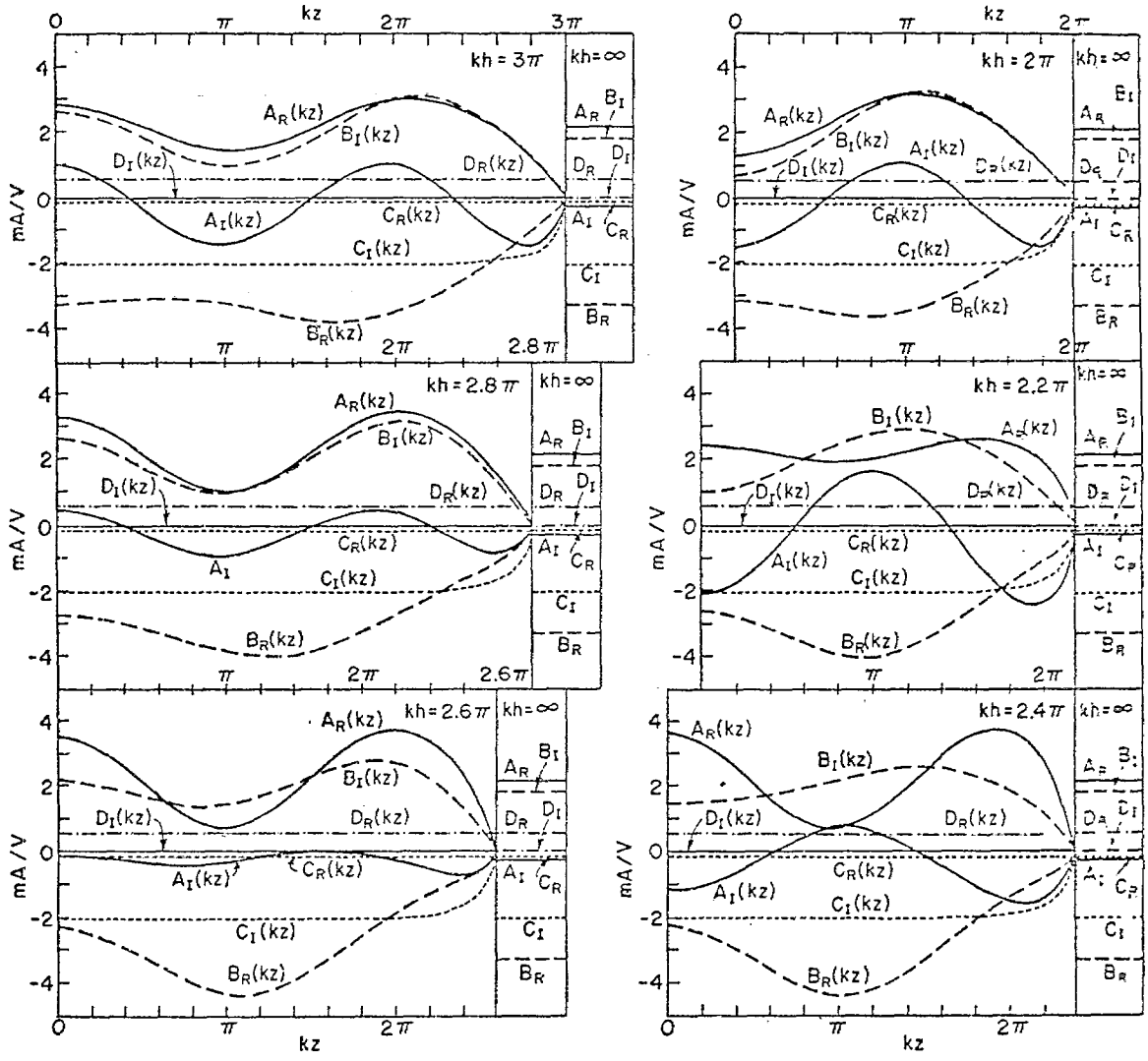

Fig. 43. Fourier coefficients of surface density of axial current on tubular cylinder, $K_z(\theta,z) = A(kz) + B(kz)\cos\theta + C(kz)\cos 2\theta + D(kz)\cos 3\theta$; E-polarization, normal incidence; ka = 1.

Fig. 44. The constants A_R, A_I, B_R and B_I are also shown. It is seen that approximations of the type $A_{fR}(kz) \doteq A_R e(kz)$ are moderately good but that the decreases to zero near the open end are all somewhat different.

When the length of the tube is not resonant, the generalized form (3.11) may be used. Thus,

$$K_z(\theta,z) \doteq [(A + A_r \cos kh) + (B + B_r \cos kh)\cos\theta + C \cos 2\theta + D \cos 3\theta] \times e(kz) + (A_r + B_r \cos\theta)(\cos kz - \cos kh) \tag{8.4}$$

An application of this formula to a tube with $ka = 1$ and $kh = 3\pi$ follows:

$$K_z(\theta,z) \doteq [(A - A_r) + (B - B_r)\cos\theta + C \cos 2\theta + D \cos 3\theta]e(kz) + (A_r + B_r \cos\theta)(\cos kz + 1) \tag{8.5}$$

From Table 1 for $ka = 1$, $A = 2.18 - i0.25$, $B = -3.28 + i1.85$. The evaluation of A_r and B_r can be carried out as follows. Consider first $A_R(kz) = (A_R - A_{rR}) \times e(kz) + A_{rR}(\cos kz + 1)$. With $A_{rR} \doteq (1/2)[A_R(0) - A_R(\pi)] \doteq (1/2)[A_R(2\pi) - A_R(\pi)]$ and the above numerical values, $A_{rR} \doteq 0.78$. Similarly, $A_{rI} \doteq 1.20$. It follows that

$$A(kz) \doteq (1.40 - i1.45)e(kz) + (0.78 + i1.20)(\cos kz + 1) \tag{8.6a}$$

Similarly,

$$B(kz) \doteq (-2.98 + i0.92)e(kz) + (-0.30 + i0.93)(\cos kz + 1) \tag{8.6b}$$

$$C(kz) \doteq Ce(kz) \doteq -(0.14 + i2.04)e(kz) \tag{8.6c}$$

$$D(kz) \doteq De(kz) \doteq 0.58e(kz) \tag{8.6d}$$

$$E(kz) \doteq Ee(kz) \doteq i0.10e(kz) \tag{8.6e}$$

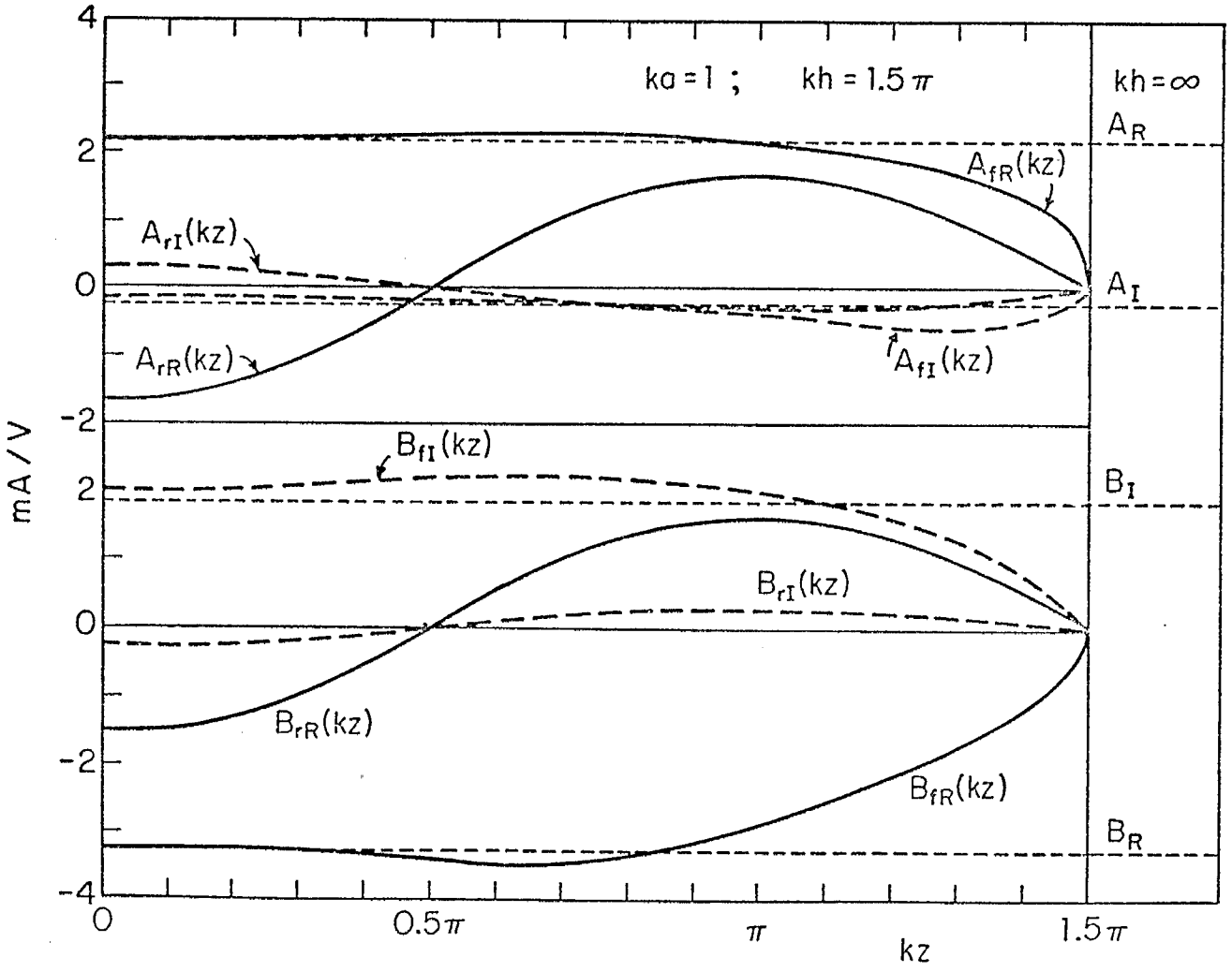

Fig. 44. Fourier coefficients A(kz) and B(kz) of $K_z(\theta,z)$ resolved into resonant and forced components.

Graphs of these coefficients as given in Table 3 are in Fig. 45 on the left, and as computed from the approximate formulas (8.6a-e) in Fig. 45 on the right. The correspondence is seen to be quite good with differences primarily in the rates of decrease near the open end due to the use of a single function e(kz) to represent all components. Graphs of the individual components of the first two modes are shown in Fig. 46.

The transverse currents on all cylinders are given by

$$K_\theta(\theta,z) \doteq i[B'(kz)\sin\theta + C'(kz)\sin 2\theta] \tag{8.7}$$

where $B'(kz)$ and $C'(kz)$ are in Table 3 for $kh = 1.5\pi$ and Table 5 for $kh = 3\pi$. They decay rapidly with increasing distance from the open end.

With the distributions of the vector surface density of current $\vec{K}(\theta,z)$ and of the surface density of charge $\eta(\theta,z)$ available on cylinders with $ka = 1$ over a range of lengths together with representations in terms of their transverse Fourier components, the information needed for a summarizing explanation of the underlying phenomena with E-polarization is at hand. For reference, note first that on the infinitely long cylinder the surface density of current $\vec{K}(\theta,z)$ reduces to $\hat{z}K_z(\theta)$ which is independent of z and entirely forced; $K_\theta(\theta) = 0$ and $\eta(\theta) = 0$. The real and imaginary parts of $K_z(\theta)$ are well approximated by

$$K_{zR}(\theta) \doteq A_R + B_R\cos\theta + D_R\cos 3\theta$$

$$\doteq 2.18 - 3.28\cos\theta + 0.58\cos 3\theta \quad \text{mA/V} \tag{8.8a}$$

$$K_{zI}(\theta) \doteq A_I + B_I\cos\theta + C_I\cos 2\theta$$

$$\doteq -0.25 + 1.85\cos\theta - 2.04\cos 2\theta \quad \text{mA/V} \tag{8.8b}$$

These distributions are shown in Fig. 22c in curves of crosses.

When the cylinder extends only from $z = -h$ to $z = h$, the condition

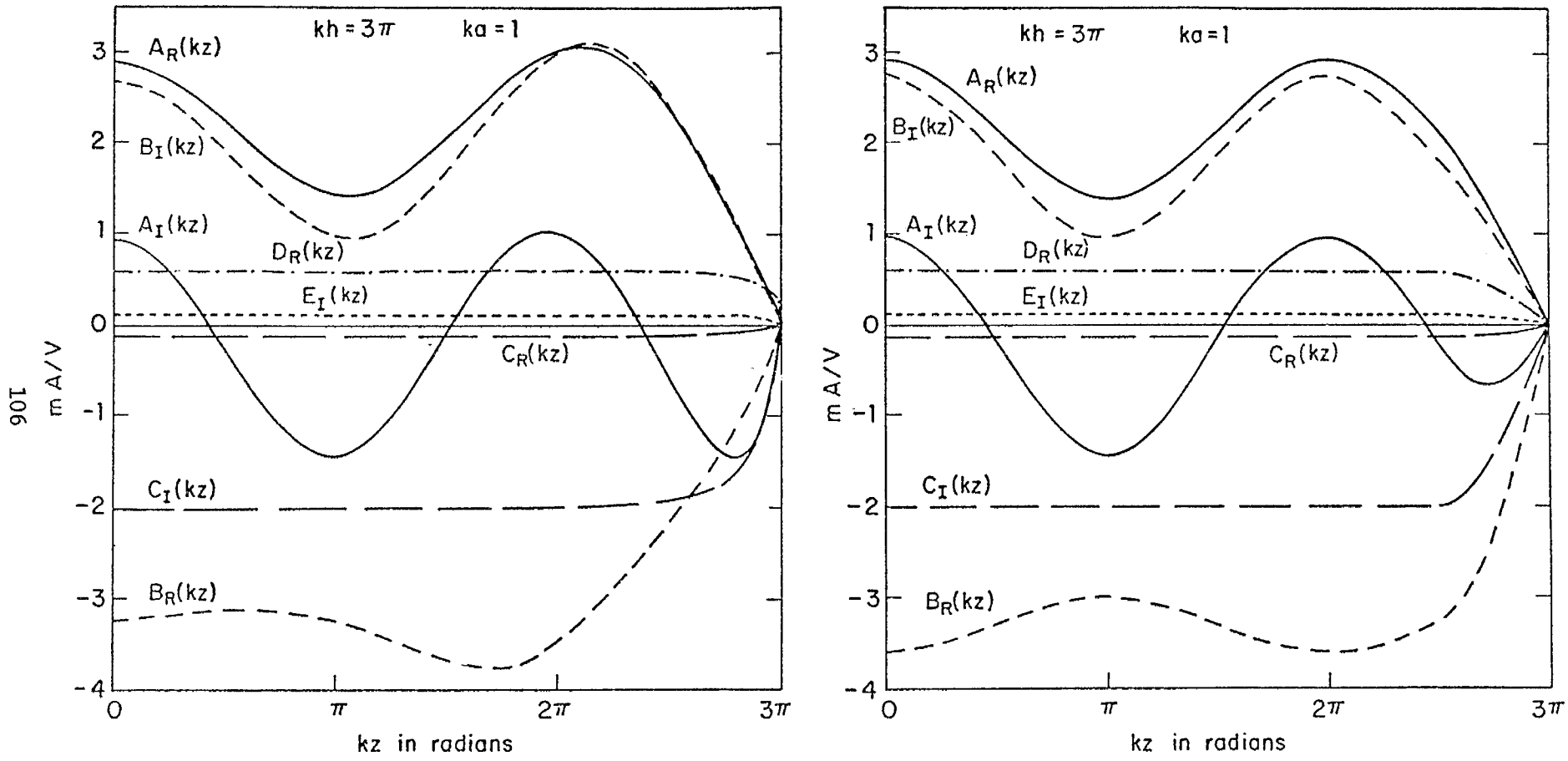

Fig. 45. Theoretical (left) and approximate (right) Fourier coefficients of surface density of axial current $K_z(\theta,z)$ on tubular cylinder; E-polarization, normal incidence.

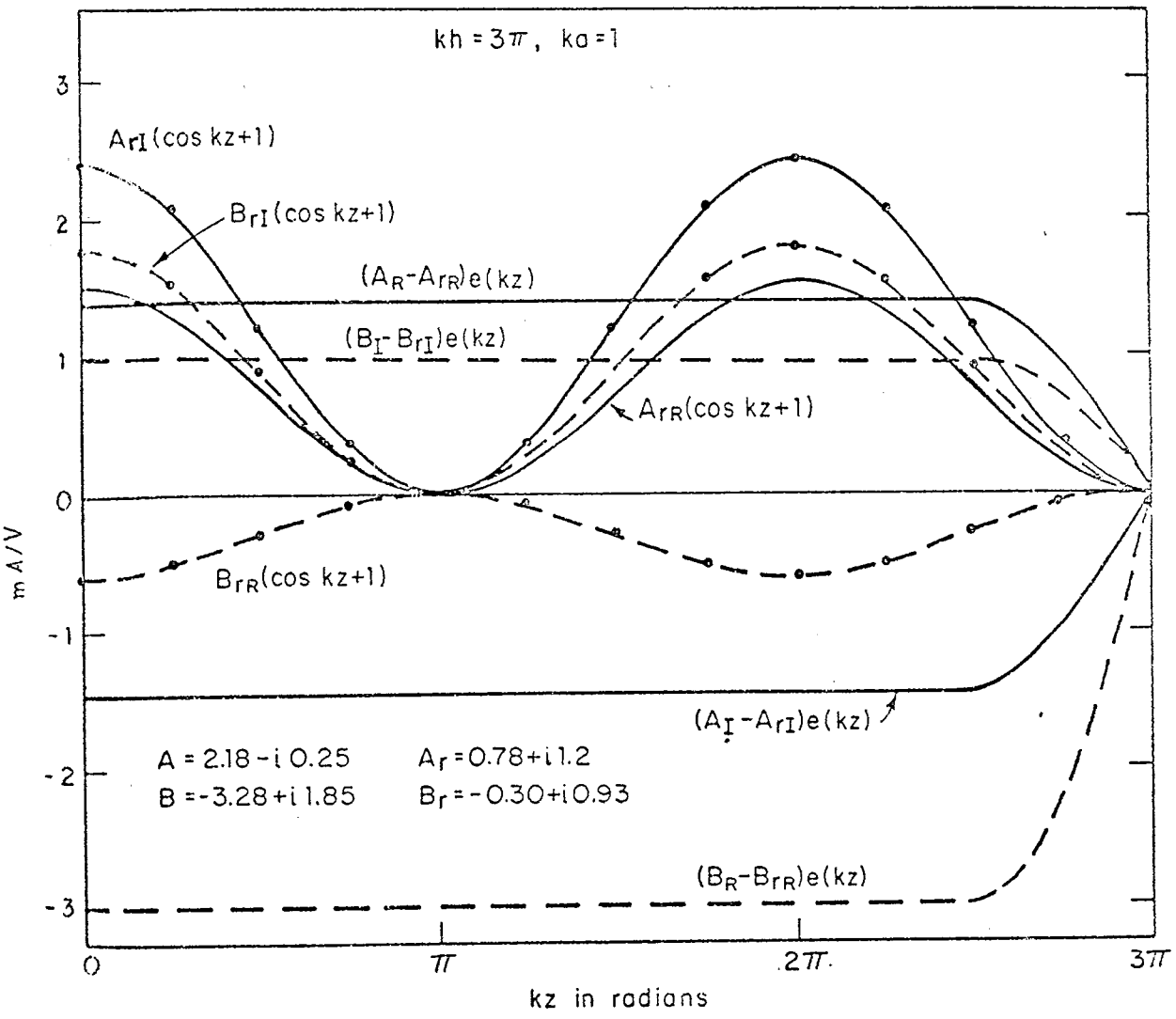

Fig. 46. Components in the approximate representation shown on right in Fig. 45: $A(kz) = (A - A_r)e(kz) + A_r(\cos kz + 1)$, $B(kz) = (B - B_r)e(kz) + B_r(\cos kz + 1)$.

$K_z(\theta,z) = 0$ at $|z| = h$ is satisfied for each Fourier coefficient. This involves high concentrations of suitably distributed charges near the ends and associated reflected currents that cancel the forced currents of the infinitely long tube within a distance of the order of a quarter wavelength of the end. Although the manner in which these reflected currents decrease varies somewhat with each Fourier component, an approximation for all of them is $1 - e(kz)$ where $e(kz)$ is defined in (3.8) and illustrated in Fig. 9. The forced part of the current on a finite cylinder is approximately like that on an infinite one in its transverse distribution and in its axially constant value except within about a quarter wavelength of the open ends where the total current decreases smoothly to zero. (On a metal tube where separate outside and inside currents exist, the outside current continues over the edges at the ends into the interior where it becomes the inside current that decays within about a quarter wavelength when $ka = 1$.)

The concentrations of charges at the ends associated with each Fourier component of forced current excite axially resonant currents. For example, when $kh = 1.5\pi$, the rotationally symmetric part of the charges excites currents of the form $A_r(kz) \doteq A_r \cos kz$ with an associated charge proportional to $(i/c)A_r \sin kz$. Similarly, the charges at the ends with the transverse distribution $B_f(kz)\cos\theta$ excite axially resonant currents $B_r(kz) \doteq B_r \cos kz$ with the transverse distribution $\cos\theta$. Evidently, the resonant currents $B_r(kz)\cos\theta$ on the illuminated side of the cylinder where $\cos\theta$ is negative are equal and opposite to the currents at the corresponding points on the shadow side where $\cos\theta$ is positive. In effect, the halves of the cylinder are equivalent to a two-conductor transmission line for the currents with the Fourier coefficient $B_r(kz)$. The associated charges vary axially as $\sin kz$, and transversely as $\cos\theta$. Since with $ka = 1$ the distance half-way around

the cylinder is a half wavelength, near resonant transverse currents are excited near the ends. Thus, the two-conductor transmission line formed by the halves of the cylinder with axial currents $B_r(kz)\cos\theta$ is, in effect, short-circuited at the ends which carry transverse currents $B'(kz)\sin\theta$ around the cylinder. The resonant part $B_r(kz)$ of the Fourier component $B(kz)$ of the axial current combines with the component $B'(kz)$ of the transverse current to form a two-dimensional standing-wave pattern on the surface of the tube. There is, of course, an associated standing-wave pattern of surface charge. The superposition of the forced currents (which are axially constant with no associated charge except near the ends) and the resonant components associated with the rotationally symmetric $A_r(kz)$ and with the non-rotationally symmetric $B_r(kz)\cos\theta$ and $B'(kz)\sin\theta$ (significant only near the ends) in a generalized two-conductor-line type of distribution, serves to characterize the distributions of current on a cylinder of resonant length. The higher Fourier modes contribute relatively little. The current on the surface of a cylinder of resonant length but not within a quarter wavelength of the ends consists primarily of the axial forced current, $A + B\cos\theta + C\cos 2\theta + D\cos 3\theta + \ldots$, like that on an infinitely long tube and the superimposed axial resonant current, $(A_r + B_r\cos\theta)\cos kz$. In the quarter wavelength at each end, the axial forced current decreases to zero in a complicated manner approximated by the function $e(kz)$ and transverse currents with large amplitudes are generated. These play the role of currents in the terminations for the non-rotationally symmetric parts of the axial currents.

SECTION IX

CROSSED ELECTRICALLY THICK TUBES; ka = 1

When two tubular cylinders with electrically large cross sections (ka = 1) intersect at right angles (as shown in Fig. 47 for a cross on a ground plane) and the entire structure is illuminated by an incident plane wave, the induced currents and charges are distributed in highly complicated patterns over the conducting surfaces even when the wave is normally incident and the electric vector is parallel to the axis of the vertical tube. The investigation of these distributions for various lengths of the four members and locations of their junction necessarily involves extensive experimental work which is far from completed. A few samples of the results obtained so far and attempts at their interpretation follow.

When the crossed cylinders shown in Fig. 47 are isolated (i.e., with the indicated ground plane removed) and the origin of coordinates is at their junction, they correspond exactly to the cross shown in Fig. 13. The vertical cylinder extends between the open ends at $z = -h_1$ and $z = h_2$, the horizontal one between the open ends at $x = -\ell_1$ and $x = \ell_2$. However, the frequency of the incident wave in Fig. 13 was assumed to be low enough to satisfy the inequality $ka \ll 1$ so that transverse currents could be neglected, approximate local rotational symmetry assumed for each conductor, and total axial currents and charges per unit length defined. Furthermore, the junction region was electrically so small that the actual distributions of the charges on its entire surface could be ignored and, hence, the geometry of that surface treated as irrelevant. When ka = 1, none of these greatly simplifying approximations can be made. The incident field is E-polarized for the vertical tube, H-polarized for the horizontal one. In terms of the local cylindrical coordinates for each tube (i.e., ρ,θ,z for the vertical one and ρ,θ,x for the horizontal one with $\theta = 0°$ the shadow center, $\theta = 180°$ the

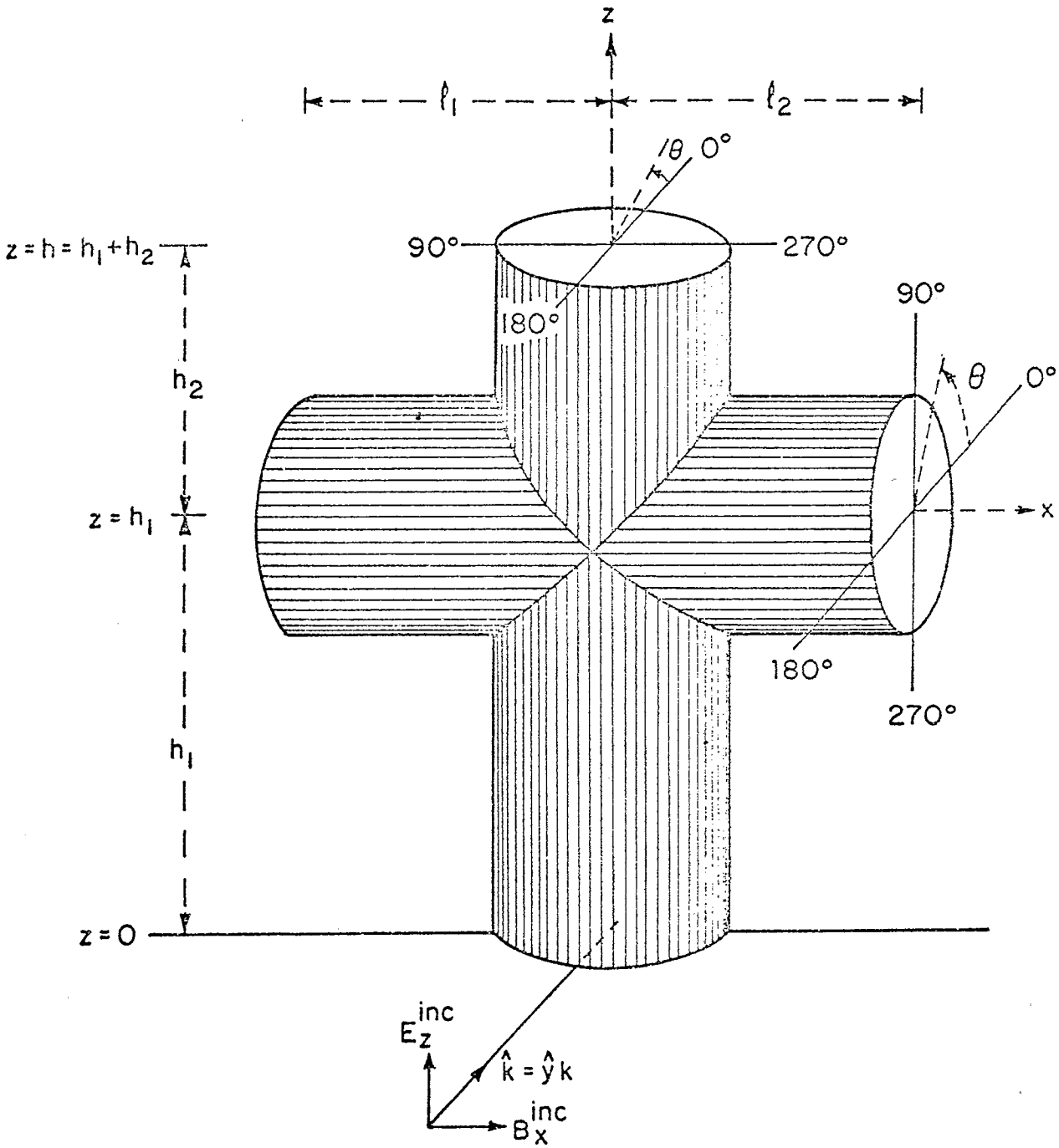

Fig. 47. Diagram of crossed electrically thick cylinders illuminated by normally incident, plane-wave field.

illuminated center for each tube) the primary induced current densities are $K_z(\theta,z)$ of the type defined in (5.7a) on the vertical tube, $K_\theta(\theta,x)$ of the type in (5.8b) on the horizontal one. Due to reflections at the ends and the junction and coupling between the tubes, transverse currents with the density $K_\theta(\theta,z)$ of the type in (5.7b) are generated on the vertical member and axial currents with the density $K_x(\theta,x)$ of the type in (5.8a) on the horizontal member. These last excite further transverse currents of the type (5.7b) that become a part of $K_\theta(\theta,x)$. Note that the component of $K_\theta(\theta,x)$ induced by the incident field is an even function of θ, that generated by the reflection of $K_x(\theta,x)$ at the ends is an odd function of θ.

The boundary conditions which determine the distributions of current and charge on the crossed tubular cylinders are: $\vec{E}_{tang} = 0$ at all points on the outside and inside surfaces of the crossed tubes, $K_z(\theta,z) = 0$ at the open ends at $z = -h_1$ and $z = h_2$, and $K_x(\theta,x) = 0$ at the open ends at $x = -\ell_1$ and $x = \ell_2$. [Note that $K_z(\theta,z)$ and $K_x(\theta,x)$ are total densities, i.e., inside plus outside currents.]

The complicated geometry of the crossed tubes makes the formulation of integral equations to determine $\vec{K}(\theta,z)$ and $\vec{K}(\theta,x)$ excessively difficult. However, it can be anticipated that at points not too close to the junction section the surface currents will be distributed in a manner that can be approximated by a superposition of the leading components in (5.7a,b) and (5.8a,b). This requires experimental verification with the probes and techniques tested on the uncrossed cylinder. The distributions of current and charge density on the surfaces of the cylinders near and in the junction region are both more complicated and more difficult to determine experimentally since probes cannot be moved over them conveniently. The junction region itself consists of sections of cylinders that meet in junction lines at angles

that range from 90° at the top and bottom ($\theta = 90°, 270°$) to 180° on the back and front ($\theta = 0°, 180°$). These lines are effectively the bottoms of grooves that wind diagonally around the junction. Although the metal surface is continuous across a junction line, its slope is not except when the angle is 180°. As a consequence, the component of the electric field normal to the surface has different directions as the junction line is approached from each side and must, therefore, reduce to zero in magnitude if it is to be continuous across that line. This means that the surface density of charge - which is proportional to the normal component of the electric field on a metal surface - must be zero along the entire junction line. (If the bottom of the junction is rounded instead of sharp, the zero becomes a minimum.) Thus, ideally in a contour diagram the junction line is a contour of constant (zero) charge density. Since the current along the groove must vanish, the current density crosses the groove at right angles and has a maximum or minimum there.

The fact that the charge density must be zero along the junction line does not mean that the sign of the charge is opposite on opposite sides or that the overall distribution in a standing-wave pattern determined by the boundaries of the structure as a whole is greatly modified. The charge density has substantially the same value and sign at short distances on each side of the junction line and may rise quite rapidly from zero in directions along the surfaces perpendicular to it. A standing-wave pattern of the charge density (determined by the overall lengths and circumferences of the tubes) can be expected to experience a locally sharp dip across the junction line and a spreading-out of the pattern in both directions from it due to the repulsion of charges with the same sign brought closer together on the sides of the groove than on a plane. But there should be no major change in the general shape of the pattern at a distance from the junction line. The zero in charge density occurs along the entire junction line except in a small

area on the front and back where the two junction lines cross and the angle of intersection of the surfaces of the horizontal and vertical cylinders is 180°. Monopole probes to measure the charge density can be moved axially along the entire lengths of both horizontal and vertical cylinders on both the front and the back ($\theta = 0°, 180°$). However, since such a probe has a small but finite length, it measures the average charge density over a small area around its base. It is, therefore, insensitive to sharp dips and nulls in the charge density that occur over distances comparable with its own length (unless the sign of the charge reverses).

The nature of the standing-wave pattern on the crossed cylinders is determined not only by the length of the four arms of the cylinders but also by the location of their junction. It is seen, for example, from Figs. 40 and 41 that if the horizontal cylinder is centered at $kz = 2.5\pi$, it will be located more or less symmetrically with respect to the charge maximum near $\theta = 0°$, $kz = 2.5\pi$; if centered at $kz = 2\pi$, it will be located symmetrically with respect to the charge minimum near $\theta = 0°$, $kz = 2\pi$. Distributions of induced current and charge densities for both of these locations must be studied for a range of lengths of the horizontal cylinder.

Measurements of surface current and charge densities have been made on crossed cylinders with $kh = 3.5\pi$ when the junction is centered near a charge maximum in the standing-wave pattern along the vertical member without cross, i.e., when $kh_1 = 2.5\pi$, $kh_2 = k\ell_1 = k\ell_2 = \pi$ as shown in Figs. 38 and 39. Graphs of $\eta(\theta,z)$ with $\theta = 0°$ and 180° are in Fig. 48. It is seen that the presence of the horizontal cylinder alters $|\eta(0°,z)|$ and $|\eta(180°,z)|$ primarily in the adjacent region where the third maximum disappears in $|\eta(0°,z)|$ and is greatly reduced in $|\eta(180°,z)|$. The overall standing-wave pattern including the first two maxima agree well with the theoretical graphs in Fig. 38

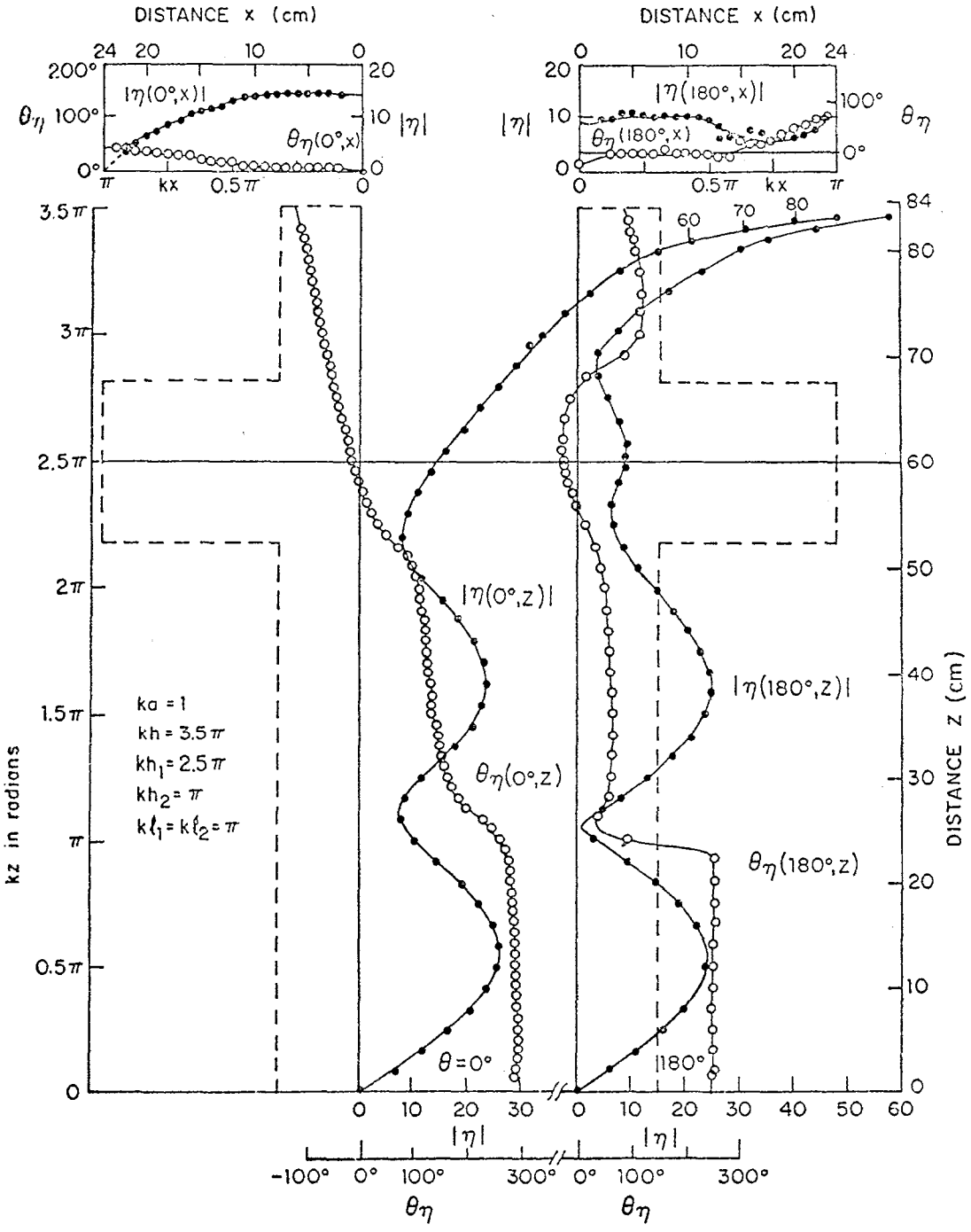

Fig. 48. Measured surface density of charge on crossed cylinder; E-polarization, normal incidence; $kh_1 = 2.5\pi$, $kh_2 = \pi$, $k\ell_1 = k\ell_2 = \pi$.

for the cylinder without cross. The anomalous disappearance of the second maximum of $|\eta(180°,z)|$ in the measured data in Fig. 39 does not occur when the cross is present. The graphs of $K_z(0°,z)$ and $K_z(180°,z)$ in Fig. 49 when compared with the corresponding curves in Fig. 32 for the same cylinder without cross also show the effect of the horizontal member to be confined primarily to the sections adjacent to the cross with no major changes in the standing-wave pattern at greater distances.

When the horizontal member is lowered and lengthened so that $kh_1 = 2\pi$, $kh_2 = k\ell_1 = k\ell_2 = 1.5\pi$, it becomes centered near a charge minimum in the unperturbed distributions in Fig. 38. The measured distributions of $\eta(0°,z)$ and $\eta(180°,z)$, shown in Fig. 50, again differ significantly from the corresponding theoretical distributions without cross (Fig. 38) only near the horizontal cylinder. The original standing-wave pattern as represented by the first and third maxima is not greatly changed. It is seen from Fig. 51 that $K_z(0°,z)$ and $K_z(180°,z)$ differ from the corresponding graphs in Fig. 32 primarily in the region at and near the horizontal cylinder.

The graphs in Figs. 48 through 51 are for the densities of surface current and charge only along the back and front ($\theta = 0°$, $180°$) where the probes can move continuously from the ground plane at $kz = 0$ to the open end at $kz = 3.5\pi$. Currents and charges on the surfaces below and above the horizontal cylinder were also measured to within a few centimeters of the junction lines. Graphs of the measured $|\eta(\theta,z)|$ with $kh_1 = 2\pi$, $kh_2 = k\ell_1 = k\ell_2 = 1.5\pi$ are shown in Fig. 52. The measured curves for values of θ other than $0°$ and $180°$ are shown extrapolated somewhat arbitrarily to the junction lines where $\eta(\theta,z) = 0$. The curves for $0°$ and $180°$ are the same as those in Fig. 50. Contours of constant $|\eta(\theta,z)|$ obtained from Fig. 52 are shown in Fig. 53 with the junction lines taken as surfaces of zero charge except near $\theta = 0°$ and

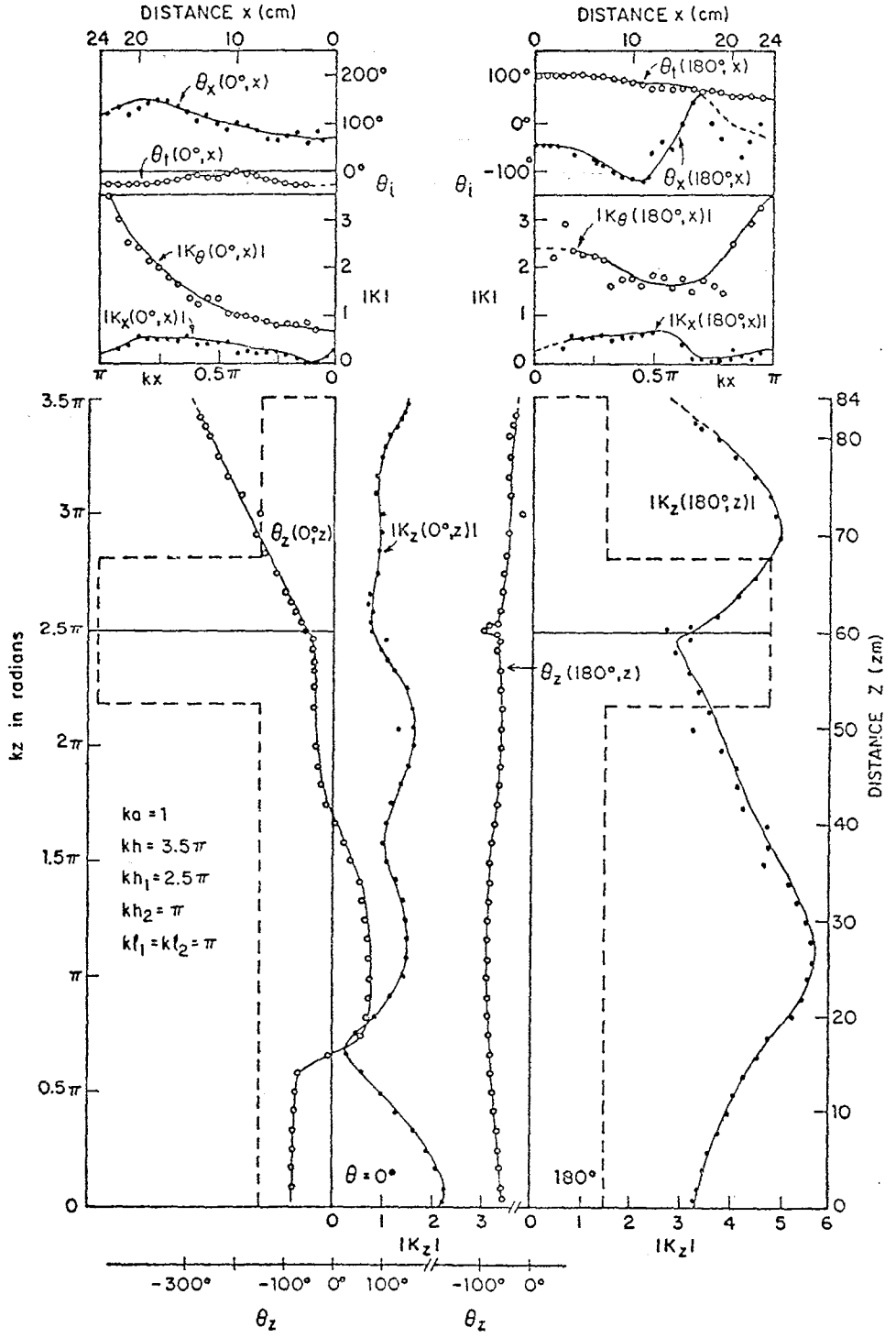

Fig. 49. Measured surface densities of current on crossed cylinders; E-polarization, normal incidence; $kh_1 = 2.5\pi$, $kh_2 = k\ell_1 = k\ell_2 = \pi$.

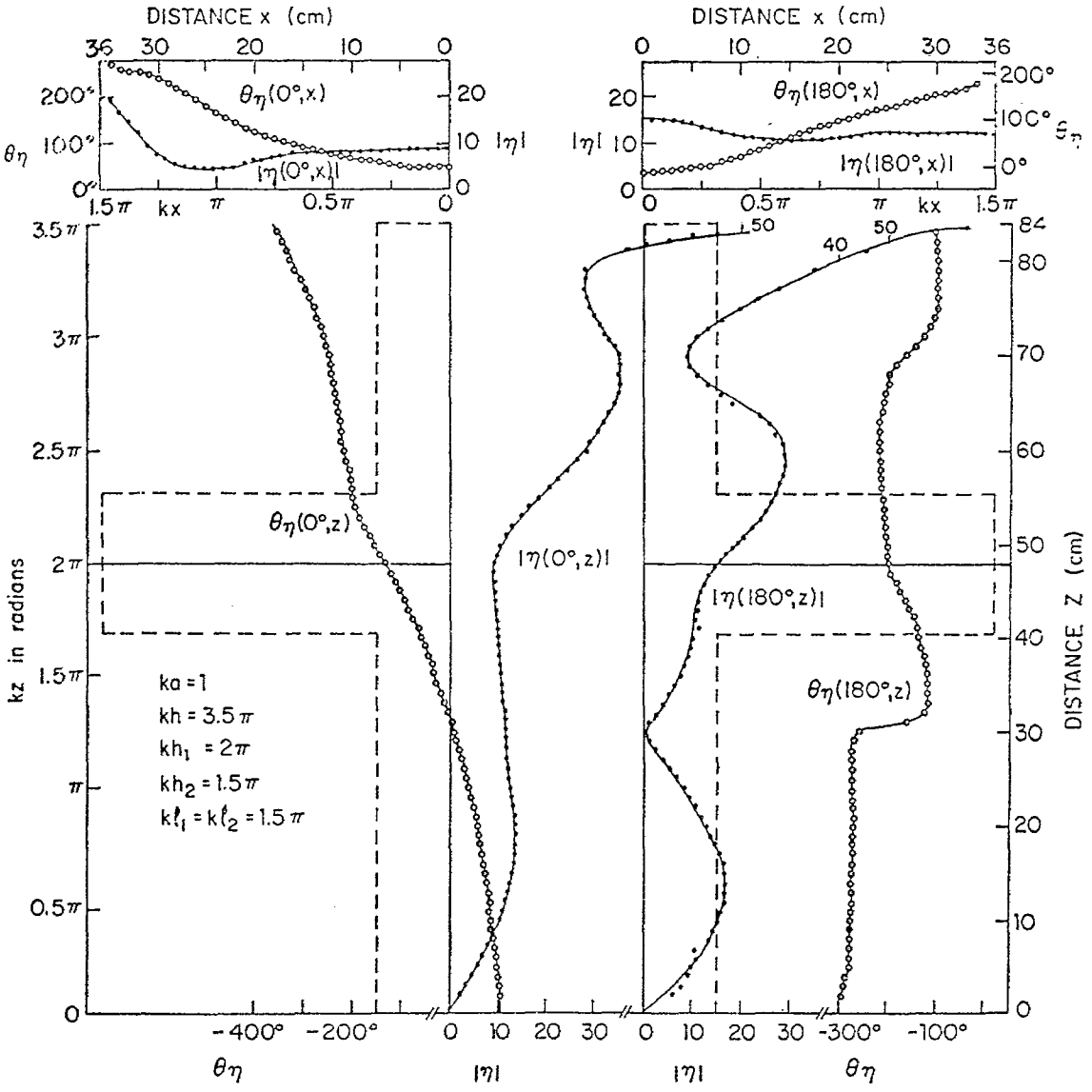

Fig. 50. Measured surface density of charge on crossed cylinders; E-polarization, normal incidence; $kh_1 = 2\pi$, $kh_2 = k\ell_1 = k\ell_2 = 1.5\pi$.

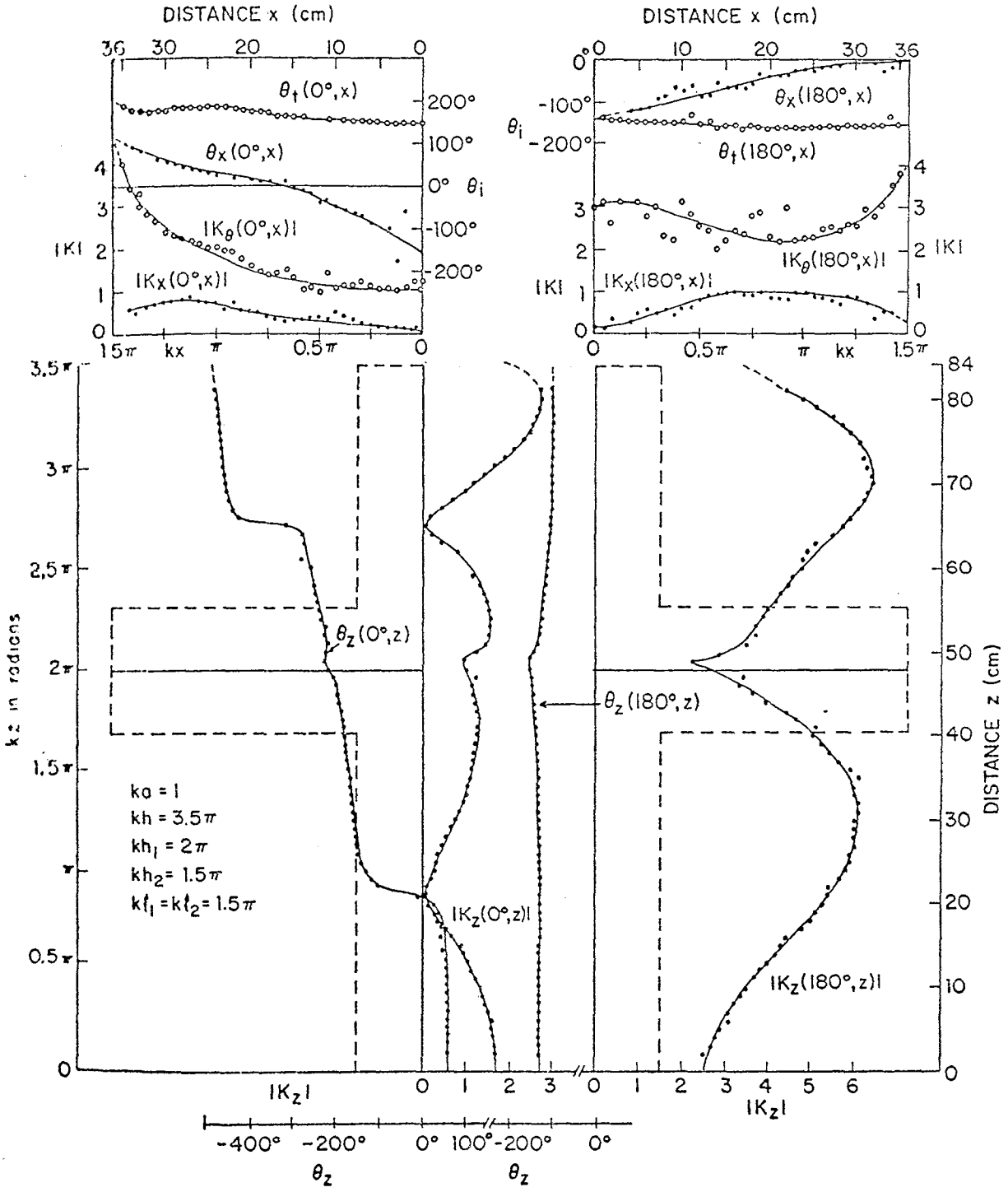

Fig. 51. Measured surface densities of current on crossed cylinders; E-polarization, normal incidence; $kh_1 = 2\pi$, $kh_2 = k\ell_1 = k\ell_2 = 1.5\pi$.

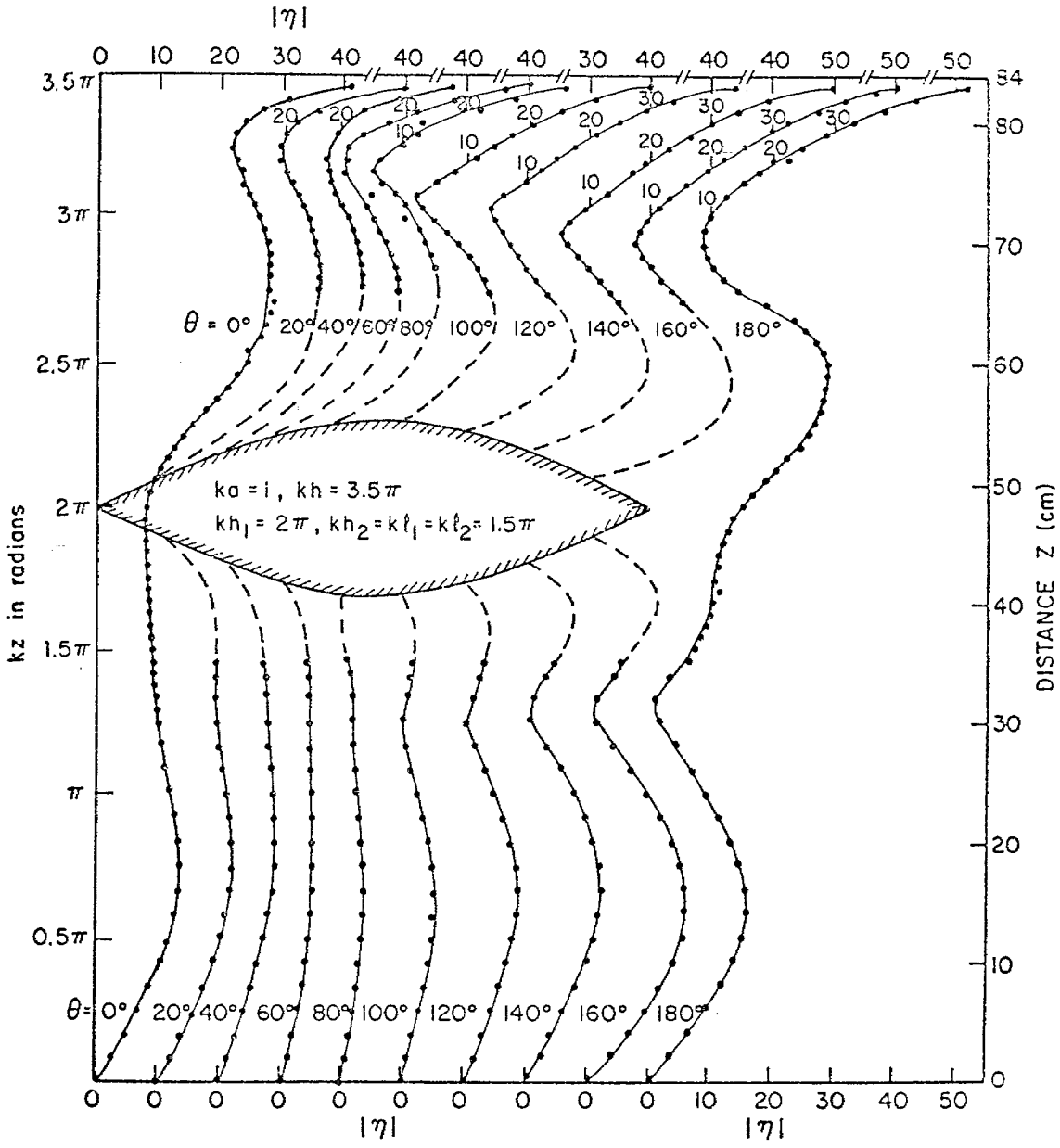

Fig. 52. Measured magnitude of surface density of charge on vertical member of crossed cylinders; E-polarization, normal incidence.

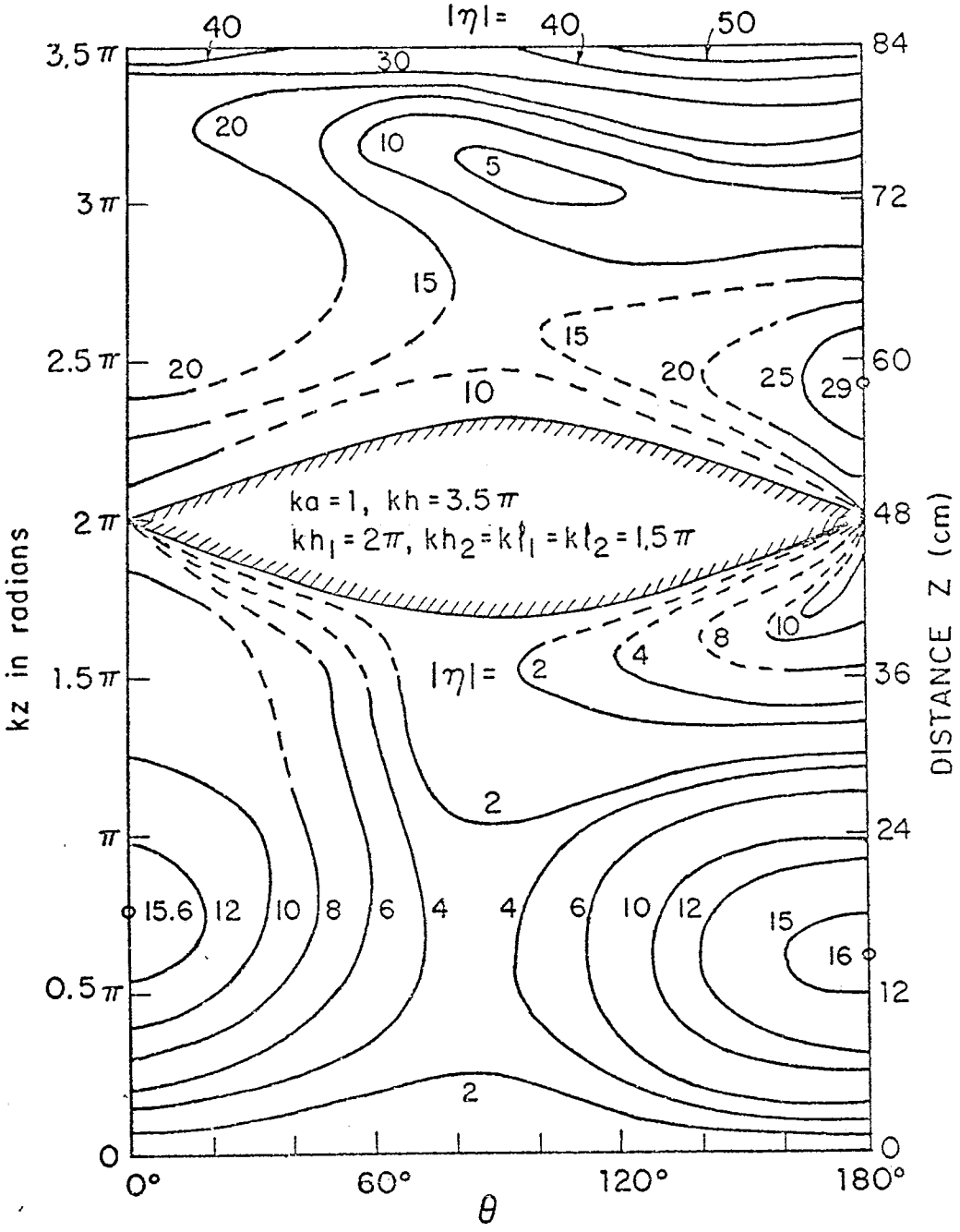

Fig. 53. Measured contours of constant density of charge on vertical member of crossed cylinders; E-polarization, normal incidence.

180°. A comparison of Fig. 52 with Figs. 38 and 39 and Fig. 53 with Figs. 40 and 41 confirms that the horizontal member has a significant effect on the general shape of the standing-wave pattern of $\eta(\theta,z)$ primarily at and near the cylinder. However, it is seen from both Figs. 52 and 53 that a relatively small charge maximum near $\theta = 180°$, $kz = 0.5\pi$ on the cylinder without cross becomes a very significant, much greater maximum with the horizontal cylinder present. The axial surface currents are in Fig. 54.

Distributions of surface current and charge on the back and front ($\theta = 0°, 180°$) of the horizontal member of the cross are included at the top in Figs. 48 through 51. The charge distributions on the entire horizontal cylinder when $kh_1 = 2\pi$, $kh_2 = k\ell_1 = k\ell_2 = 1.5\pi$ are shown in Fig. 55 with θ as a parameter at the bottom and as a contour diagram at the top. Since there is no angular symmetry, the graphs are shown for the full 360°. As for the vertical cylinder, the measured graphs have been extrapolated to $|\eta(\theta,x)| = 0$ at the junction lines. The extrapolated sections are necessarily somewhat arbitrary but they yield reasonable contours. It is seen that there are maxima of charge at the open ends ($kx = 1.5\pi$) at $\theta = 90°$ and 270°, i.e., the top and bottom. This transverse distribution is also shown in Fig. 56 at the top. On the same figure are the transverse distributions of both $K_x(\theta,x)$ and $K_\theta(\theta,x)$. It is seen that $K_x(\theta,x)$, like $\eta(\theta,x)$, has its maximum near $\theta = 90°$ and 270°. $K_\theta(\theta,x)$ includes induced currents excited by the H-polarized incident field and currents generated by the charges maintained near the ends by the axial current $K_x(\theta,x)$. These latter are large only near the open ends and account for much of the oscillation in the curve for $x = 32$ cm. At $x = 23$ cm the current is due primarily to the H-polarized incident field. Complete graphs of both $K_x(\theta,x)$ and $K_\theta(\theta,x)$ on the horizontal cylinder are in Fig. 57.

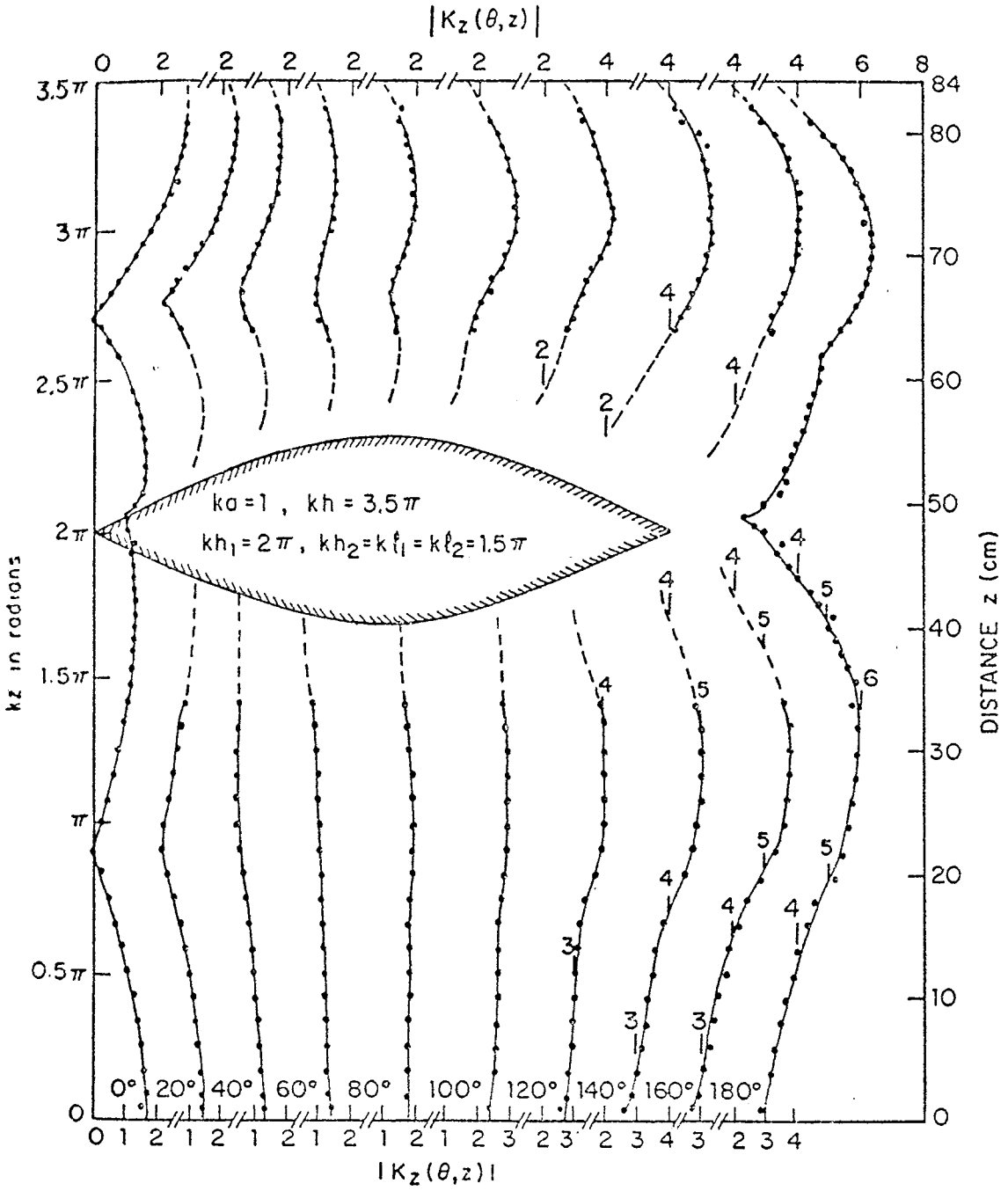

Fig. 54. Measured magnitude of surface density of axial current on vertical member of crossed cylinders; E-polarization, normal incidence.

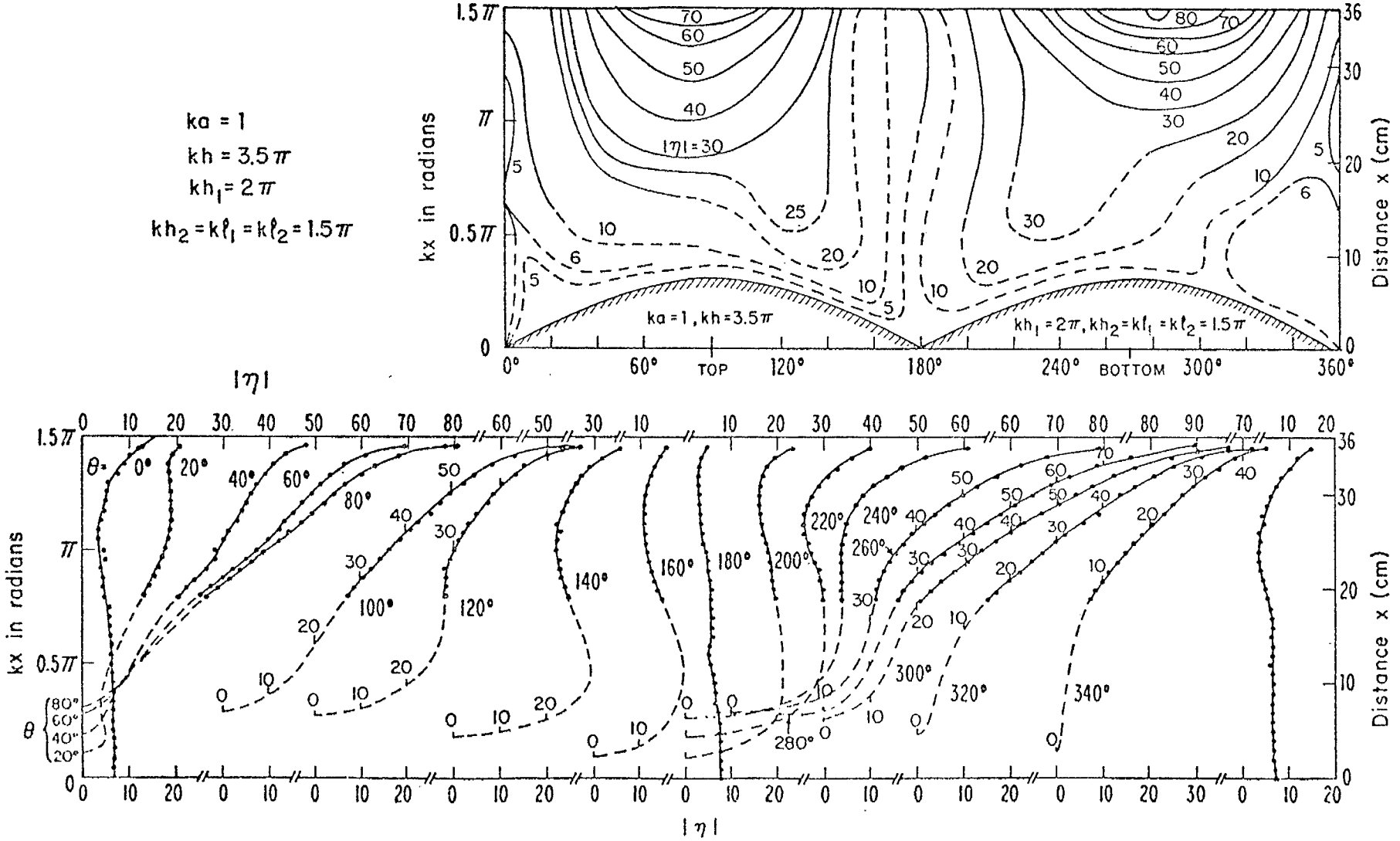

Fig. 55. Measured magnitude of surface density of charge on horizontal member of crossed cylinders; E-polarization for vertical cylinder, normal incidence.

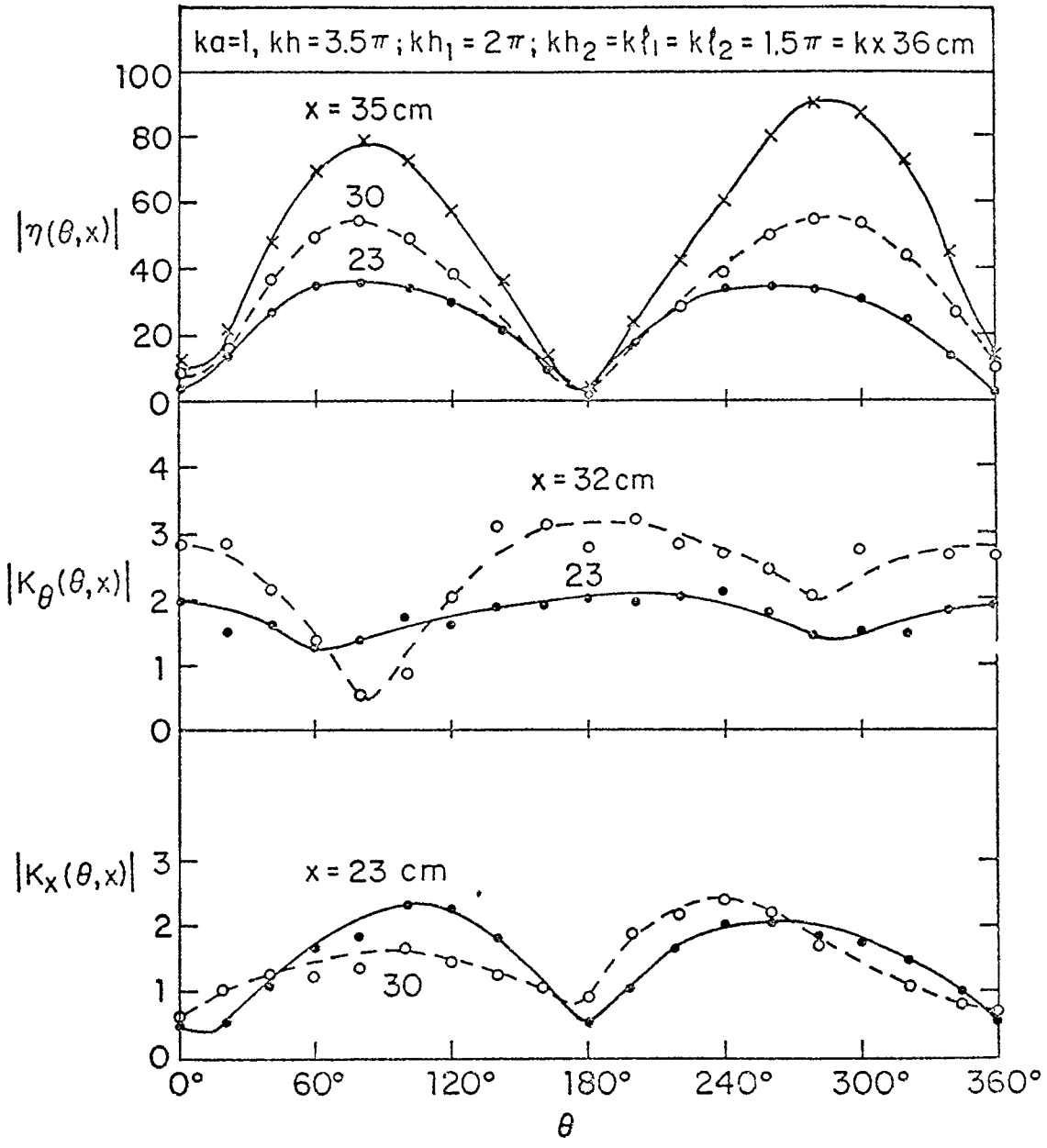

Fig. 56. Measured magnitudes of surface densities of charge and current on horizontal member of crossed cylinders; E-polarization for vertical cylinder, normal incidence.

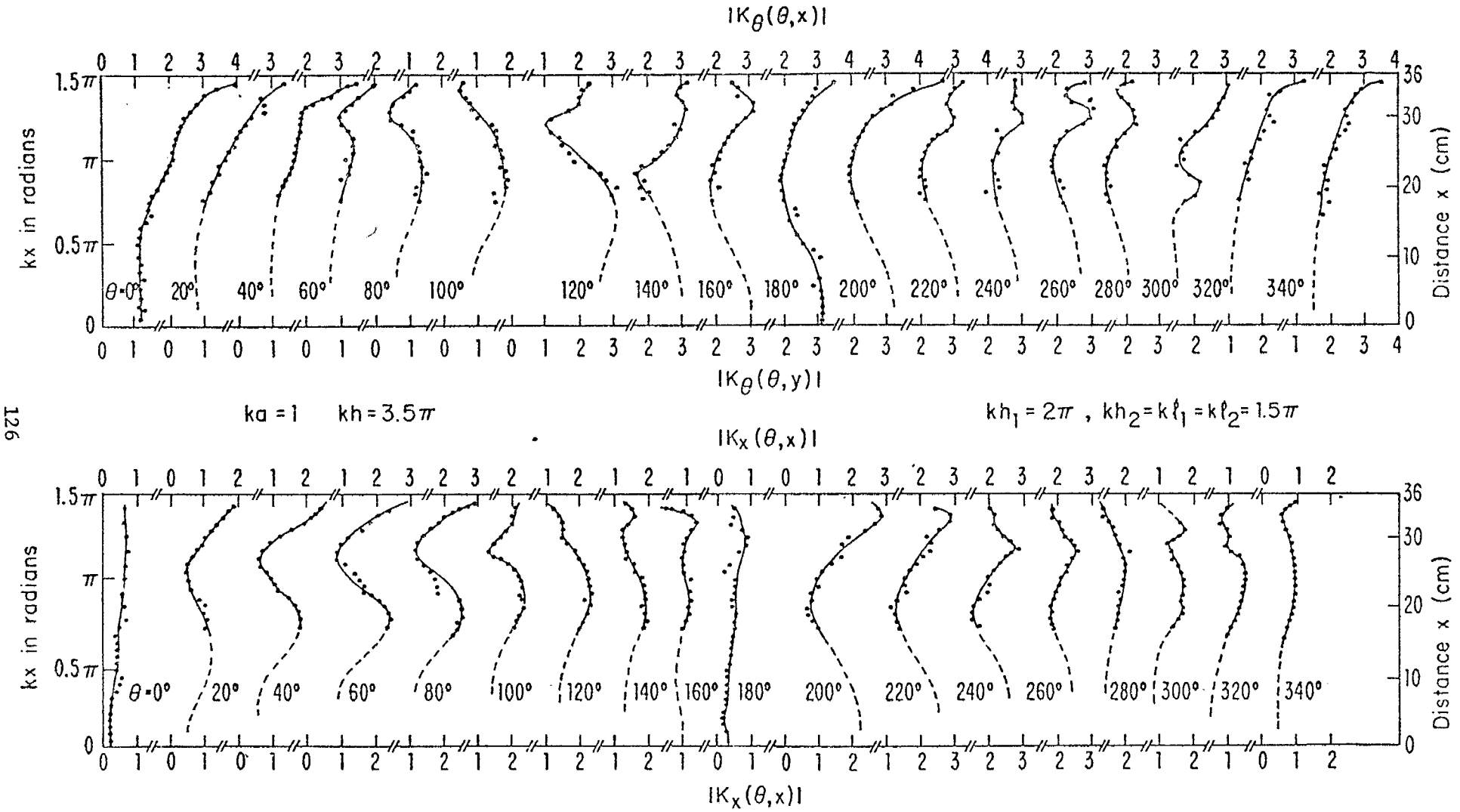

126

Fig. 57. Measured magnitudes of surface densities of current on horizontal member of crossed cylinders; E-polarization for vertical cylinder, normal incidence.

SECTION X

CONCLUSIONS

An introduction has been given to the problem of determining the distributions of surface current and charge on crossed metal structures, in particular, tubular cylinders. Pertinent knowledge about distributions of current and charge induced in thin wires, crossed thin wires, and cross-sectionally large tubes is presented as a foundation for acquiring an understanding for currents and charges induced in crossed electrically thick cylinders. It is shown that a representation of the distribution of current along a conductor excited by an E-polarized plane wave in terms of the transverse Fourier components and suitable combinations of forced and resonant components offers an attractive relatively simple approximation. Preliminary experimental investigation of crossed cylinders with ka = 1 indicates that the original standing-wave distributions of charge and current density are not greatly altered by the addition of the horizontal cylinder except in the vicinity of that member. Outside this vicinity the general nature of the standing waves is not changed significantly with respect to their location but large changes in the relative distributions of amplitude can occur. No data are yet available on crossed cylinders with other than normal incidence with the E-vector parallel to the vertical member.

REFERENCES

[1] C. D. Taylor and C. W. Harrison, Jr., "On the excitation of a coaxial line by an incident field propagating through a small aperture in the sheath," IEEE Trans. Electromag. Compat., vol. EMC-15, pp. 127-131, Aug. 1973, and also Interaction Notes, Note 104, Jan. 1972.

[2] C. W. Harrison, Jr. and R. W. P. King, "Excitation of a coaxial line through a transverse slot," IEEE Trans. Electromag. Compat., vol. EMC-14, pp. 107-112, Nov. 1972, and also Interaction Notes, Note 87, Oct. 1971.

[3] C. W. Harrison, Jr. and R. W. P. King, "Cylindrical shields," IRE Trans. Antennas Propagat., vol. AP-9, pp. 166-170, Mar. 1961, and also Interaction Notes, Note 30, Mar. 1961.

[4] C. W. Harrison, Jr. and R. W. P. King, "Transmission line coupled to a cylinder in an incident field," IEEE Trans. Electromag. Compat., vol. EMC-14, pp. 97-105, Aug. 1972, and also Interaction Notes, Note 72, May 1971.

[5] C. D. Taylor, "Electromagnetic scattering from arbitrary configurations of wires," IEEE Trans. Antennas Propagat., vol. AP-17, pp. 662-663, Sept. 1969, and also Interaction Notes, Note 42, 15 Nov. 1968.

[6] C. D. Taylor, S. M. Lin and H. V. McAdams, "Scattering from crossed wires," IEEE Trans. Antennas Propagat., vol. AP-18, pp. 133-136, Jan. 1970.

[7] C. M. Butler, "Currents induced in a pair of skew-crossed wires," IEEE Trans. Antennas Propagat., vol. AP-20, pp. 731-736, Nov. 1972.

[8] H. H. Chao and B. J. Strait, "Radiation and scattering by a configuration of bent wires with junctions," IEEE Trans. Antennas Propagat., vol. AP-19, pp. 701-702, Sept. 1971.

[9] J. C. Logan, "A comparison of techniques for treating radiation and scattering by wire configurations with junctions," Tech. Rept. TR-73-10, Dept. of Elec. and Computer Engineering, Syracuse University, Syracuse, N.Y., Aug. 1973.

[10] R. W. P. King and T. T. Wu, "Analysis of crossed wires in a plane-wave field," IEEE Trans. Electromag. Compat., vol. EMC-17, pp. 255-265, Nov. 1975, and also Interaction Notes, Note 268, Nov. 1975.

[11] T. T. Wu and R. W. P. King, "The tapered antenna and its application to the junction problem for thin wires," IEEE Trans. Antennas Propagat., vol. AP-24, pp. 42-45, Jan. 1976, and also Interaction Notes, Note 269, Jan. 1976.

[12] C. D. Taylor, K. T. Chen and T. T. Crow, "An improvement on wire modeling for determining the EMP interaction with aircraft," Interaction Notes, Note 241, October 1974.

[13] R. W. P. King and T. T. Wu, The Scattering and Diffraction of Waves. Cambridge, Mass.: Harvard University Press, 1959, Ch. II.

[14] C. C. Kao, "Electromagnetic scattering from a finite tubular cylinder: numerical solutions and data. I. Development of theory. II. Tables," A.F. Contract F19628-68-C-0030 Sci. Rept. No. 6, Div. of Engrg. and Appl. Phys., Harvard University, Cambridge, Mass.

[15] C. C. Kao, "Three-dimensional electromagnetic scattering from a circular tube of finite length," J. Appl. Phys., vol. 40, pp. 4732-4740, Nov. 1969.

[16] C. C. Kao, "Electromagnetic scattering from a finite tubular cylinder: numerical solutions," Radio Science, vol. 5, pp. 617-624, March 1970.

[17] C. C. Kao, "Currents on semi-infinite tube illuminated by electromagnetic waves," Radio Science, vol. 5, pp. 853-859, May 1970.

[18] R. W. P. King, B. Sandler, T. T. Wu, R. W. Burton, C. C. Kao and L. C. Shen, "Surface currents and charges on an electrically thick conducting tube in an E-polarized, normally incident plane-wave field. I. Theory," accepted for publication, Radio Science (scheduled for August 1976).

[19] R. W. Burton and R. W. P. King, "Induced currents and charges on thin

cylinders in a time-varying electromagnetic field," IEEE Trans. Electromag. Compat., vol. EMC-17, pp. 140-155, Aug. 1975, and also Interaction Notes, Note 257, Aug. 1975.

[20] R. W. Burton and R. W. P. King, "Measured currents and charges on thin crossed antennas in a plane-wave field," IEEE Trans. Antennas Propagat., vol. AP-23, pp. 657-664, Sept. 1975.

[21] C. C. Kao, "Measurements of surface currents on finite circular tube illuminated by an electromagnetic wave," IEEE Trans. Antennas Propagat., vol. AP-18, pp. 569-573, July 1970.

[22] R. W. Burton, R. W. P. King and D. Blejer, "Surface currents and charges on an electrically thick conducting tube in an E-polarized, normally incident plane-wave field. II. Measurements," accepted for publication, Radio Science (scheduled for August 1976).

[23] J. J. Bowman, T. B. A. Senior and P. L. E. Uslenghi, Eds., Electromagnetic and Acoustic Scattering by Simple Shapes. Amsterdam: North-Holland Publishing Co., 1969, Ch. 2.

[24] J. H. Van Vleck, F. Block and M. Hammermesh, "Theory of radar reflection from wires and thin metallic strips," J. Appl. Phys., vol. 18, pp. 274-294, Mar. 1947.

[25] C. T. Tai, "Electromagnetic back-scattering from cylindrical wires," J. Appl. Phys., vol. 23, pp. 909-916, 1952.

[26] R. W. P. King, Theory of Linear Antennas. Cambridge, Mass.: Harvard University Press, 1956, pp. 503-511.

[27] R. W. P. King, "Current distribution in arbitrarily oriented receiving and scattering antenna," IEEE Trans. Antennas Propagat., vol. AP-20, pp. 152-159, Mar. 1972.

[28] R. W. P. King, A. W. Glisson, S. Govind, R. D. Nevels, and J. D. Prewitt, "Current distribution in arbitrarily oriented conductor in plane-wave

field," submitted for publication.

[29] C.-L. Chen and T. T. Wu, Antenna Theory, Part I, R. E. Collin and F. J. Zucker, Eds. New York: McGraw-Hill Book Co., 1969, pp. 446-454.

[30] C.-L. Chen, "On the scattering of electromagnetic waves from a long wire," Radio Science, vol. 3, pp. 585-598, June 1968.